Computational modelling of Dielectric Barrier Discharge Plasma Actuators for Aerospace Flow control applications

MASTER OF SCIENCE THESIS

FOR THE DEGREE OF MASTER OF SCIENCE IN AEROSPACE ENGINEERING AT

DELFT UNIVERSITY OF TECHNOLOGY

SYED ZAID ALI

SEPTEMBER 6. 2016

FACULTY OF AEROSPACE ENGINEERING (LR) : DELFT UNIVERSITY OF TECHNOLOGY

I dedicate this work to my Father (Abbu).

DELFT UNIVERSITY OF TECHNOLOGY

DEPARTMENT OF

AERODYNAMICS

The undersigned hereby certify that they have read and recommend to the Faculty of Aerospace Engineering for acceptance of the thesis entitled **"Computational modelling of Dielectric Barrier Discharge Plasma Actuators for Aerospace flow control applications"** by **Syed Zaid Ali** in partial fulfilment of the requirements for the degree of **Master of Science.**

Dated: 06-09-2016

Supervisors:

Dr. Marios Kotsonis

Dr. Bas van Oudheusden

Dr. Steven Hulshoff

Dr. Daniele Ragni

Acknowledgements

The thesis appears in its present form due to assistance and guidance of my Supervisor; Dr. Marios Kotsonis. I would therefore like to offer my sincere gratitude and appreciation to him. Dr. Kotsonis always had motivating suggestions for me. He was extremely patient and his suggestions immensely helped me in to gain expertise in Computational modelling. Moreover I thank him for correcting my thesis numerous times and helping me with the graduation process.

Also, I would like to thank Dr. Annette Meiners from COMSOL technical support in Germany, Research group at the High Temperature and Plasma Laboratory at University of Minnesotta. They helped me a lot to better understand the challenges and the limitations of developing DBD model using COMSOL Multiphysics.

I would like to dedicate this thesis to my father whom I lost to cancer during my MSc. Without his sacrifices, trust, and support I would not have progressed in life. He made sure that me and my elder brother got the best education. Even with limited resources at his disposal, he was able to send my brother to Imperial College London, and myself to TU-Delft. I haven't come across a man of his calibre and with will power as strong as his. Even when the Doctors gave up hope, he joked about his death to mentally prepare us to not feel his loss. He fulfilled all his roles and responsibilities as a father, husband, brother, father-in-law, and a son.

Last but not the least, I want to thank my family; Ammi, Samad Bhai, Shagufta Baaji, and Shabbi. Thank you for always being there with me.

Delft University of Technology

Syed Zaid Ali

Nomenclature

Symbols

Symbol	Unit	Definition
F_b		Body force
ρ_c		Charge density
E	V/m	Electric field
$\nabla V_{\text{applied}}$	Volts	Applied potential
n_e		Electron density
τ_e	`	Electron flux vector
R_ϵ		Energy gain or loss due to inelastic collisions
R_e		Electron source or sink
x_k		Mole fraction of specie k
x_j		Mole fraction of target specie for reaction j
k_j	m^3/s	Rate coefficient
N_n	$1/m^3$	Neutral number density
D		Electric displacement
F_c		Computational body force
F_e		Experimental body force from Kotsonis PMMA and Kapton experiments
ρ		Density of fluid for CFD simulation
μ		Dynamic viscosity
r	-	Reflection coefficient
a	-	1 for electron flux directed towards the wall or 0 otherwise
$v_{e,th}$	m/s	Thermal velocity
γ_p	-	Secondary emission coefficient from the p_{th} positive ion species
Γ_p	$1/m^2s$	Ion flux of the p_{th} positive ion species at the surface
Γ_t	$1/m^2s$	Thermal emission flux
ε_p	Volt	Mean energy of the p_{th} positive ion species at the wall.
ε_t	Volt	Mean energy of thermally emitted electrons
n	-	Outward normal

Abbreviations

DBD	Dielectric Barrier Discharge Plasma Actuator
AC	Alternating Current
FEM	Finite Element Model
FEA	Finite Element Analysis
DOF	Degrees Of Freedom
EEDF	Electron Energy Distribution Function
1-D, 2-D	One Dimensional, Two Dimensional
CFD	Computational Fluid Dynamics
N-S Equations	Navier Stokes Equations

Table of contents

List of figures

Figure 42 Potential and Electric field at concluding time step of 102 second of the Electrodynamic-Fluid model. The results corroborate with the results of Electrostatic model [Figure 18, 19] confirming the correct implementation of boundary conditions and the coupling of NS-equations with Poisson equation.

Figure 43 Spatially and temporally varying body force distribution and for one complete cycle from t=0 seconds to t=2e-4 seconds with frequency of 5000 Hz.

Figure 44 Velocity ditribution and issuing of wall jet under quiescent condition, evident from Kotsonis[11]

Figure 45 Velocity vectors for a series of time steps for the Electrodynamic-Fluid model.

List of tables

Chapter 1

Introduction

Plasma actuators are comparatively new devices that have been devised for flow control. A Dielectric Barrier Discharge (DBD) plasma actuator is a commonly used plasma actuator. It typically consists of a set of asymmetrically placed electrodes and a dielectric. One of the electrode is exposed to the surrounding air whereas the other electrode is encapsulated within the dielectric material. The characteristic size of the DBD plasma actuator is of the order of millimetres in vertical direction and several centimetres in the horizontal (streamwise) direction. Figure 1 shows the schematic of a DBD plasma actuator configuration.

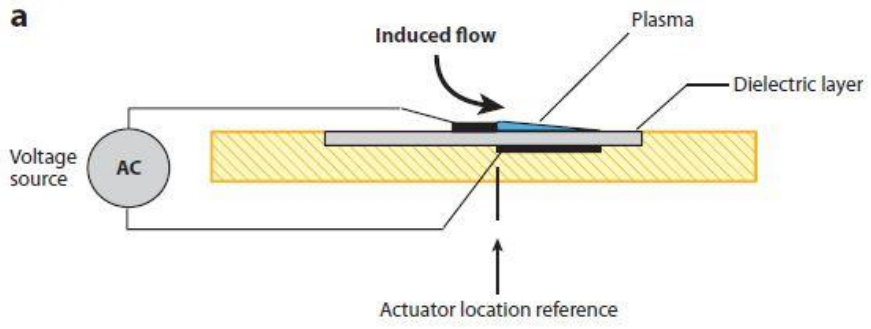

Figure 1 Schematic drawing of an asymmetric DBD plasma actuator

The actuator is driven by high frequency (typically in kHz range) AC voltage of several thousand volts. At sufficiently high voltages, the air in the vicinity of the exposed electrode ionizes. This ionized air is plasma which has a characteristic blue colour. The plasma so formed can be seen with a naked eye, but it requires a darkened room since the emission intensity is very low. In the presence of strong external electric field the ionized air results in a body force which acts on the ambient (neutrally charged) air. This body force is the mechanism for active aerodynamic control. The underlying physics behind the operation of DBD's will be discussed in the subsequent chapter.

Much of the research has undergone into the enhancing the performance of plasma actuators. The influence of electrical and geometrical parameters such as electrode length, dielectric thickness and applied waveform, applied frequency etc. have been a subject of a number of studies. Also, much attention has gone into visualizing the flow patterns and velocity distributions induced by the plasma actuator.

Although plethora of applications of DBD's have been realized till date but the complex interaction of charged species in a non-thermal plasma with the bulk gas and the dielectric barrier is the underlying physical aspect which has to be understood in order to improve plasma actuators efficiency and to make them reliable for flow control applications.

1.1 Project Rationale

The following Master thesis project has been performed with a goal to create a computational model of an Alternating Current Dielectric Barrier Discharge (AC-DBD) plasma actuator configuration using COMSOL Multi-physics software package. Studies aimed at modelling a plasma are challenging because they combine elements of reaction engineering, statistical physics, fluid mechanics, physical kinetics, electrodynamics, electromagnetics, heat transfer and mass transfer. This results in a multi-physics problem which has to account for the complicated coupling between the different physics. COMSOL Multi-physics software has an inbuilt plasma module, comprising of different plasma physics interfaces.

The COMSOL plasma module is designed to simplify the process of modelling low-temperature plasmas. The module will aid us in delving into the physics of plasma and to comment on complex process of Plasma-fluid interaction. Also, as stated prior, the model will be able to compute the body force, and possibly, also show its distribution. The study will also help us to comment on the capabilities of COMSOL's Plasma module and also on the challenges that are faced in the computational modelling of a DBD Plasma Actuator.

The final goal is to compare the results of the computational model with the available experimental studies and comment on the model's agreement with the experiments.

Thus, the core objectives of this thesis can be stated as follows:

1. Development of a computational model for AC-DBD plasma actuators. This part will be accomplished by first developing an electrostatic model and then finally, a time dependent (Electrodynamic) model.

2. Comparison of results with experimental studies done in the past.

1.2 Research question, aims and objectives

This research project aims at developing a reliable computational model of a Plasma actuator in Alternating Current Dielectric Barrier Discharge configuration (AC-DBD). Also the model will enable better understanding of plasma physics through plasma modelling and plasma-fluid interaction through a CFD study. So far, there is little literature involving plasma-fluid interaction to analyse and optimize the momentum coupling between plasma and the neutral fluid. The final envisioned goal of the thesis is to validate the model's results with experimental studies done in the past and to calibrate computational body force with experimentally determined body forces. The research will be based on plasma modelling and CFD simulations using commercially available software's and codes.

1.2.1 Research question

Is it possible to develop a reliable and accurate model for a AC-DBD plasma actuator which provides an insight into plasma behaviour at atmospheric pressure, accurately predicting the body force which acts on the neutral fluid due to plasma formation, taking into account the extremely

short and disparate time scales between plasma discharge formation and the reaction of the fluid to plasma?

1.2.2 Objective

To develop an efficient computational model for AC-DBD plasma actuator quantifying the body force. The accuracy of the quantified body force will be dependent on defined plasma chemistry and involved reactions and plasma processes (electron-ion impact, secondary electron emission etc.). Apropos to this research, experimental studies have been carried out at the Aerodynamic faculty at TU-Delft which have quantified the body force and induced thrust using PIV flow measurement technique. In addition, the final AC-DBD model developed in this research will also be complemented by the results from these experimental studies, calibrating computational body force with experimentally determined body forces.

1.2.3 Sub-objectives

1. To identify the most influential parameters that affect the performance of a plasma actuator.

2. Validation of the calculated body force derived by multi-physics study which solves for coupled plasma-fluid interactions (plasma model and CFD model), with the experimental results.

3. To contribute to the understanding of the challenges involved in computationally modelling an AC-DBD Plasma Actuator using COMSOL.

4. Attempt to identify and appropriately model the reactions and processes involved, which affect the discharge formation, namely: electron impact reactions, secondary electron emission, electron-ion impact etc.

1.3 Approach

In this work, we will start by developing an electrostatic model for the DBD configuration, whereby we will solve for Electric field and potential using Poisson equation. Using the electrostatic model, we shall be able to see the behaviour of electric field and potential with and without a plasma discharge, which will be modelled/represented by a charge density. Furthermore, we will also introduce Gaussian charge distribution in the vicinity of exposed electrodes and along the dielectric surface to model the decay plasma discharge of as one moves away from the exposed electrode, and notice the behaviour of the electric field.

The next and the final goal of this work is then to develop a time-dependent model for a DBD plasma actuator or a species-based Electro-dynamic model which shall quantify the body force and also detail its distribution. An AC circuit will be modelled which will be coupled to the DBD configuration. The plasma in the vicinity of the exposed electrode will be modelled using a

simplified Argon based chemistry. Notable phenomenon's responsible for plasma formation; like secondary electron emission, surface charge accumulation over dielectric surface will also be modelled. The resulting simulation will give us vivid details and aid in visualizing different stages of plasma formation.

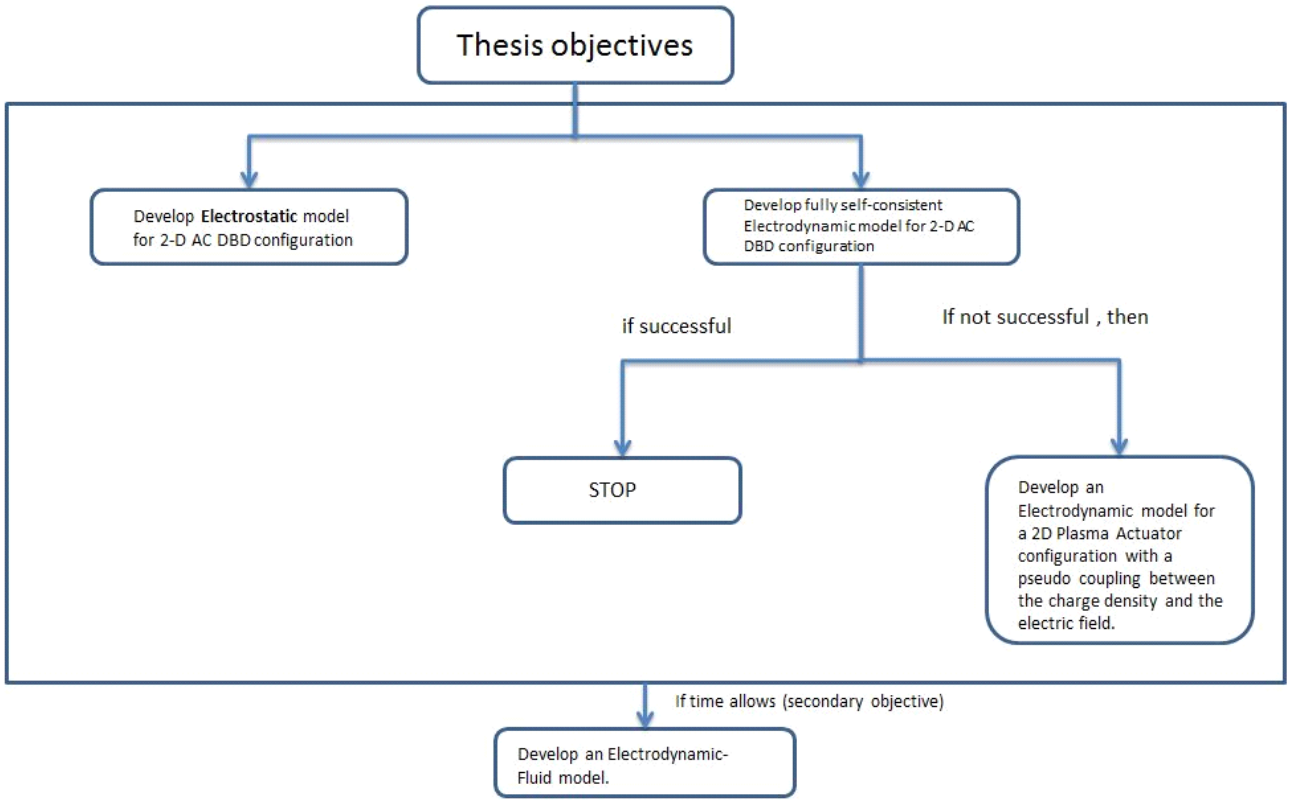

Figure 2 Detailing the thesis approach

Chapter 2

Literature Review

The goal of the research is to create a computational model of an Alternating Current Dielectric Barrier Discharge (AC-DBD) plasma actuator. COMSOL Multi-physics software has a inbuilt plasma module, comprising of different plasma physics interfaces. The COMSOL plasma module is designed to simplify the modelling of low-temperature plasmas. This module will be used extensively in the study to delve into the physics of plasma and to comment on complex process of Plasma-fluid interaction. Also the model will be able to quantify the body force. The study will also help us to comment on the results of numerical and experimental studies of AC-DBD's conducted in the past. Another goal of this research will be to come up with a comprehensive set of geometrical and electrical parameters which affect the AC-DBD's performance , thus realizing an optimum configuration for a particular application. Thus, this research will be conducive to

1. Development of an efficient AC-DBD plasma actuator model.
2. Improved design and operation of Dielectric Barrier Discharge (DBD) plasma actuators.

2.1 Introduction

In the past decade there has been an increasing interest in plasma actuators[1] in the domain of active flow control. A low-weight ,fully electronic configuration with no mechanical moving parts with a fast time response for unsteady application; these features make plasma actuators a lucrative solution for active flow control applications. Particularly in the aerospace industry, plasma actuators have displayed the potential for plethora of applications such as prevention of flow separation on wing surface or controlling boundary layer instabilities in hypersonic flows.

The DBD configuration used for plasma actuators consists of two electrodes, one exposed to the air and the other encapsulated in dielectric material which are arranged asymmetrically. An example configuration is shown in Figure 1. The electrodes are supplied with an AC voltage that causes the air over the covered electrode to weakly ionize. This ionized air is a plasma and has a characteristic blue color. The intensity of plasma is very low and requires darkened space to view by eye. In the presence of the external electric field, the ionized air in the vicinity of the exposed electrode results in a body-force vector field that acts on the ambient (non-ionized, neutral) air. The body force is made use of in the active aerodynamic flow control.

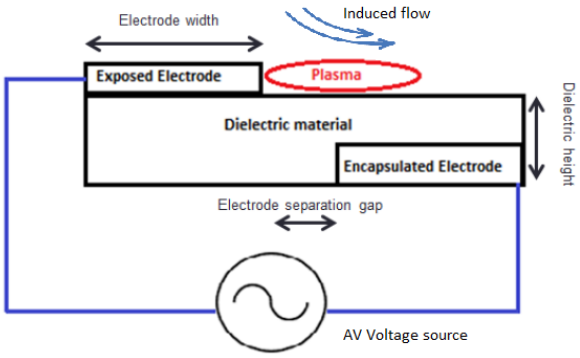

Figure 3 Geometrical configuration and operation of a plasma actuator in DBD configuration.

Although plethora of applications of plasma actuators have been realized till date but the complex interaction of plasma with the neutral fluid is the underlying physical aspect which has to be understood, to improve plasma actuators efficiency and to make them reliable for flow control applications. Because the timescale of plasma formation is typically 10^{-4} seconds, hence very less is known about momentum coupling between plasma and fluid flow . Therefore, resolving the time scales for different phases of plasma formation or capturing them using experimental or computational techniques is very difficult. This fosters a need to develop efficient computational models which can predict the plasma behavior ,to better understand the physics involved, giving a lucid picture of interaction between plasma and neutral fluid. As the defining characteristic of plasma actuators which makes them lucrative in flow control applications is the creation of body force ; these models should also be able to accurately quantify the body force.

Increased need to employ plasma actuators in the engineering industry calls for developing efficient computational models which model the induced flow by plasma along-with reproducing changes in performance with a change in operating conditions/ parameters. The focus of discussion of plasma actuator models is to study how different studies have modelled the plasma, the assumptions that are involved while modelling and how these studies arrive at the derivation of body force. This discussion delineates the contrast between different studies and aids in adopting methods which capture essential plasma physics and accurately quantify the body force at manageable computational costs.

Plasma actuator models can be briefly divided into 2 categories :Models based on first principles and Algebraic models. Models based on first principles require the solution of complicated chemistry, species transport equations, Poisson's equation, and the Navier-Stokes equations self-consistently. Though these models accurately predict the plasma discharge processes, they are very computational intensive which hinders their application in an iterative design process. An example of model based on first principles includes the chemistry based models. A widely accepted chemistry based plasma model has been developed by Likhanskii[17]. However, the model of Likhaanski has severe limitations like high spatial resolution for moderate voltages and unsteady ionization constants. Furthermore, in his experimental study Hoshkinson[18] notices that the performance of plasma actuator doesn't change with change in dielectric material. Intuitively, this should not be the case according to first principle based models which depend on

secondary electron emission. Since different dielectric materials have different secondary electron emissions, the performance of plasma actuator should vary for different dielectric materials. However, this is not the case in real world, as proved by Hoshkinson's experiments. These are the primary reasons for not implementing/preferring models based on first principles in plasma actuator modelling studies.

In contrast to the chemistry based models, algebraic models capture the resulting plasma phenomenon without a need for very high spatial resolution. Different algebraic models developed in the past use different methods to solve for the body force while avoiding the need for a high degree of spatial resolution. The algebraic models can be distinguished from each other on the basis of simplicity.

Shyy and Jayaraman[19] developed a model for the glow discharge-induced fluid flow which computes the body force by simplifying the electric field, assuming that the electric field lines are parallel everywhere except in a region near the exposed electrode. This saves the trouble of providing a detailed description of the electric field. With this assumption standing, the electric field in the vicinity of the exposed electrode is linearized keeping in mind that the electric field strength should decrease as one traverses laterally away from the exposed electrode edge. A time averaged expression for the body force gives the body force along x and y axis. These body force expressions are plugged directly into the Navier-Stokes equations as a source term for studying the plasma-neutral fluid interactions.

Suzen and Hwang[20] developed an electrostatic model to calculate the body force. This model is slightly more sophisticated than the model of Jayaraman and Shyy. The prime feature of this model compared to the former is that it makes use of less variables while capturing more of the essential plasma physics. It starts by assuming that the plasma is quasi steady which means that the charges in the plasma have sufficient time to rearrange themselves resulting in plasma neutrality, before the plasma actually forms. This is a valid assumption owing to the large time scales between plasma formation (10^{-4} seconds) and charge rearrangement (10^{-8} seconds). This assumption leads to simplification of equations reducing originally the four Maxwell's equation to two (one Poisson and one Helmholtz equation). For the applied electric field the Poisson equation is solved giving the value of potential due to applied electric field and for the electric field due to charge density, the Helmholtz equation is solved giving the value of charge density. The calculation of body force requires only these 2 parameters, which is then calculated. However, a prior assumption of charge density distribution is to be incorporated in this model. This serves as the initial point for the model during iteration. Suzen and Hwang originally assume a half Gaussian charge density distribution in their study.

A complex but enhanced model was developed by Corke and Orlov[21]. The authors also compare the models results with experimental results from Enloe [16], which corroborate really well. The physical space surrounding the exposed electrode is discretized into N small sub-regions. Each region is modelled as a circuit, hence consisting of N circuits. Each circuit consists of 2 capacitive elements (air capacitor and a dielectric capacitor) and 1 resistive element. The resistive element models plasma. Each circuit is time dependent to account for the evolution of plasma with each half cycle. The governing equations are a set of 5 ordinary differential equations which are solved for induced voltage and induced current in the Nth circuit. The current is

indicative of the charge density in the region adjacent to the N^{th} circuit. The derived induced voltage in the N^{th} circuit serves as a boundary condition to solve for potential due to the charges which is substituted in the expression for the body force, thus calculating it. Unlike Suzen and Hwang one does not need a prior assumption of boundary condition for charge density when solving this model. This is to be counted among one of the advantages of Orlov's Lumped circuit model.

The motivation behind optimizing the plasma actuator performance is to optimize the momentum coupling between ionized fluid resulting due to the plasma action and the ambient fluid. In other words, enhancing the body force acting on the ambient fluid. The optimum configuration rests on various parameters. These parameters can be broadly classified under 2 major categories :

1. Geometrical parameters: Electrode thickness, electrode width , electrode separation gap.

2. Electrical parameters: Applied voltage, type of waveform, frequency.

Electrode thickness: Enloe[16] and Corke[21] showed that change in thickness of the exposed electrode has no effect on the structure of the plasma. Also, the thrust due to the plasma was found to linearly decrease with the increase in thickness and the diameter of the exposed electrode. But unlike Enloe and Corke, Hoshkinson[18] observed an exponential decrease in induced thrust with the exposed electrode thickness. Also, as discussed prior, Hoshkinson's experiments showed that the induced thrust is independent of the exposed electrode material. This is suggestive of a serious limitation of chemistry based plasma models which rely on secondary electron emission. Hence, the results from Hoshkinson's suggest that the induced force will not change if one changes the secondary electron emission coefficient. This can be an interesting study to simulate in computational models and comment on Hoshkinson's conclusion.

Electrode width**:** Enloe[16] and Corke[21] found that the induced thrust increases with increase in width of the "encapsulated" electrode. This claim was further corroborated by Forte[25] who confirmed the same with his parametric study's results.

Electrode separation gap: Effects of the electrode separation gap on the maximum induced velocity were studied by Forte[25]. The separation gap was varied from -5 to 15 mm. The results showed a parabolic increase in maximum induced velocity and an optimum at electrode separation gap of 5 mm. Further increase in the electrode separation gap beyond 5mm showed a decline in the electric field magnitude. Hence, increasing the electrode separation gap may strongly alter the electric field distribution since the ions accelerate for longer distances. The Electric field falls down with a larger gap because the effective dielectric thickness between the electrodes increases. The ions cannot accelerate as much when the electrodes are one above the other (d=5mm) because of the symmetric electric field distribution

Applied voltage: Enloe[13] noticed an increase in induced thrust with the increase in applied voltage. Also, a power-law relationship was found to exist between the applied voltage and induced thrust. Likewise to Enloe, Corke and Thomas[15] also found a power-law relationship betwee

n applied voltage and induced thrust with an exponent of 7/2. Though the dependent variables in Corke's study are different than Enloe, but the similar observed trend in both the studies is interesting. In contrast, Forte's result are not suggestive of a power law relationship like the two previously discussed studies but the increase in induced thrust with increasing applied voltage is suggested by Forte too. The mismatch between Forte's compared to Enloe and Corke's results can be because of the operating conditions and experimental setup used by Forte are different from the Corke's and Enloe's study. The dielectric thickness is 7 times in comparison to Corkes study and the maximum voltage reached is 25 kV, which is two order magnitude larger than that reached in Enloe's and Corke's study.

Enloe[13] and Orlov studied the maximum extent of plasma over a range of applied voltages. Orlov's work bolstered the work of Enloe which also showed an increase in the extent of plasma with an increase in applied voltage magnitude. Study conducted by Likhanskii [17] showed an increase in plasma extent with increase in the amplitude of negative cycle. The reason can be that as the voltage is applied, the cathode begins to loose potential and emit electrons due to secondary electron emission. Most of electrons distribute themselves over the dielectric while some ionize the oxygen molecules, giving them a negative charge. This results in a gradient between positive and negative charges. Thus plasma moves along the dielectric surface due to this charge distribution. Increasing the amplitude of the negative half cycle results in increasing of the duration of this phase which results in plasma going even further along the longitudinal axis. This plasma is retained till the potential difference between the dielectric and the exposed electrode is greater than the breakdown electric field strength.

Waveform: Enloe[13] and Thomas[15] studied the effect of different applied waveforms on the induced thrust. Both of their studies showed that a positive sawtooth waveform results in better plasma actuator performance in comparison to sinusoidal or negative sawtooth waveforms. Furthermore it was seen that for any AC waveform the negative going half cycle of waveform, produced more plasma and possessed less discharge asymmetry than the positive going portion.

Frequency: Forte[25] shows that the induced velocity increases with increase in applied frequency. The study was conducted for an applied voltage of 20kV and frequency values between 0 to 2000 Hz. A steep increase in induced velocity is noticed with increase in frequencies upto 1500 Hz. This might happen because with the increase in frequency, the slope of the voltage-time graph also increases. This could result in enhanced ionization. But with further increase in frequencies beyond 1500 Hz, a plateau is observed, whereby the increase in induced velocity is not noticeable or almost negligible. The reasoning given by author for this phenomenon is that ,though the ionization is increased with increase in frequency but the dielectric relaxation time is decreased. At the ignition of discharge the dielectric charges and then relaxes. Since the relaxation time is considerably low, this results in an unstable discharge at frequencies beyond 1500-2000 Hz. Orlov[14] observed no effect in the extent of plasma with change in frequency. This observation suggests that the propagation velocity increases with increase in applied frequency because at higher frequencies the plasma has less time to spread over a given area. Since the plasma extent is the same for all frequencies, the velocity must increase, which is indeed the case. Thomas[15] also found an increase in induced thrust with increase in frequency of the applied voltage. Thus the observations from the study of Orlov, Forte and Thomas corroborate really well to each other.

2.2 Analysis

The focus of discussion of numerical models is to study how different studies have modelled the plasma actuator, the assumptions that are involved while modelling and how these studies arrive at the derivation of body force. This discussion is conducive to realize a best suited study for capturing plasma physics and quantify the body force at manageable computational cost. Further in the literature study we discuss the geometrical and electrical parameters that affect the performance of a AC-DBD plasma actuator. We gauge the performance of a plasma actuator by the magnitude of induced thrust which quantifies the body force in experimental studies. Variation in geometrical and electrical parameters affects the induced thrust, and hence the performance of the plasma actuator. Among one of the goals of thesis is to vary most of the governing parameters and notice if the models results match with the trends from the studies discussed in the literature study. Since there are contradicting trends amongst some studies, our model will aid us in supporting claims from competing studies.

2.3 Discussion and Conclusions

Alongwith development of an efficient AC-DBD plasma actuator model which accurately models the plasma and plasma-fluid interaction by precisely quantifying the body force, this research will also help us in identifying the gaps between our model , and the experiments and models developed in the past. Also it will help us in identifying the challenges faced while computationally modelling a plasma actuator and the variables that affect its performance subsequently helping us to deduce the reasons behind these and contributing to improved design and operation of AC-DBD for varied applications.

Chapter 3

Methodology

The goal of the research is to create a computational model of an Alternating Current Dielectric Barrier Discharge (AC-DBD) plasma actuator.. The model should be able to quantify the body force. The study will also help us to comment on the capabilities of COMSOL's Plasma module and on the results of computational studies of AC-DBD's conducted in the past. Another envisioned goal of this research is to develop a species based electro-dynamic model of an AC-DBD plasma actuator that self consistently solves for electron and ion density with a given set of initial conditions. The final goal is to compare body force computed from the computational model with the experimental body force measurements [10, 22]. Thus, this research will be conducive to

1. Development of a computational model of an AC-DBD plasma actuator.
2. Calculation and distribution of body force.
3. Improved design and operation of Dielectric Barrier Discharge (DBD) plasma actuator.

3.1 Objective

The final goal of the research is to develop species based self-consistent computational model for an AC-DBD plasma actuator quantifying the body force, whereby the body force and hence the performance of the plasma actuator is a function of various geometrical, electrical and flow parameters and the accuracy is dependent on defined/modelled plasma chemistry, reactions and plasma processes (electron-ion impact, secondary electron emission etc.).

In relation to this research, experimental studies carried out at the Aerodynamic faculty at TU-Delft which have quantified the body force and induced thrust using PIV flow measurement technique will be used for comparison with the results from the computational model. One of the goal of the thesis is to validate the model's results with experimental studies done in the past and calibrate computational body force with experimentally determined body forces.

3.2 Hypothesis

Is it possible to develop a computational model for AC-DBD plasma actuator using COMSOL Multiphysics software, which provides an insight into plasma behaviour at atmospheric pressure, computing the body force close to experimental values, and takes into account various AC-DBD plasma processes like secondary electron emission, electron impact reactions, electron-ion recombination etc?

3.3 Research Methodology

In our research, a deductive approach is adopted. Based on studies conducted in the past, less accurate approaches to computationally model a plasma actuator will be discarded whereas comparatively more accurate modelling techniques will be adopted.

With this knowledge we proceed on to develop our computational model which predicts the body force by modelling the plasma and plasma processes. With this model at hand, we will be able to compare and calibrate the results with the experimental measurements of body force at TU-Delft for a given set of same geometrical and electrical parameters.

3.4 Theoretical Basis

3.4.1 Calculating the body force due to the plasma discharge

The resulting plasma discharge on operation of the AC-DBD exerts a force on the ambient fluid, exchanging momentum with it which prevents flow separation [1]. The expression of the body force is given as follows:

$$F_b = \rho_c \, E \tag{3.1}$$

Where ρ_c is the charge density (C/m^3) and E is the electric field.

Since the applied potential is varying in time, and thus the name AC-DBD, the Electric field too varies in time since it is related to the potential via the Poisson's equation, given below

$$E = -\nabla V_{applied} \tag{3.2}$$

Thus, the Electric field is the negative gradient of the applied potential. Therefore, as the electric field reaches its breakdown value at a given time step, the initiation of discharge takes place. As evident, the space charge density (plasma discharge) is a function of the electric field and thus varies in time.

Since ρ_c and E are both variable in time, thus the body force also varies in time. Hence, the body force and plasma discharge are coupled with the electric field and therefore the applied potential.

An electro-dynamic model should take care of this coupling and this is one of the challenges in modelling the AC-DBD.

3.4.2 Modelling the plasma discharge

The challenge in developing a computational model of an AC-DBD lies in modelling the plasma discharge itself and to find a complete and physically correct chemical mechanism for the plasma of interest. The chemical mechanism from experimental studies is largely unknown and it is only in computational or numerical studies where this can be modelled. The plasma so modelled, can involve just a handful of reactions and species or tens and hundreds of species. This is important with regards to the convergence speed of the solution. Even with simple chemistry, the solution for simple DBD's can be time intensive.

A set of equations called Drift Diffusion equations are solved for the plasma discharge to calculate the electron density and the electron energy density. Drift Diffusion equations[30] are a combination of convection-diffusion equations that describe the physical phenomenon where particles (ions and electrons), energy and physical quantities are transported inside a physical system due to two processes; diffusion and convection.

Drift diffusion equations are simplified form of Boltzmann equations. The Boltzmann equation is an extremely complicated integro-differential equation and presently solving them in an efficient manner is not deemed possible. However, the Boltzmann equation can be approximated by fluid equations by multiplying a weighting function and then integrating over velocity space. This reduces the Boltzmann equation to a three dimensional time dependent problem. The fluid equations describe the electron number density, the mean electron momentum and the mean electron energy which are a function of space and time.

COMSOL Multiphysics allows for solving the Drift diffusion equations for calculation of electron density and electron energy density, for any type of plasma, except those which are formed at pressure below 0.133 Pascal and where the number density of the charged species is much less than the background gas[30]. In other words, the plasma is weakly ionized. For example; the drift diffusion equations cannot be solved for fusion plasmas.

The Drift diffusion equations solved for electron density and electron energy density by COMSOL drift diffusion interface are as given below, respectively.

$$\frac{\partial(n_e)}{\partial t} + \nabla.\Gamma_e = R_e - (u.\nabla).n_e \qquad 3.3$$

Where

$$\Gamma_e = -(\mu_e.E).n_e \qquad 3.4$$

$$R_e = \sum_{j=1}^{M} x_j k_j N_n n_e$$

3.5

$$x_k = \frac{w_k}{M_k} M_n$$

3.6

The subscript e refers to an electron. The equation is solved for n_e. Γ_e is the electron flux vector and R_e is either a source of sink of the electrons. The source coefficient R_e is determined from the plasma chemistry. For instance, in the above equation, there are M reactions that contribute to the growth or decay of electron density, x_j is the mole fraction of the target species for reaction j, k_j is the rate coefficient (m^3/s) for reaction j and N_n is the total neutral number density ($1/m^3$). x_k is the mole fraction of a specie k and it is computed from mass fraction of the specie k and the mean molar mass of the whole mixture.

$$\frac{\partial(n_\varepsilon)}{\partial t} + \nabla.\Gamma_\varepsilon + sE.\Gamma_e = R_\varepsilon - (u.\nabla).n_\varepsilon$$

3.7

$$\Gamma_\varepsilon = -(\mu_\varepsilon.E).n_\varepsilon - \nabla(D_\varepsilon n_\varepsilon)$$

3.8

$$R_\varepsilon = \sum_{j=1}^{P} x_j k_j N_n n_e \Delta\varepsilon_j$$

3.9

The subscript ε refers to electron energy and R_ε is the energy loss or gain due to inelastic collisions.

As evident from the drift diffusion equations, in order to account for the electron density and electron energy density, an initial guess for both should be provided before starting the simulation. The initial values for both are crucial in achieving convergence and for the solver to initiate. Values too far from the solution will result in an error message when initiating the simulation on COMSOL.

Furthermore, in order to calculate the electron transport properties by solving drift diffusion equations, it is deemed necessary to incorporate the dependency of a particular reaction on the electron energy. This is achieved by specifying the cross section data of all species.

1. **Cross section data for each species.**

Numerous species are present in a plasma, which can either be in ground or excited state. There are variety of processes via which electrons interact with these atomic particles and each of these processes is characterized by a distinct cross section.

When modelling plasma physics, we need to specify complete cross section data in order to model these processes. Such processes include elastic and inelastic processes (electronic and vibrational excitation, partial and total ionization, dissociative electron attachment, etc.)

2. **Electron energy distribution function**

A distribution function of electron energy (EEDF) is required to calculate reaction rates for reactions of electron collision[30]. Electron transport properties are derived from the EEDF, and therefore choosing a EEDF greatly influences the results of plasma model. The EEDF or can be approximated, based on the degree of ionization or plasma can be calculated self-consistent by solving the Boltzmann equation using two approximation term.

A Maxwellian distribution results when the electrons are in thermodynamic equilibrium with high degree of ionization. Whereas the electron electron collisions at low degree of ionization result in a Druyvesteyn distribution function.

Maximum consistency is obtained between the kinetic and fluid description of plasma when we explicitly compute the EEDF using Boltzmann Two term approximation. Solving the Boltzmann equation also makes it possible to calculate the drift velocity . The drift velocity is an important quantity because it depends on all the collisions which make up the plasma chemistry.

COMSOL only solves Boltzmann two term approximation equations for a 1D model. This renders us unable to self-consistently compute the EEDF from imported cross section data. Thus, for our electro-dynamic model, we assume a Maxwellian EEDF owing to the high degree of ionization and thermodynamic equilibrium of plasma formed on a DBD's actuation.

3.4.3 Modelling the electron exchange and the associated electron exchange mechanism

In the AC-DBD configuration, electron exchange takes place through different mechanisms. Thus, it is essential to model these mechanisms. The different mechanisms through which electron exchange happens are as follows:

1. Gain of electrons due to secondary electron emission.
   The exposed metal electrode and the dielectric emit electrons with some probability when it is stuck by a positive ion. The chemical reaction resulting in generation of the secondary electron is added under the drift diffusion interface in COMSOL and the appropriate surface is selected where the electron exchange takes place.

2. Gain of electrons due to thermionic emission.
   As a surface is heated up, it releases electrons. This typically occurs when the thermal energy of the electron is higher than the work function of the material.

3. Loss of electrons from *plasma bulk* to the surface.
   The electrons present in the plasma strike the metal and the dielectric surface and reattach back to these surfaces.

These electron exchange mechanisms are modelled by solving for electron flux normal to the surface. The resulting reactions are specified under the drift diffusion interface in COMSOL. Two equations are solved; one for electron density normal to the surface and the other for electron energy density normal to the surface.

The electron flux's normal component is given by:

$$-n.\Gamma_e = \frac{1-r}{1+r}\left(\frac{1}{2}v_{e,th}.n_e\right) - \frac{2}{1+r}(1-a)\left[\sum_p \gamma_p(\Gamma_p.n) + \Gamma_t.n\right] \quad 3.10$$

The electron energy density's normal component is given by:

$$-n.\Gamma_\varepsilon = \frac{1-r}{1+r}\left(\frac{5}{6}v_{e,th}.n_\varepsilon\right) - \frac{2}{1+r}(1-a)\left[\sum_p \gamma_p\varepsilon_p(\Gamma_p.n) + \varepsilon_t\Gamma_t.n\right] \quad 3.11$$

The meaning of the symbols and the units are given in Table 1 below:

Symbol		Unit
r	Reflection coefficient	-
a	1 for electron flux directed towards the wall or 0 otherwise	-
$v_{e,th}$	Thermal velocity	m/s
γ_p	Secondary emission coefficient for p_{th} positive ion species	-
Γ_p	Ion flux of the p_{th} positive ion species	$1/m^2s$
Γ_t	Thermal emission flux	$1/m^2s$
ε_p	Mean energy of the p_{th} positive ion species at wall.	V
ε_t	Mean energy of thermally emitted electrons	V
n	Outward normal	-

Table 1 Detailing the symbols with their meanings and units.

3.5 Discretization schemes in COMSOL

COMSOL Multiphysics is a finite element analysis simulation software package for various physics and engineering applications, especially coupled problems known as Multiphysics problems. The finite element method (FEM) is a numerical technique which is used for finding approximate solutions to complex partial differential equations. Finite element method divides a large problem into smaller, simpler, parts, which are called finite elements (discretization). The system is then reduced to simple algebraic equations which model these finite elements which can then be solved easily.

Discretizing means translating an object-based model into a mathematical model that is appropriate for analysis. Finite Element method is a discretizing procedure which creates a network of elements connected by nodes. Each of these element copies and simulates the properties of the local material. With properly defined boundary conditions, a numerical definition of the object based model can be defined, resulting in a computational model.

In COMSOL, FEM analysis of a particular problem can be time dependent, stationary, or an eigenvalue. And the problem can be non-linear, linear, parametric, and sometimes combinations of those. Based on the physics of a problem, COMSOL automatically selects a solver.

Concepts related to COMSOL Solvers are introduced and discussed in the following section:

3.5.1 Solutions to Linear Systems of Equations: Direct and Iterative Solvers

COMSOL uses direct and iterative solvers to solve linear system of equations. COMSOL selects the optimized solver and its settings based on the chosen space dimension and the associated physics. Fundamental understanding of these methods provide an insight into how the solvers actually work and for understanding how the problem size affects the memory requirements. Linear Static Finite Element Problem.

Consider a simple linear system.

$$\begin{Bmatrix} f_{u1} \\ f_{u2} \end{Bmatrix} = \begin{bmatrix} k_2 + k_3 & k_3 \\ -k_3 & k_1 + k_3 \end{bmatrix} \begin{Bmatrix} u_1 \\ u_2 \end{Bmatrix}$$

3.12

This system can also be represented as;

$$f(u) = b - ku$$

3.13

If we define a quadratic function

$$r(u) = b.u - (ku.u)1/2$$

3.14

The solution to a quadratic function is given by Newton's method. If we give an initial value of u_0, we get a solution for a given quadratic equation in one iteration. The solution is as follows

$$u_{solution} = u_0 - \frac{r'(u_0)}{r''(u_0)}$$

3.15

The $r'(u_0)$ and $r''(u_0)$ values for equation 3.16 are given by:

$$r'(u_0) = b - ku$$

3.16

$$r''(u_0) = -k$$

3.17

Plugging the values of $r'(u_0)$ and $r''(u_0)$ in equation 3.17, we get the solution for equation 3.16, which is given by

$$u_{solution} = k^{-1}b$$

3.18

Though this is a simple linear system, but in actuality, there can be hundreds or thousands of linear equations which results in large matrices. Solution to equation 3.20 is then computationally the most demanding part of the problem.

This method of finding solution to a linear system of equations by finding the minimum of a quadratic function is called Gaussian elimination or LU factorization. All COMSOL direct solvers discussed in the next section use LU decomposition for solving linear systems.

There are two fundamental classes of algorithms that are used to solve for $k^{-1}b$: direct and iterative methods. We introduce both of these methods and solvers in COMSOL that are based on these algorithms.

Direct Solvers

Direct solvers are based on Gaussian elimination/LU factorization.

The direct solvers in COMSOL are;

1. MUMPS
   The MUMPS solver is fast and has cluster multi core capability.
2. PARDISO
   The PARDISO solver is robust and has better multi-core capability than MUMPS since it scales better than the former on a single node with multiple cores.
3. SPOOLES:
   The SPOOLES solver is slow but it uses least memory.

If we are solving a problem that does not have a solution, then the direct solvers will return an error message. This error message hints that we should look whether we have properly constrained our problem or not.

Iterative Solvers

All Iterative solvers in COMSOL at their highest level make use of Conjugate-gradient method to find solution to linear system of equations. The iterative solvers approach the solution gradually unlike the direct solvers, which solve the linear system of equations in one step.

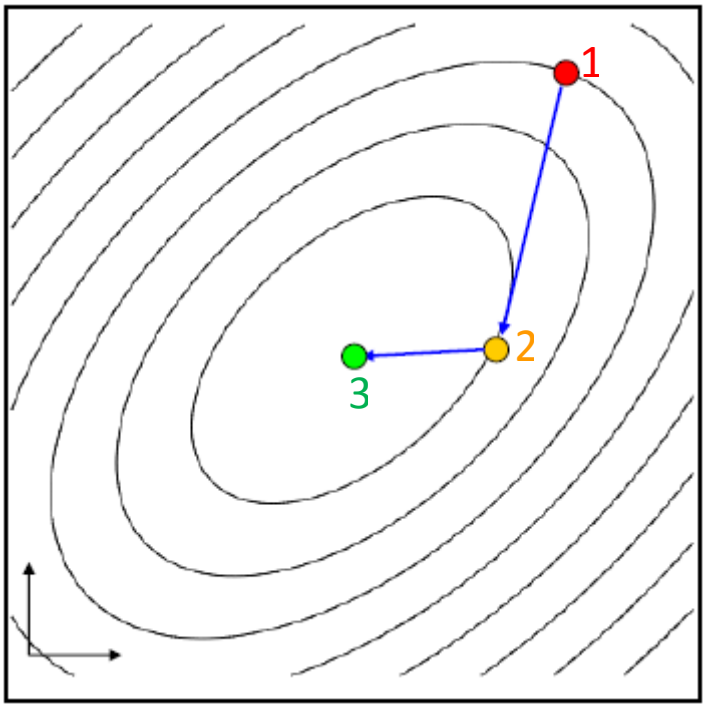

Figure 4 Iterative method for finding minimum using the Conjugate-gradient method [source: Wikipedia]

In a conjugate gradient method, we initially start at a point, for instance Point 1 in Figure 4. Then, gradient vector is computed and minimum (point 2 in Figure 4) along that vector is found. We then find a conjugate gradient vector with respect to the gradient vector at the minima point.

Then again we find a minimum along the conjugate gradient vector (point 3 in Figure 4) and find a conjugate gradient vector at that point with respect to the previous conjugate gradient method. The iterations are repeated until the solution is converged. The conjugate gradient method necessitates that we can calculate $r(u_0)$ $r'(u_0)$ and $r''(u_0)$. However, we cannot compute k^{-1}using conjugate gradient method while its choice can significantly affect the solution. Numerical errors increase with higher values of k, also known as the condition number.

Fundamentally, all COMSOL iterative solvers make use of some form of Conjugate gradient method. In order to decrease the numerical errors associated with condition numbers, all iterative methods make use of pre-conditioners. The linear system equation $ku = b$ is multiplied with a preconditioner N as shown in Figure 5 [right[, to improve the conditioner number and thus decrease the numerical errors associated with solving the linear system of equations..

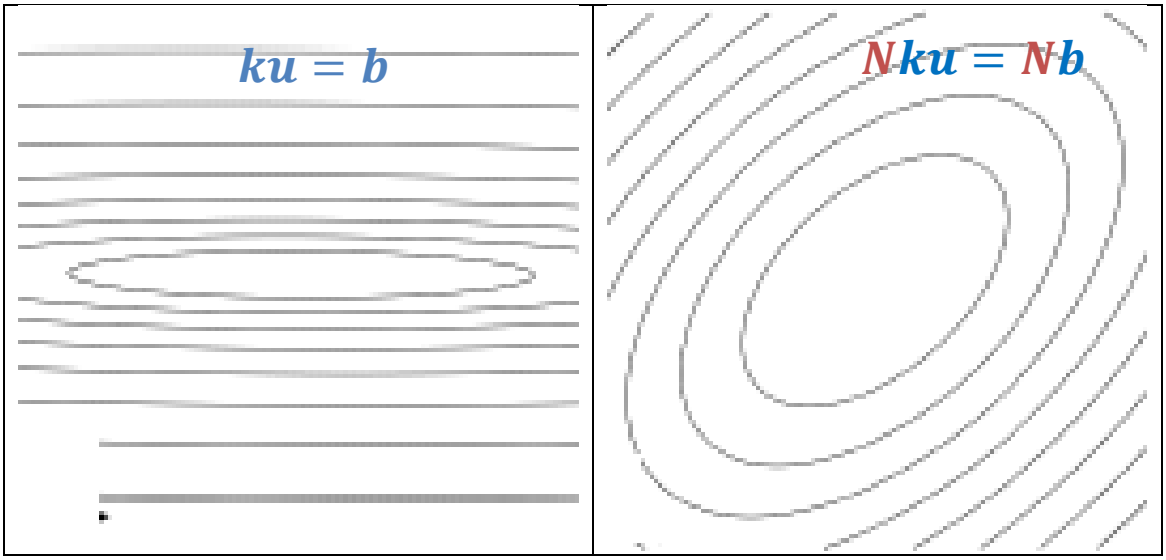

Figure 5 Decrease in numerical error associated with Conjugate gradient method by introducing a preconditioner *N*in the linear system of equation $ku = b$.

Iterative solvers are less robust than the direct solvers because condition number affects the convergence speed of the iterative solvers. Whereas, a disadvantage with direct solvers is that they use more memory than iterative solvers

One of the advantages that COMSOL offers is that it automatically detects the best solver for solving linear system of equations for a given physics and study type and does not require any user input.

3.5.2 Solutions to Nonlinear Static Finite Element Problems

Solving a non-linear system of equations is quite alike to solving linear system of equations except that we take several Newton Raphson iterations to obtain the solution.

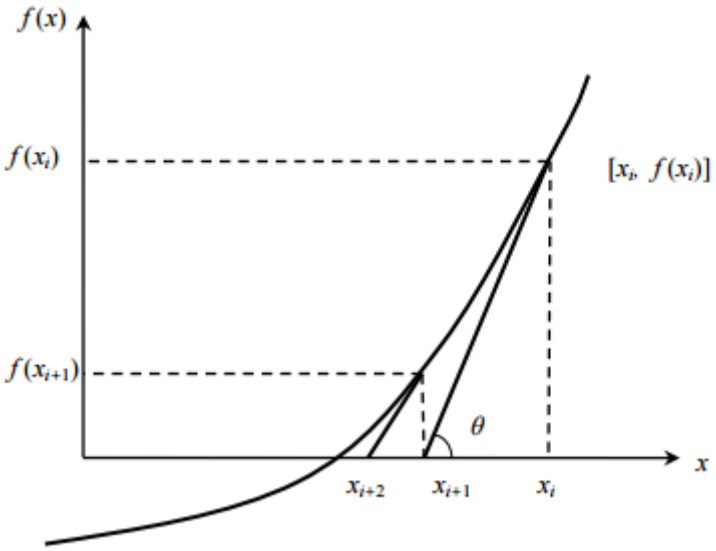

Figure 6 Plot of a non-linear function $f(x)$

Consider a non-linear function $f(x)$ shown in Figure 6. We first evaluate the gradient of the function $f(x)$ and then make an initial guess of the root x_i in order to make an estimate of the new root x_{i+1} as follows:

$$x_{i+1} = x_i - \frac{f(x_i)}{f'(x_i)}$$

3.19

The approximate error is calculated as follows

$$Approximate\ Error = \left(\frac{x_{i+1} - x_i}{x_{i+1}}\right).100$$

3.20

The calculated approximate error is compared with the aprior specified relative tolerance. If the value of the approximated error is larger than the relative tolerance, then again, the gradient of function $f(x)$ is computed at point x_{i+1} and a closer approximation to the root x_{i+2} is obtained. This is done until the solution no longer changes with further iterations and thus, it converges.

However, when solving a problem with hundreds, thousands, or even millions of degrees of freedom, it is desirable to take as few Newton-Raphson steps as possible since computing the inverse of the derivative is computationally the most rigorous step. COMSOL uses a damping factor to avoid regions of no solution when solving non-linear problems. This, thus also minimizes the number of Newton Raphson iterations taken.

3.6 Thesis approach

The work plan is elucidated in successive points and followed accordingly.

1. Develop an Electrostatic model for a 2-D AC-DBD configuration that solves the Poisson equation, computing the electric field magnitude and distribution.

2. Attempt to develop a "species-based" 2-D self-consistent Electrodynamic model for an AC-DBD which solves the Drift diffusion equations for electron and species mobility and distribution.

    2.1 If successful, then stop.

    2.2 If not successful, then attempt to develop a simpler Electrodynamic model with a pseudo-coupling between the charge density and the electric field that solves the Poisson equation for the electric field.

        2.2.1 If not successful, then stop.

        2.2.2 If successful and if time permits, then couple the Electrodynamic model with Navier Stokes equation, solving for the body force as a source term in NS-equations and computing the magnitude and distribution of the body force.

.

Chapter 4

Plasma actuator models and results

In total, 4 different models of the AC-DBD have been developed, as follows:

1. 2-D Electrostatic model.
2. 2-D Electrodynamic model.
3. 2-D Electrodynamic model 1.
4. 2-D Electrodynamic-Fluid model.

All of these models and the associated results will be discussed in this chapter, in the respective order.

4.1 2-D Electrostatic model

This section describes the development of the electrostatic model of the DBD configuration.

Initially, the focus of the thesis is to develop an electrostatic model to investigate the behaviour of the electric potential and hence electric field with and without charge densities which are representative of Plasma. This is achieved by solving the Poisson equation for the 2-D DBD model. The mathematical expression for body force is also incorporated in the model. The noticeable trend of change in electric field and the body force with introduction of different charge densities is conducive in furthering the development of an electrodynamic model and to later validate the results and trends arising from the electrodynamic model(s).

A detailed overview of the assumptions used in the development of the model, the associated geometry, the boundary conditions, the governing equations, the specific COMSOL settings, and the results from the model are discussed in the following sections.

4.1.1 Configuration and Computational set-up.

In computational modelling studies of a plasma actuator, the initial goal is to develop an electrostatic model for the respective configuration. The aim is to delve into the behaviour of electric field and other important parameters such as body force, with and without plasma. Therefore, we aim to replicate the plasma with a charge density, in order to get a rough idea of how the electrodynamic model should behave, when one actually models the plasma by defining appropriate plasma chemistry, reactions, reaction rates etc. for a self-consistent model.

Thus, we proceed by developing an electrostatic model for our study. The reference geometry of the DBD configuration, as shown in Figure 7, is taken from [24], with a goal to later compare latter's experimental results with the computational results. As evident from Figure 7, the

computational geometry used is a 2-D geometry. We can adequately assume the geometry to be 2-D because the length to thickness ratio of a DBD configuration is quite large.

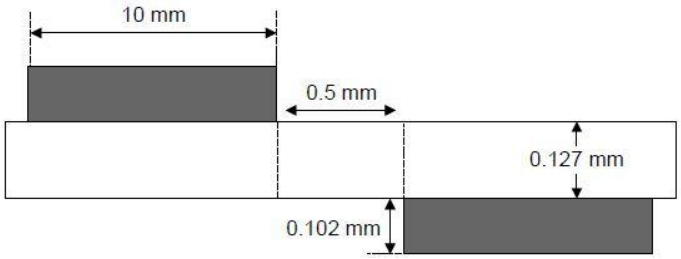

Figure 7 Schematic of the DBD geometry used for the electrostatic model.

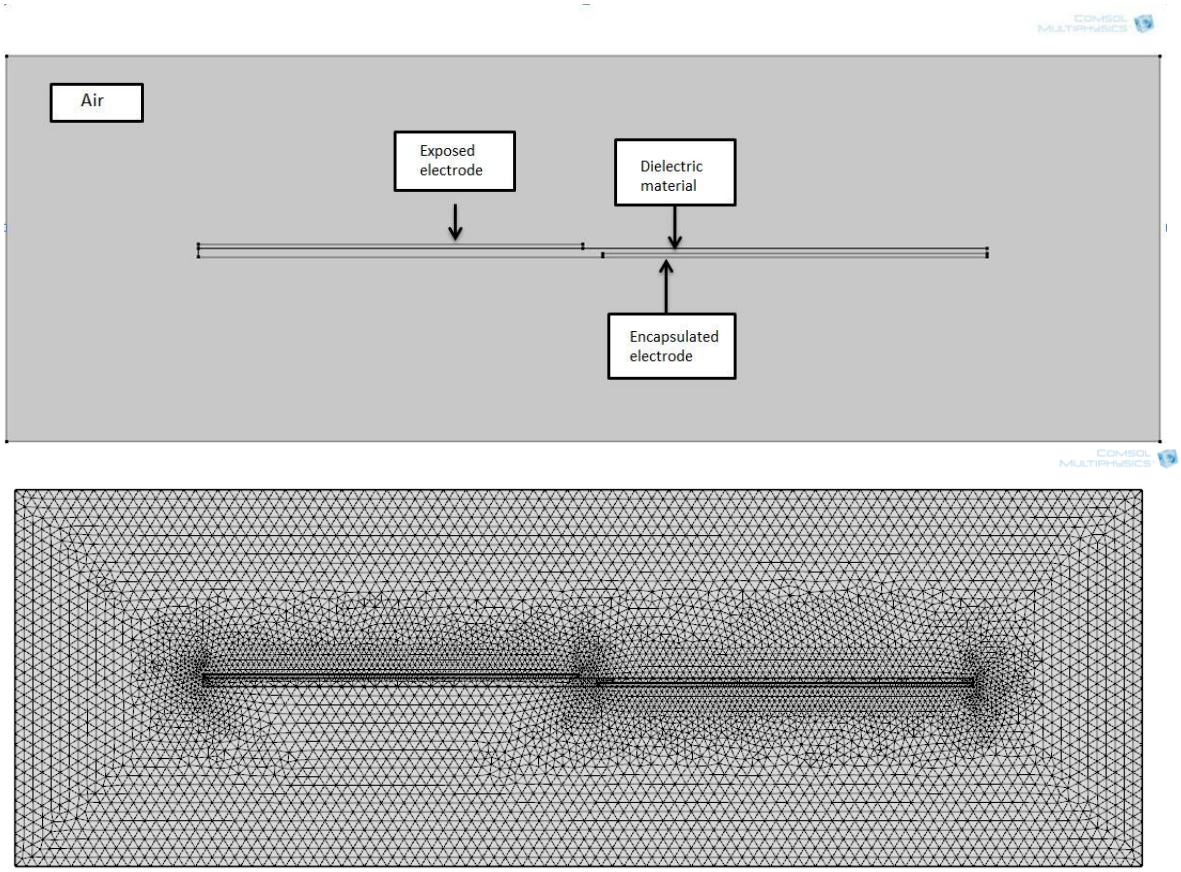

Figure 8 Reference computational geometry and discretized meshed domain.

Figure 8 shows the reference computational geometry and the meshed computational domain. Triangular elements are used to mesh the geometry and the mesh setting is selected to be "extremely fine". Triangular elements are default meshing elements in COMSOL for 2D models and are a first choice because they allow least user interaction.

Copper is selected as the electrode material and glass is selected for the dielectric material. Air is selected in the domain surrounding the DBD.

4.1.2 Boundary conditions for Charge density is equal to 0

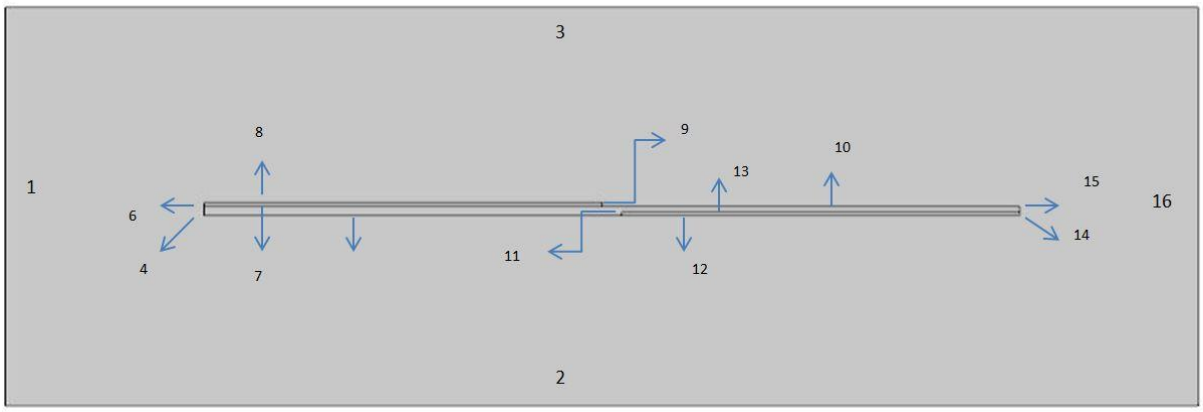

Figure 9 Boundaries of simulation domain. Boundary conditions given by numbers are given in Table 3.

Boundary	Boundary condition
1,3,2,16	$\mathrm{n}.D = 0$
6,7,8,9	$V = V_{applied} = 8000\ Volts$
11,12,13,14	$V = 0\ Volts$
All domains	$E = -\nabla V;\ \nabla.(\varepsilon_0 \varepsilon_r E) = \rho_v$

Table 2 Boundary conditions for Poisson's equation.

Charge conservation is applied to all domains and boundaries. This solves the Poisson's equation and hence the electric field and potential for all domains and boundaries. For present case, the charge density ρ_v is 0 hence there is no potential due to the charge density. Therefore, the Poisson equation is solved only for the applied potential. A zero charge boundary condition at the exterior boundaries (1,3,2,16) makes sure that the electric displacement ($D = (\varepsilon_0 \varepsilon_r E$)) and thus the potential normal to these boundaries is 0. The relation between electric displacement and the electric field is a constitutive relation that takes into account the macroscopic properties of the medium. An initial value of V=0 volts is set for all the domains.

A stationary direct solver is used (a solver available in COMSOL). Direct solvers can handle most non-singular systems and are very robust and fast for small models.

Mesh convergence study

To see how well an FEM solution is to a PDE, on a particular mesh, a common strategy is to refine the given mesh and then calculate solution on a finer mesh and then use solutions on the different meshes to qualitatively compare them. A mesh convergence study of this type enables us to get accurate solutions with a mesh that is sufficiently dense and doesn't demand much computation resources.

We conduct the mesh convergence study for 6 different meshes. The maximum element size of the respective meshes is shown in Figure 10. The Maximum electric field magnitude, which is the

solution to the Poisson equation is plotted versus the respective mesh configuration in Figure 11. As evident from the Figure 11, the Electric field magnitude converges as we discretize the domain with finer mesh configurations.

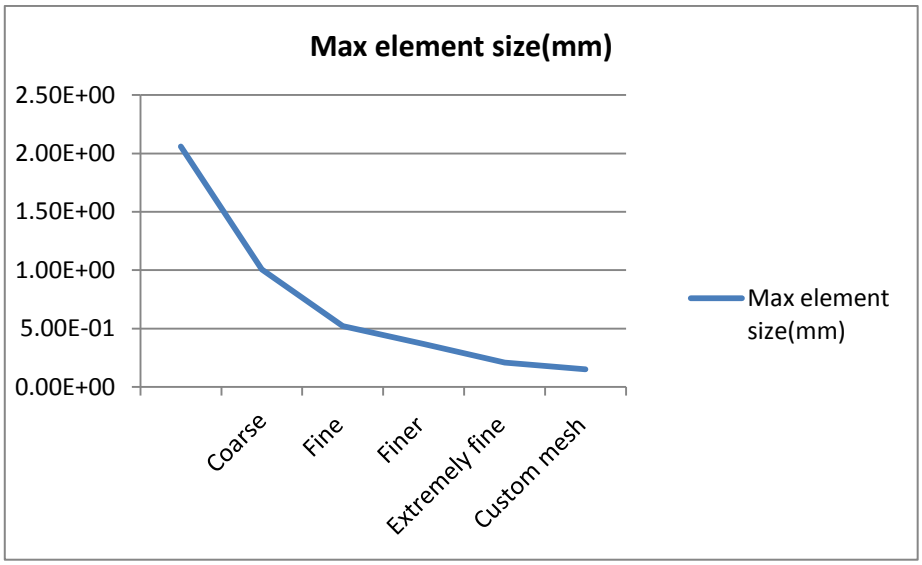

Figure 10 Mesh configurations versus the maximum element size for respective mesh configuration

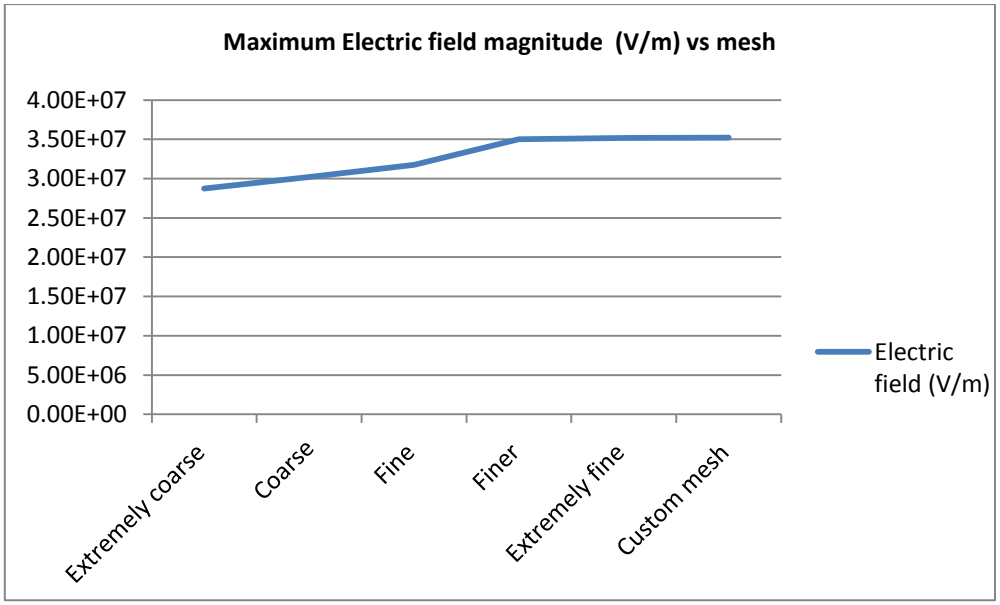

Figure 11 Maximum Electric field magnitude versus different mesh configurations.

Simulation results

A voltage of 8 kV is applied to the exposed electrode. The charge density in the adjoining domain is 0. The accompanying surface plots of the potential in Figure 12 show the solution to the Poisson's equation for the DBD configuration. The results are compared with literature[28]

and the solution is similar to that found in literature. Zooming in to see the electric field contours and vectors in Figure 13, we can confirm that indeed, the electric field magnitude is highest near the exposed electrode edge and decreases as we move longitudinally along the exposed dielectric surface.

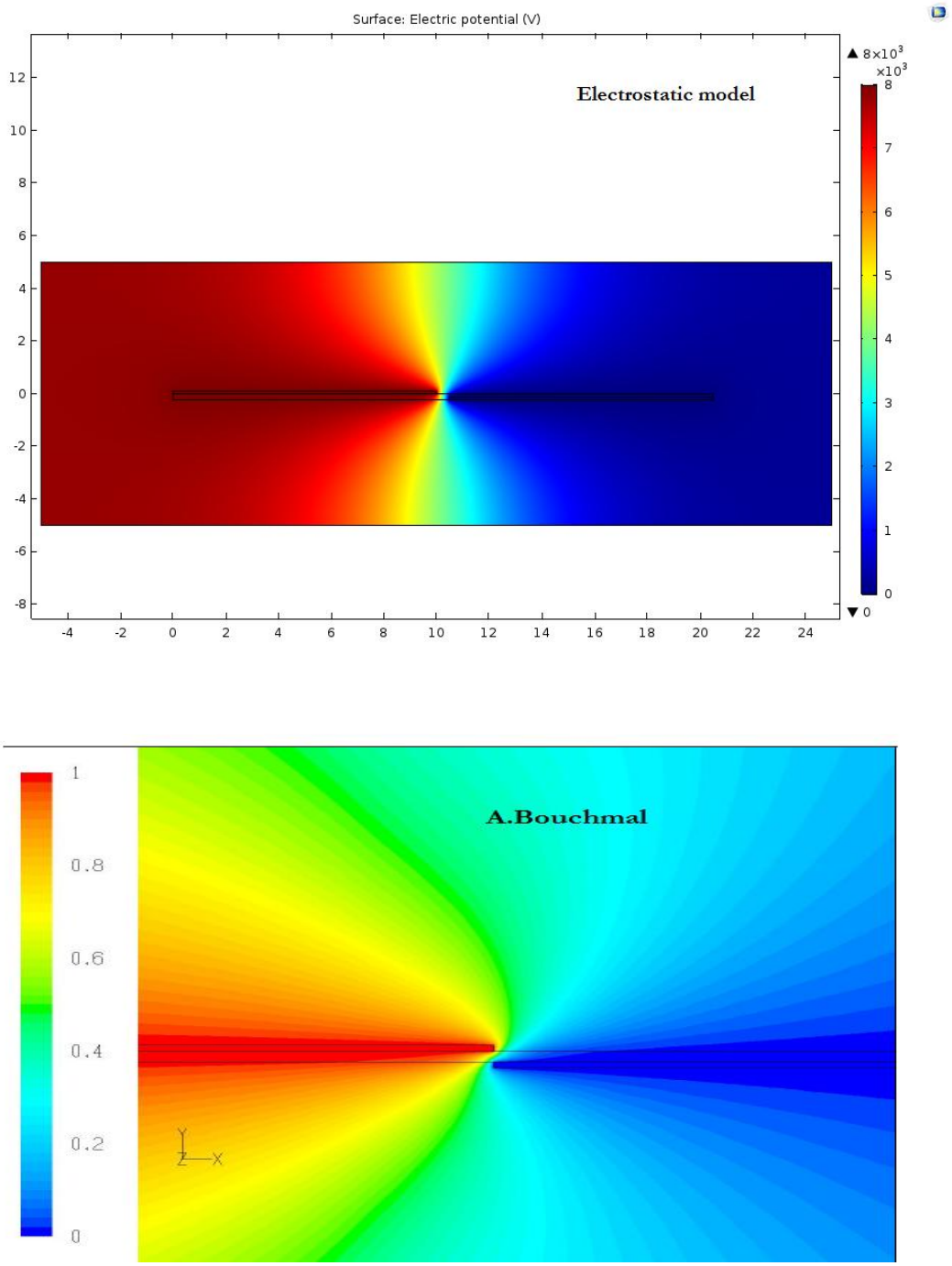

Figure 12 Surface plot of the electric potential from Electrostatic model compared with normalized potential surface plot from Bouchmal [28].

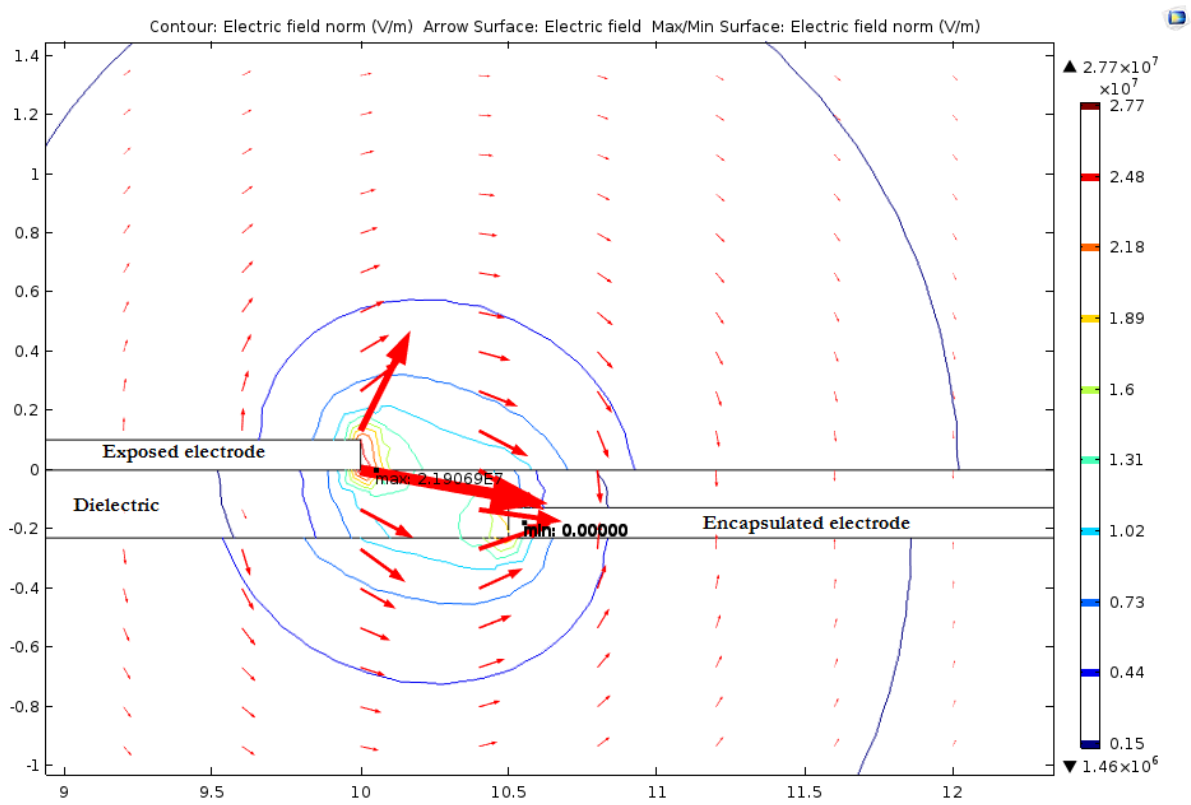

Figure 13 Electric field vectors, contours, and max-min plot from the Electrostatic model confirming a cogent electric field distribution and also confirming that the electric field is highest near the edge of the exposed electrode.

4.1.3 Boundary conditions for Finite charge density

A. Uniform Charge distribution.

For this case, the boundary conditions remain the same for all boundaries except that a rectangular domain adjacent to the exposed electrode is defined, in which a charge density which is representative of plasma, is defined. It is validated from the literature study that the plasma starts forming near the exposed electrode hence a rectangular charge density region near the vicinity of the exposed electrode can show us the variation in electric field and potential due to plasma.

Initially, we define a Uniform charge density. However, the charge density decreases as we move along the exposed dielectric surface because the charge density is coupled with the electric field strength. Higher the electric field strength, higher will be the ionization of species. Simulations from the previous case show a similar trend suggested from the literature study that the electric field magnitude is highest near the exposed electrode. Thus, moving farther away from the exposed electrode along the dielectric surface results in decrement of the plasma strength.

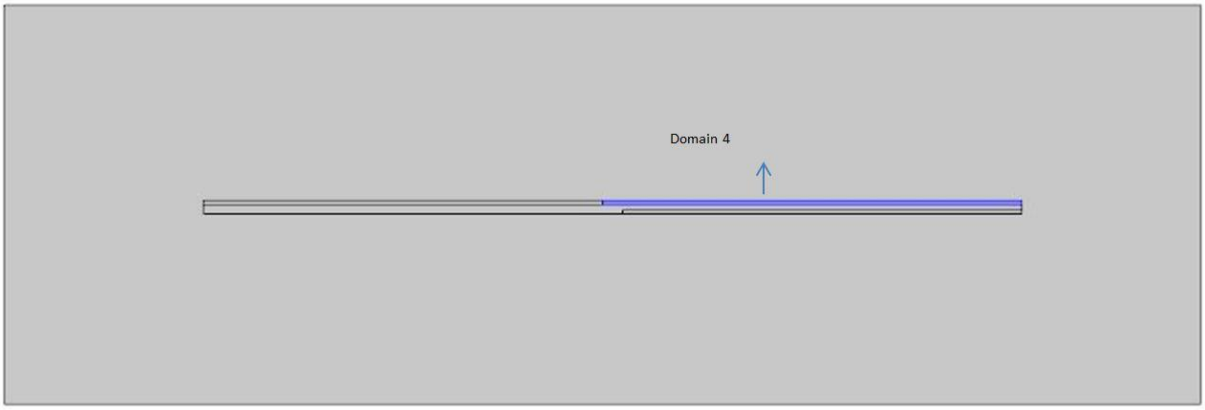

Figure 14 Domain 4 with associated boundary condition in Table 4. All other boundaries and boundary conditions are same as in the previous case listed in Table 3.

Boundary	Boundary condition
Domain 4	$\nabla . D = \rho_v$

Table 3 Boundary conditions for Uniform charge distribution.

Charge density ρ_v is defined in the Domain 4 shown in Figure 14. Initially the width of the charge volume is equal to the width of the electrodes and length equal to the exposed dielectric length. However, a sensitivity analysis of the charge volume can be carried out to determine the best dimension for the charge volume. Initially we are not aware of feasible charge densities, therefore we test our model with charge densities from 0.35 C/m^3 to 5 C/m^3. However, during the development of our self-consistent electrodynamic model (discussed later), we noticed that these charge densities are considerably larger than feasible values. From the self-consistent electrodynamic model, we typically noticed a maximum charge density value of 0.36 C/m^3. We will thus also check our model around this value to determine its feasibility.

As evident from the literature study, the plasma formed is very feeble in strength therefore it does not alter the electric field and thus the iso-potential contours considerably. This observation is critical in determining the feasibility of the model and to comment on the divergence of the electrostatic model. If the iso-potential contours vary considerably on introduction of a charge density, then it indicates that the model is not correct.

The uniform charge densities for which the model is simulated are given in Table 4.

Case	Charge density (C/m^3)
A	0.36
B	0.45
C	0.75
D	1
E	3
F	5

Table 4 Uniform charge density values for which the model is simulated.

The results from the simulation, for the successive values of uniform charge density tabulated in Table 4, are shown below in Figure 15.

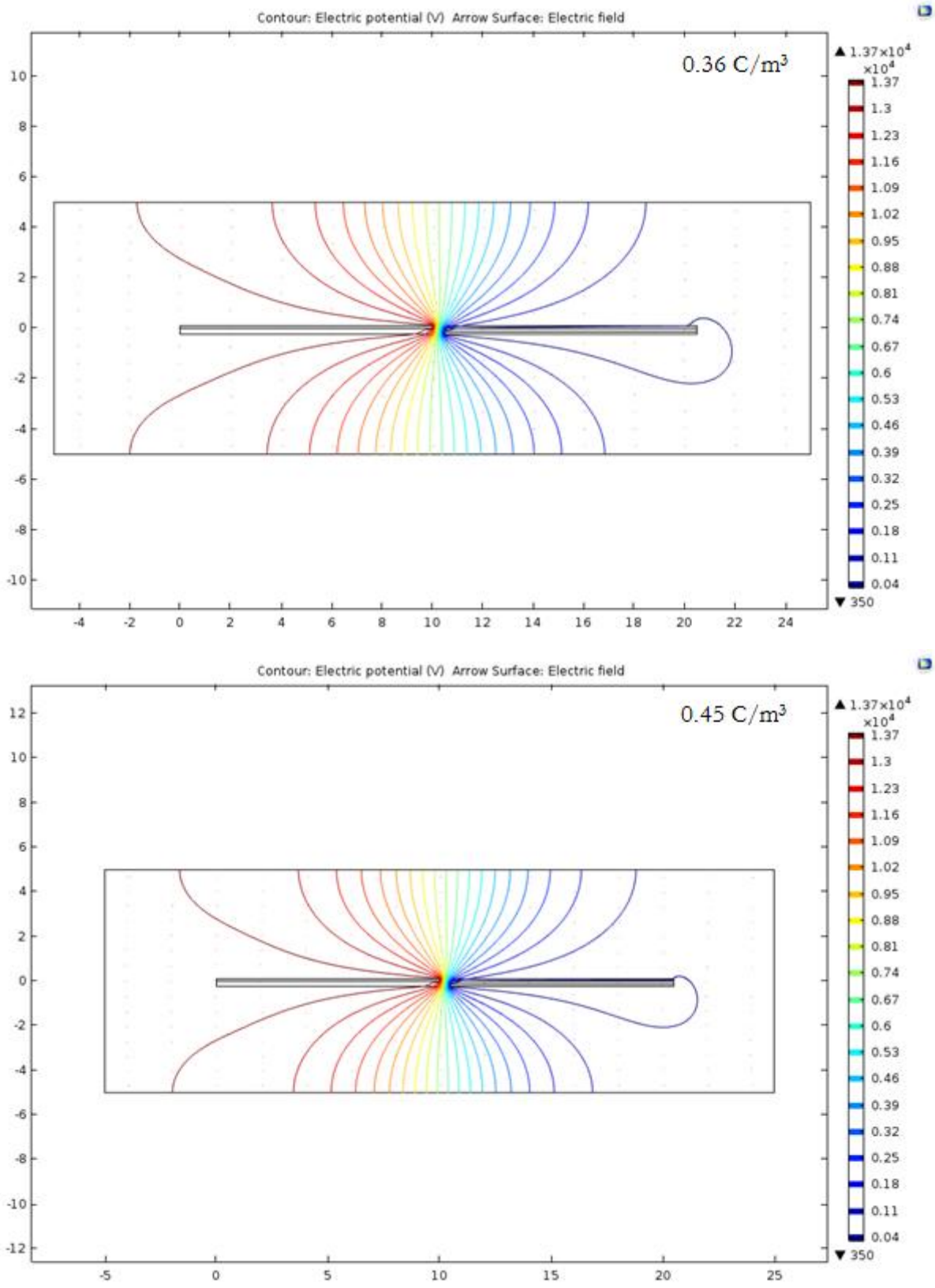

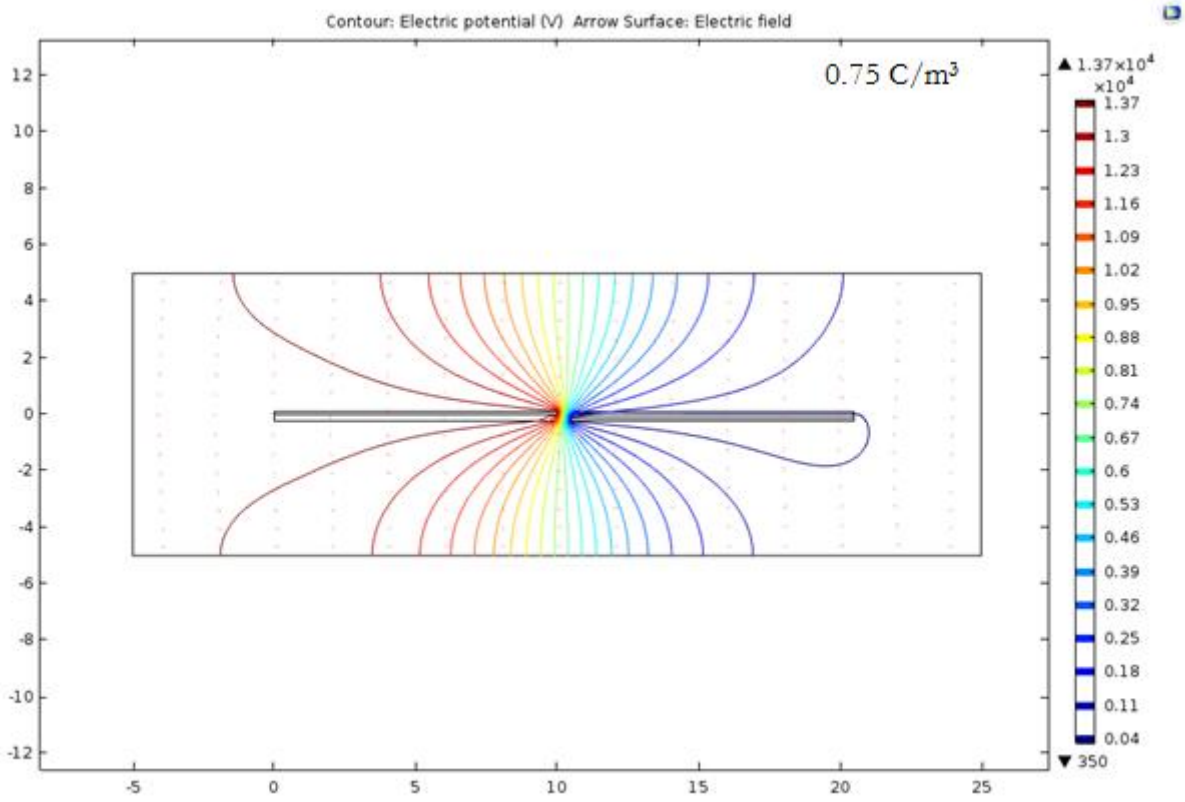
Contour: Electric potential (V) Arrow Surface: Electric field
0.75 C/m³
▲ 1.37×10⁴
×10⁴
1.37
1.3
1.23
1.16
1.09
1.02
0.95
0.88
0.81
0.74
0.67
0.6
0.53
0.46
0.39
0.32
0.25
0.18
0.11
0.04
▼ 350

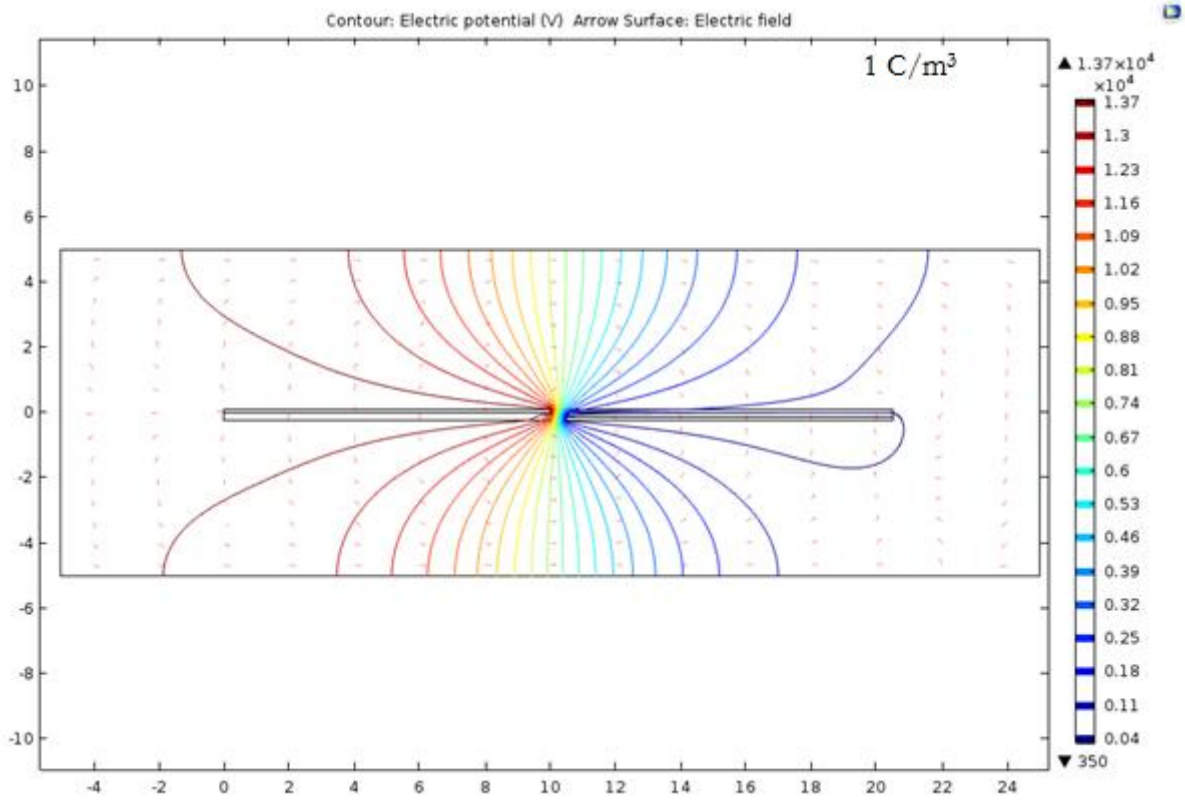
Contour: Electric potential (V) Arrow Surface: Electric field
1 C/m³
▲ 1.37×10⁴
×10⁴
1.37
1.3
1.23
1.16
1.09
1.02
0.95
0.88
0.81
0.74
0.67
0.6
0.53
0.46
0.39
0.32
0.25
0.18
0.11
0.04
▼ 350

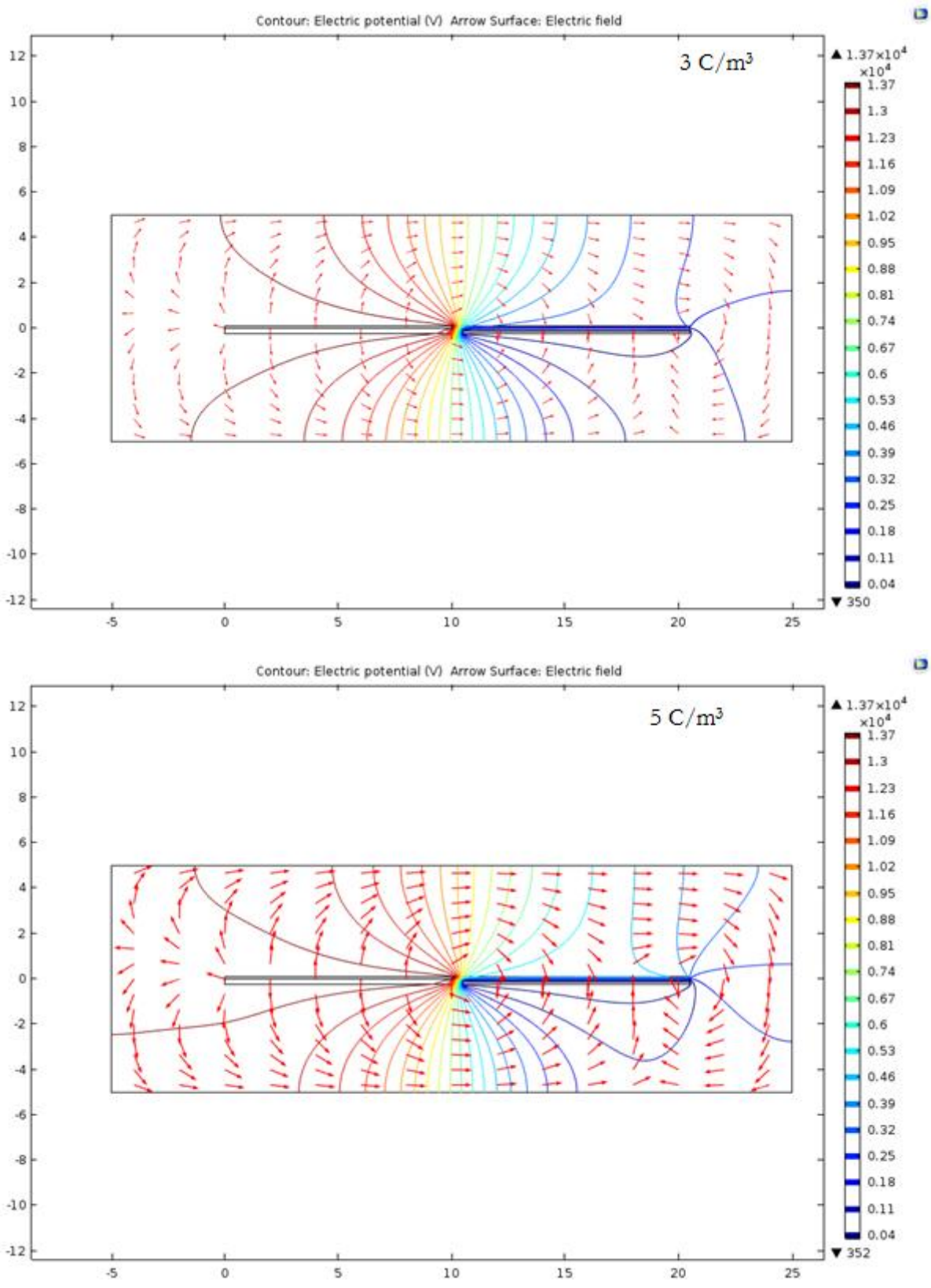

Figure 15 Simulation for successive uniform charge densities given in Table 5.

B. Gaussian charge distribution.

The uniform charge distribution in the previous case was defined to comment on the feasibility of the model and to check the boundary conditions. However, in order to correctly model the plasma, the intensity of plasma should fall as one moves away from the exposed electrode, longitudinally and laterally, along the dielectric surface. To model this, we introduce a Gaussian charge distribution in Charge volume (Domain 4 from Figure 14). The cases for which simulations are performed are as below:

i. A half Gaussian along X axis.

A half Gaussian charge distribution was defined along X axis in the electrostatic model. The following function defined the charge distribution along X-axis : 10^{-9} *exp $\left(\frac{-x^2}{100}\right)$. The plot for the equation and the charge density values along X axis are shown in Figure 16 and Figure 17.

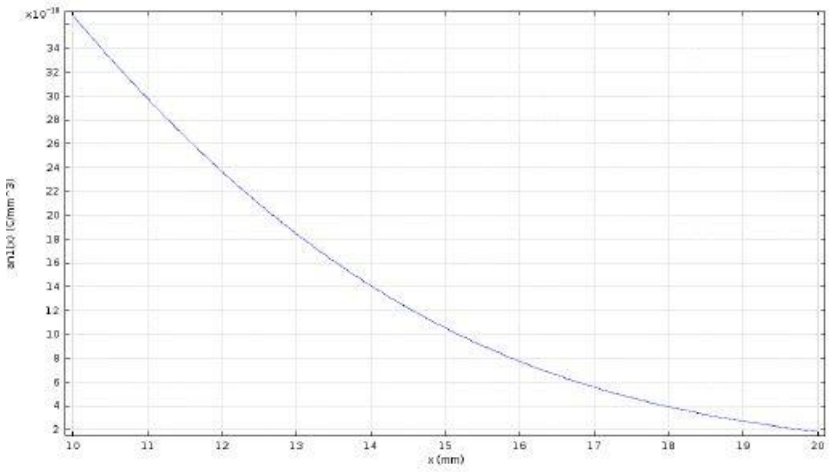

Figure 16 Plot of function an1(x), introduced as a half-Gaussian charge density along x-axis.

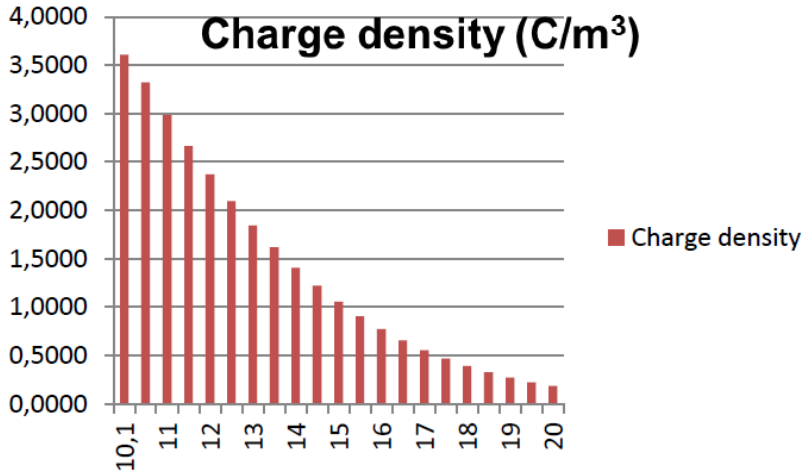

Figure 17 Charge distribution along X-axis depicting a half gaussian and the associated values along X-axis.

The results from the simulation are shown in Figure 18.

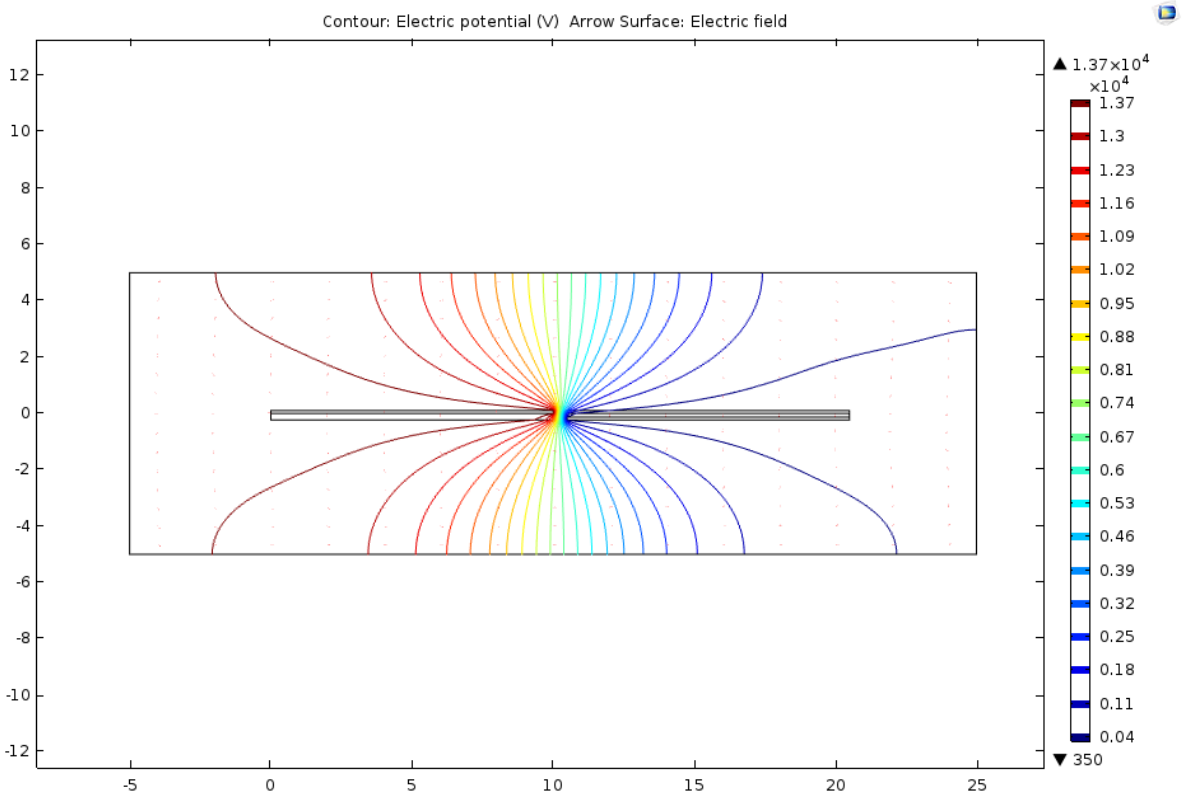

Figure 18 Iso-potential contours for Gaussian charge density along x-axis only.

ii. A half Gaussian along Y axis.

Next, a half Gaussian distribution is defined along Y axis. The equation for the distribution is 10^{-1} *exp $\left(\frac{-y^2}{100}\right)$. The plot for the equation and the charge density values along Y axis are shown in Figure 19 and Figure 20.

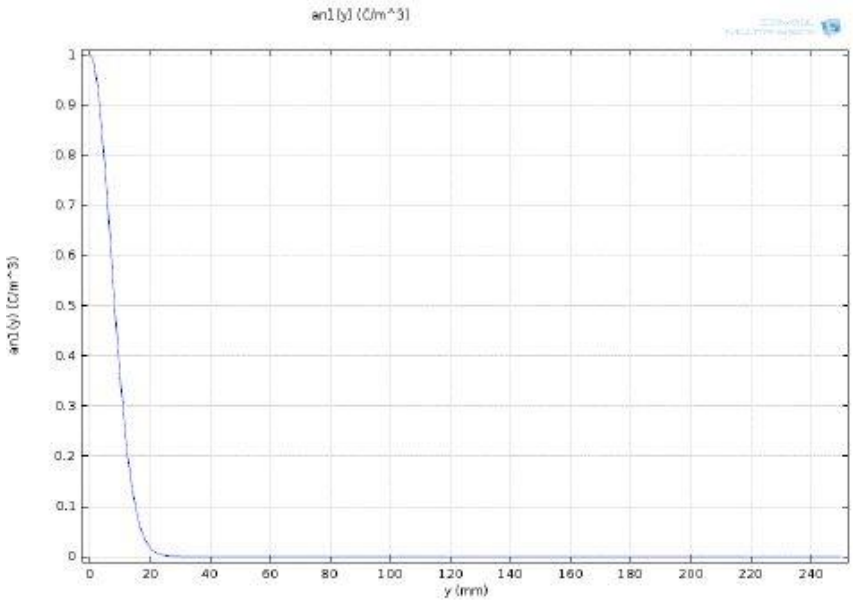

Figure 19 Plot of function an1(y), introduced as a half-Gaussian charge density along x-axis.

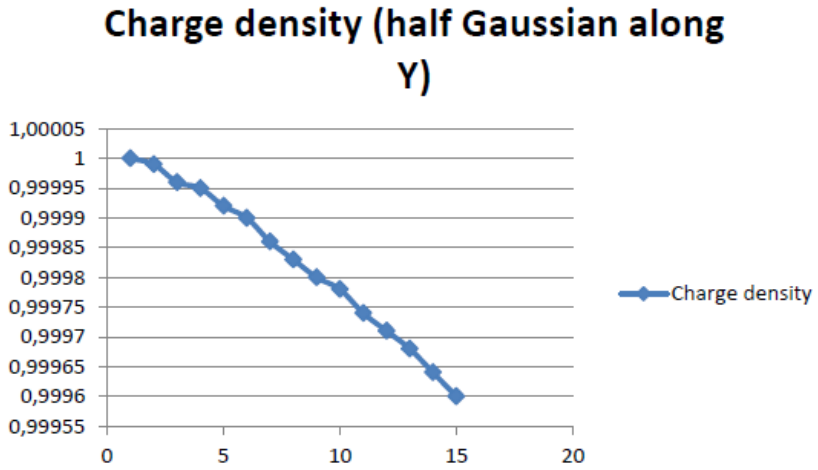

Figure 20 Charge distribution along Y-axis depicting a half gaussian and the associated values along Y-axis.

The results from the simulation are shown in Figure 21.

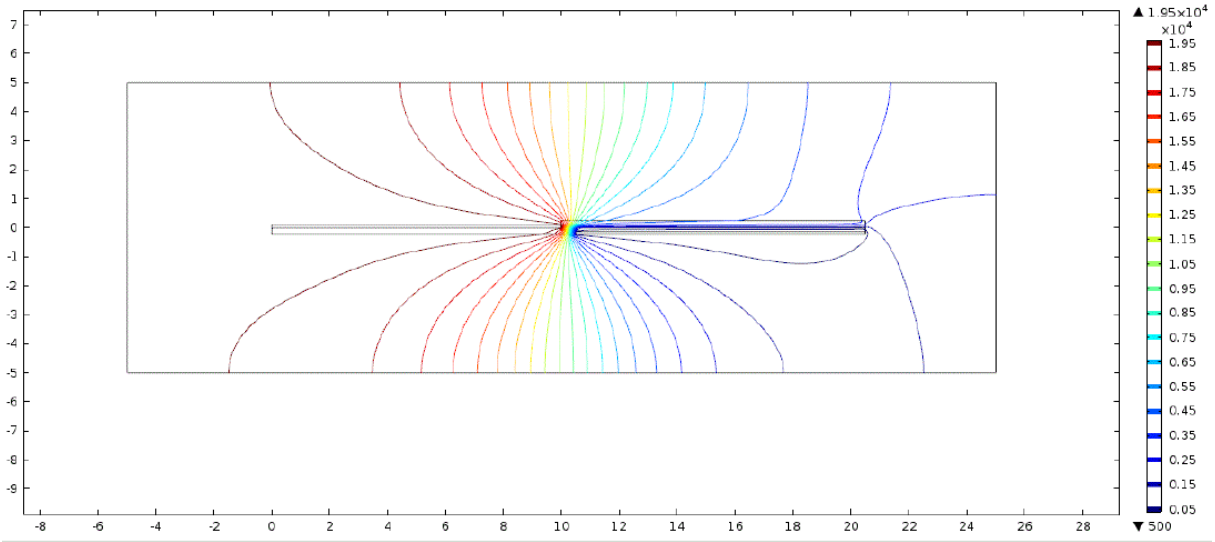

Figure 21 Iso-potential contours for Gaussian charge density along Y-axis only.

iii. **A half Gaussian along X and Y axis**

Next, we shall try to introduce a half Gaussian distribution, both along X and Y axis. A charge density of 10^{-1} *exp $\left(\frac{-x^2}{100}\right)$ is defined along X axis and in the same volume a space charge density of 10^{-9} *exp $\left(\frac{-y^2}{100}\right)$ is defined along Y-axis. The charge density values along X and Y axis are shown in Figure 22. The results from the simulation shown in Figure 23 show a very small noticeable changes in the curvature of the iso-potential lines which have been highlighted (in rectangle) for comparison with no charge density case.

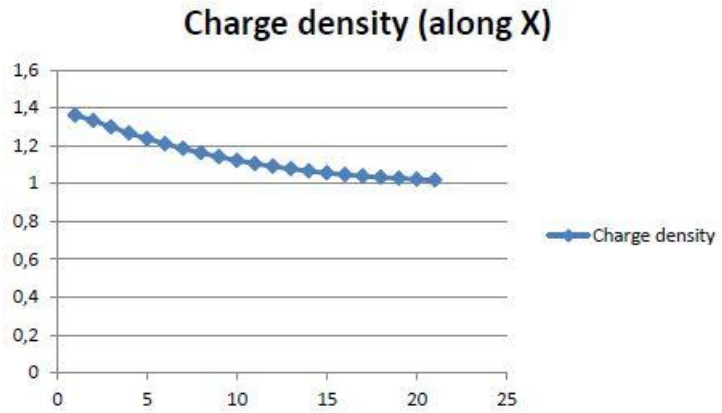

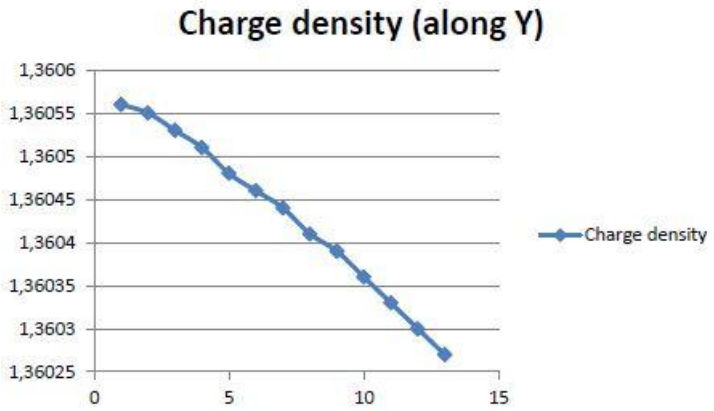

Figure 22 Charge distribution along X and Y-axis depicting a half gaussian and the associated values along both the axes.

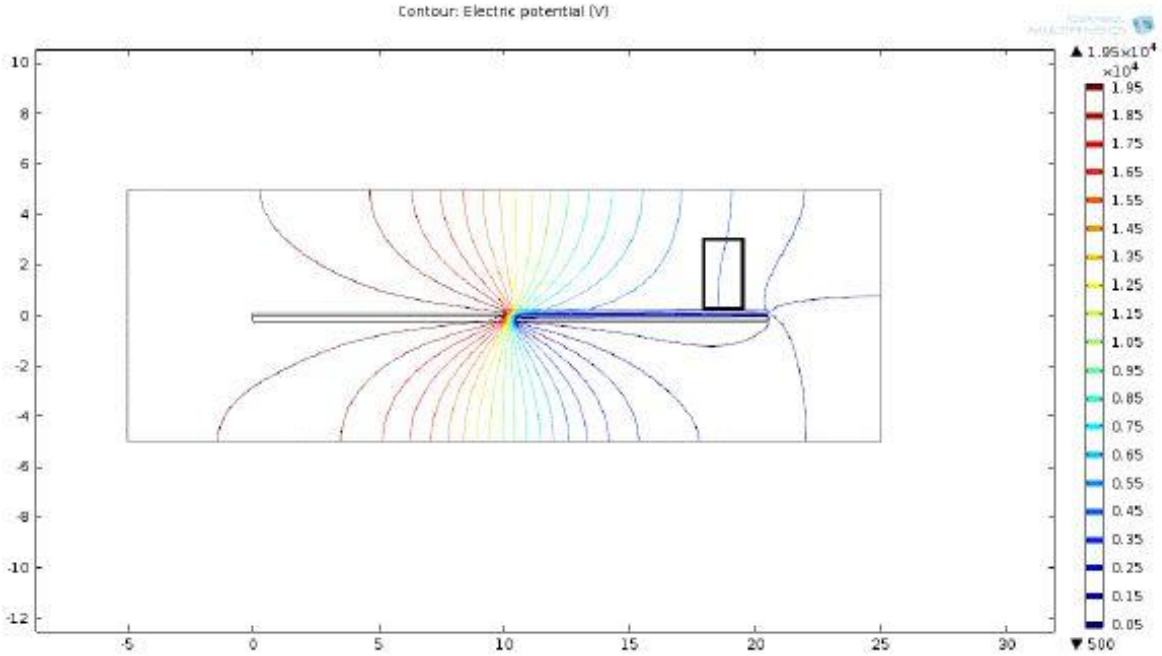

Figure 23 Iso-potential contours for half Gaussian charge density along X and Y axes.

An Electrostatic model for an AC-DBD has been successfully developed. The feasibility of the model is checked by modelling uniform charge densities, which are representative of plasma, and a check on the imposed boundary conditions is thus performed. The introduced charge density does not alter the Potential due to the applied Electric field.

In order to model the decay in the plasma strength, laterally and longitudinally along the exposed dielectric surface, we model a Gaussian charge distribution along X and Y axis along the exposed dielectric surface.

Further, the results confirm that for Gaussian charge distribution, the charge density does not alter the electric field and thus the iso-potential contours considerably and thus the results are in coherence with the literature.

4.2 2-D Electro-dynamic model 1

The next aim is to develop a species based Electrodynamic model for the AC-DBD configuration by modelling the plasma itself and the associated processes on DBD's actuation.

A very basic Helium based plasma chemistry is defined including just a handful of reactions. Associated processes such as the migration and convection of charge particles, the electron exchange and associated mechanisms at room temperature and atmospheric pressures and a given set of input parameters such as applied voltage, frequency etc are also modelled.

The externally modelled AC-Circuit is coupled with the Drift diffusion interface. This couples the Poisson equation with the Drift Diffusion equations. As discussed in Chapter 3, the Drift Diffusion equations are only solved for the plasma domain while the Poisson equation is solved for the entire computational geometry.

Discretization

The next step is to build a mesh that is in agreement with the conflicting requirements of resolving relevant details sufficiently while also keeping the computational costs in check. The main factors that determine the mesh resolution are the characteristic length scales of the domain geometry and of the relevant finest flow details.

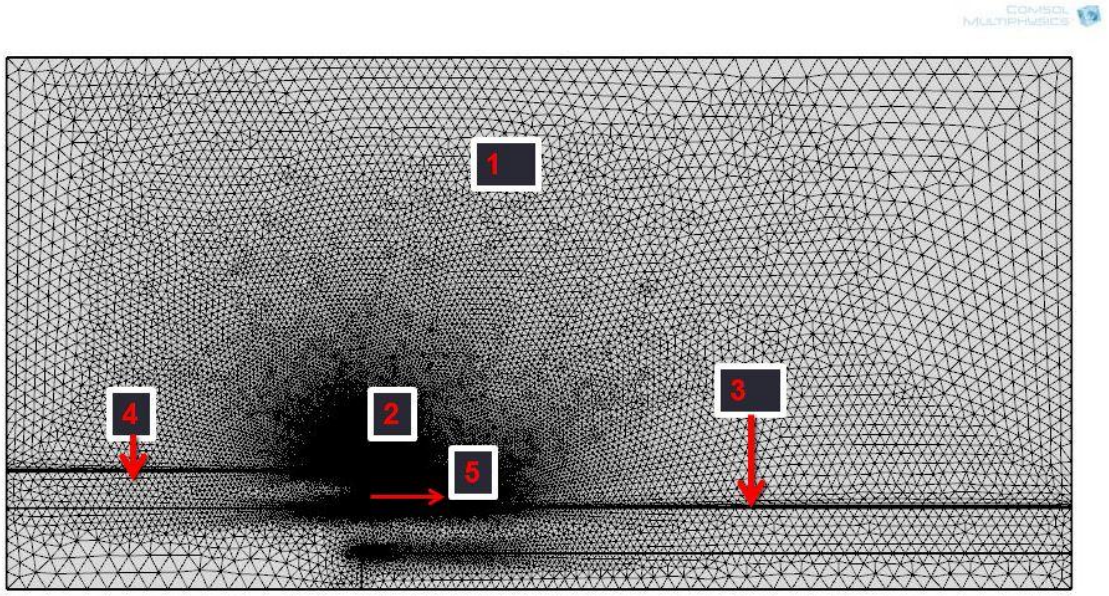

Figure 24 Discretized computational domain for electrodynamic model 1.

Fine meshing must be used in places where

- Plasma formation initiates (Region 2 and Edge 5)
- Plasma is in contact with the surface (Edge 4, Edge 5 and Edge 3)
- Plasma transport takes place (Region 2, Edge 5 and Edge 3)
- Electron transport takes place.
- Surface reactions occur. (Edge 3, Edge 4 and Edge 5).

Free triangular meshing is used in the whole domain, discretizing it with 118580 elements, about 70% of which lie in the finely meshed region. We now have a discretized simulation domain on which governing flow equations can be solved.

4.2.1 Results and discussion

As discussed prior, the model solves the coupled drift-diffusion equations (transport equations for electron), Poisson equation and the transport equations for ions. The plasma is visualized by plotting a net space charge density at a given time. Since Plasma is a quasi-neutral mixture of charged species, hence the plasma can be visualized by plotting a net space charge density.

- The model does not converge. It reaches a value of 63% of convergence in 7 days and doesn't proceed further. The reasons for this might be:

1. General computational studies making use of COMSOL for modelling AC DBD configurations generally provide considerably high frequencies which are in the range of 10^6-10^{10} Hz. The motivation behind such studies is to capture just the sheath development and propagation. Applied frequency plays an important part in charge distribution and plasma formation, thus these studies don't give a conclusive picture and hence cannot be used to compare with the experiments, keeping all the other factors same. Our study models the plasma at realistic experimental frequencies which might be a drawback.

2. COMSOL is not recommended to work with at atmospheric pressures when the plasma consists of positive ions. This was suggestive from the experience of a PhD at University of Minnesota High Temperature Plasma Laboratory [27].

3. For atmospheric pressure discharges, the plasma naturally tries to arc. This might cause problems to the solver, suggested from COMSOL technical support. Thus, arcing could be prevented by modelling a series RC- Circuit between the exposed electrode and the external circuit. This might ensure glow discharge, preventing arcing and allowing the solver to converge. Hence, a series RC circuit was modelled in the driving circuit but the same problem persisted and solution did converge beyond 63%. Thus, the non-convergence can be attributed to either of the 2 points mentioned before.

Since the idea was first to develop a working plasma model and then couple the model with the fluid flow interface, solving the Navier Stokes equation and giving us a velocity field due to the body force induced by the plasma action, that work also could not be proceeded for this model.

Multiple solutions are tried to get the model to converge but for any of them, the model either does not converge or it or does not initialize. The solutions tried are

1. Further Mesh refinement.
2. Modelling a series RC circuit to prevent arcing.
3. Considerable reduction in model size.

4. Running the model at lower voltages and frequencies.
5. Reducing the time range for which the model is simulated.
6. Choosing a different solver.

Thus, having not completely succeeded in developing a 2-D self-consistent plasma actuator model, we further our study in developing a simple 2-D Electrodynamic model which is simple than the Electrodynamic model 1. Though not self-consistent but it is developed so that it imitates the space-time averaged body force values from Kotsonis's experiments [10,11] . A relation is deduced for calibrating the experimental and computational body forces. Furthermore, the electrodynamic is coupled with a fluid interface whereby the body force resulting from the electrodynamic model is solved as a source term in the Navier-Strokes equation for a incompressible laminar flow regime. This coupled model will be referred as the Electrodynamic-Fluid model in rest of the part of the thesis.

4.3 2-D Electro-dynamic model 2

The goal behind developing a plasma actuator model is to quantify the body force. Unable to develop the species based Electrodynamic model, we proceed to develop another model in which we are able to quantify body force for a charge density and then develop a relation that gives a match between experimentally determined body force values from Kotsonis [10,11] and the body force from this electrodynamic model.

We introduce a spatial and temporal charge density adjacent to the exposed electrode. The spatial and temporal components of the charge density are in close semblance to the applied potential to incorporate/replicate the dependency of charge density on the applied external potential. This ensures that there is a pseudo-coupling between the charge density and the applied potential.

Besides correlating the body force, it is also desired that the plasma looks visually realistic in the vicinity of the exposed electrode.

Thus the modelled charge density (discharge) in the vicinity of the exposed electrode should be such that:

1. Its magnitude varies spatially and temporally, in a manner which is suggested from the experimental studies.
2. The plasma is low or negligible in the positive going half cycle and high in the negative going half cycle.
3. The charge density is the strongest near/at the edge of the exposed electrode.
4. The charge density decreases as we move further downstream of the exposed electrode along the dielectric surface. Because the electric field decreases as we move further downstream of the exposed electrode, the ionization becomes weak which results in a weak charge density due to plasma formation.
5. The charge density should also decrease orthogonally to the exposed electrode.

The body force is then calculated by integrating the product of the charge density and the electric field in the defined charge volume. The body force so calculated should also vary in space and time because the electric field and the charge density vary in space and time. This is also expected in real world but could not be confirmed from the experiments (load cell measurements etc., owing to the extremely small time steps that cannot be captured. Thus, in experiments a space integrated-time averaged value is generally deduced. But in our computational study we calculate the average body force integrated over a given volume. This enables us to see the variation in body force with each time step in the voltage cycle. This integrated body force in space is then averaged over the time range to get a single value of the body force which is then compared with the experimental body force.

4.3.1 Configuration and Computational set-up.

The configuration and the computational set-up are same as in the case of Electrostatic model except that a larger rectangular volume adjacent to the exposed electrode is defined. In this volume, we define a charge density which is representative of a plasma, as we did previously. The resulting configuration is shown in Figure 25.

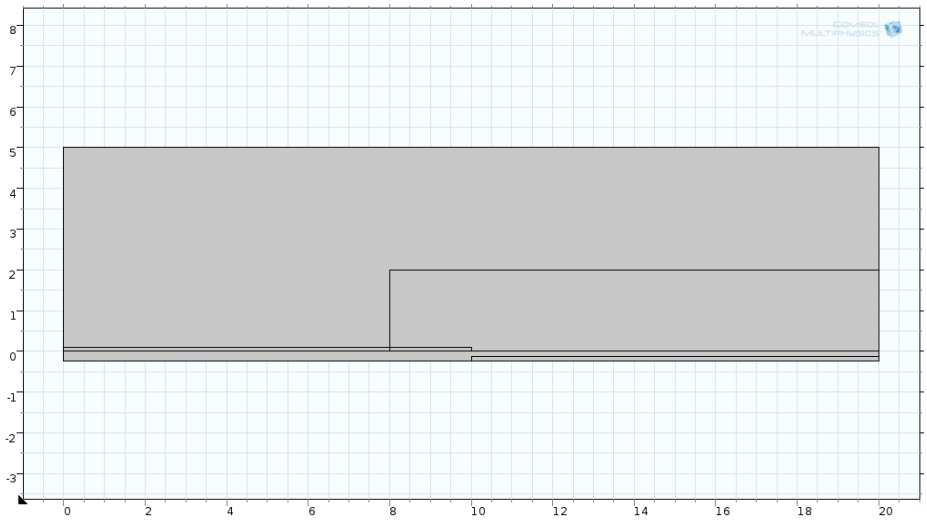

Figure 25 Schematic of the DBD geometry used for the 2D Electro-dynamic model 2.

Boundary Conditions

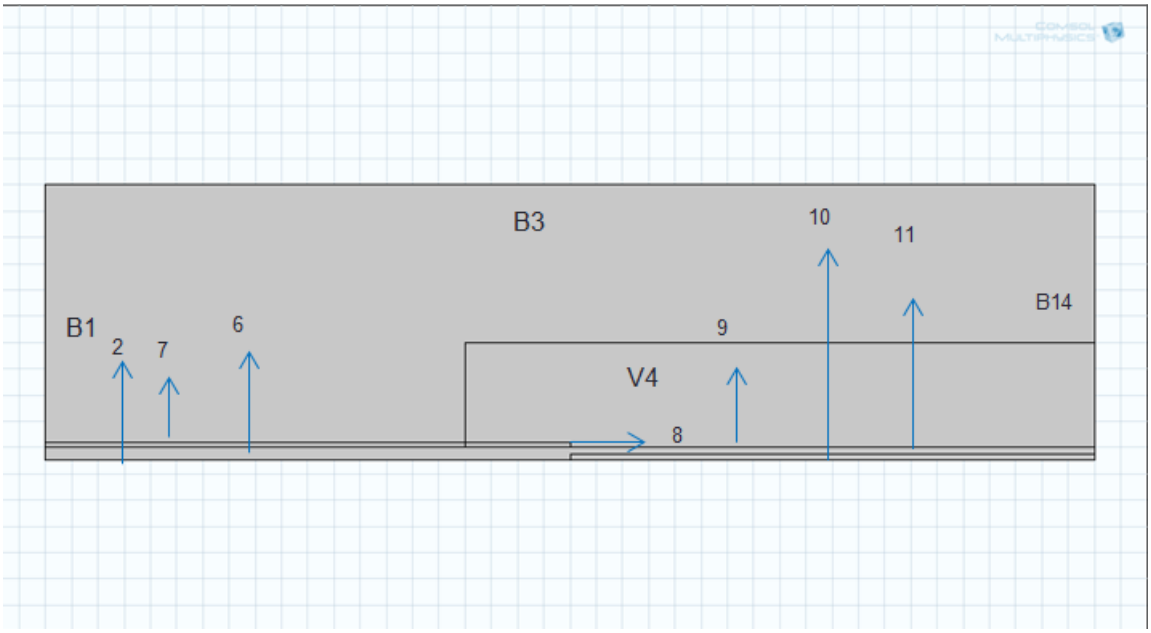

Figure 26 Boundaries of simulation domain. Boundary conditions given by numbers are given in Table 7.

Boundary	Boundary condition
5,6,7,8	$V = V_{applied} = V_0 sin(2 * pi * 10000 * t)$
10,11,12	$V = 0$
All domains	$E = -\nabla V;\ \nabla.(\varepsilon_0 \varepsilon_r E) = \rho_v$
V4	$\rho_s = \rho_s(x, y, t)$
B1,B3,B14	$\mathrm{n}.D = 0$

Table 5 Boundary conditions for 2D Electro-dynamic model 2.

The boundaries and the associated boundary conditions are listed in Figure 26 and Table 5. A charge density is defined in the rectangular volume in the vicinity of the exposed electrode. This charge density varies both in space and time and is synchronized with the applied potential. An AC sine wave is applied on the exposed electrode while the encapsulated electrode is kept at ground. The Poisson equation is solved for all the domains and the space charge density is calculated by taking the gradient of the displacement electric field.

The net flux through the model boundaries is 0. This is ensured by keeping the displacement electric field normal to the walls equal to 0.

Discretization

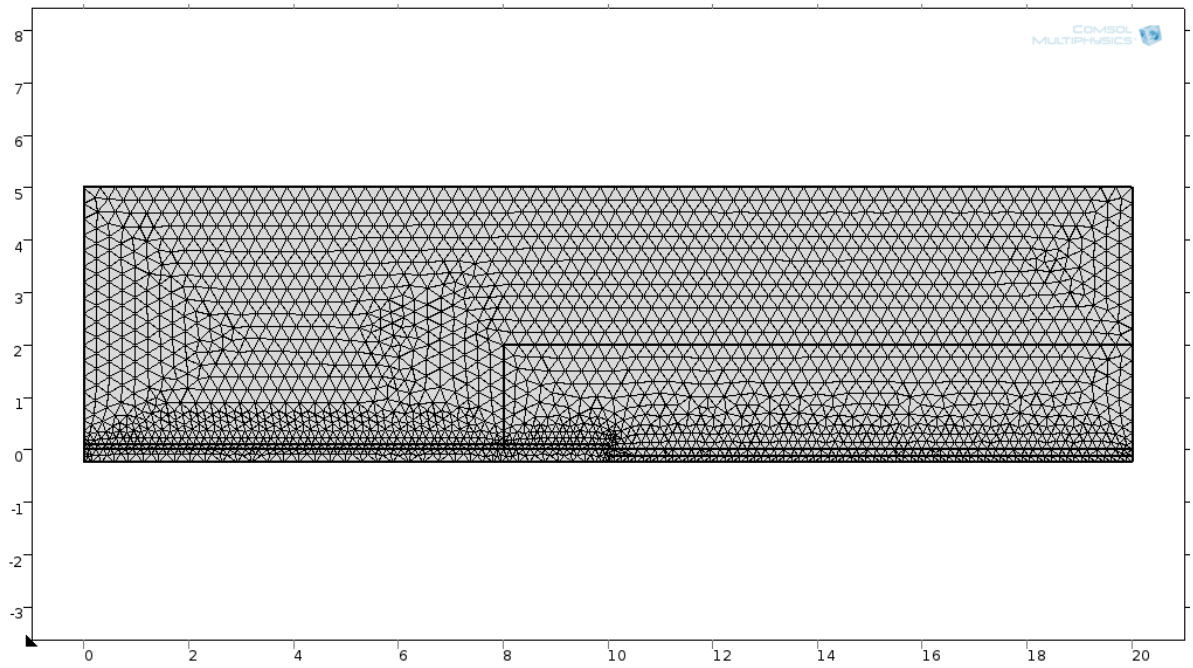

Figure 27 Discretized computational domain for 2D Electro-dynamic model 2.

The geometry is discretised using a free triangular mesh as shown in Figure 27. This number of mesh elements are 25247. A predefined fine meshing customized to Plasma simulations is selected in COMSOL.

Initialization

The time range for the simulation starts at 0 seconds and converges at the final time step of 10^{-2} seconds in steps of 10^{-7} seconds. The simulation is first run without space charge density to confirm the correct evolution of potential and electric field in time and to check if the boundary conditions are correct. In the second simulation various test cases are simulated, replicating a realistic charge density distribution (plasma), in the volume adjoining to the exposed electrode and the body force is computed which varies both in space and time. A realistic distribution of the body force is also obtained and a relation for the charge density is developed which results in duplicating the computationally derived space integrated -time averaged body force values with the experimentally deduced space-time averaged body force values.

4.3.2 Results and discussion

1. No charge density

Firstly, in order to check the boundary conditions, we first simulate the model without charge density. The results for the given time range from the simulation are as shown in the Figure 28.

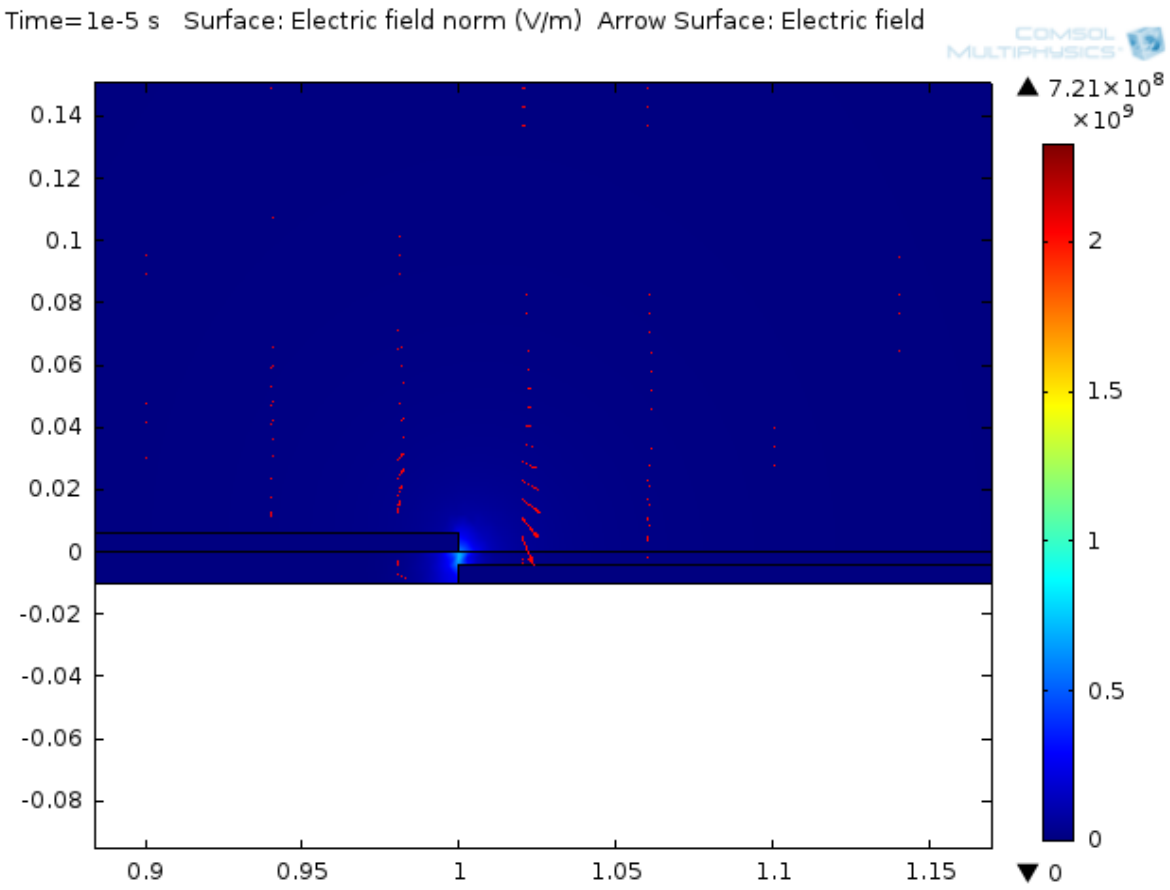
Time=1e-5 s Surface: Electric field norm (V/m) Arrow Surface: Electric field
▲ 7.21×10^8
×10^9
2
1.5
1
0.5
0
▼ 0
0.14
0.12
0.1
0.08
0.06
0.04
0.02
0
-0.02
-0.04
-0.06
-0.08
0.9
0.95
1
1.05
1.1
1.15

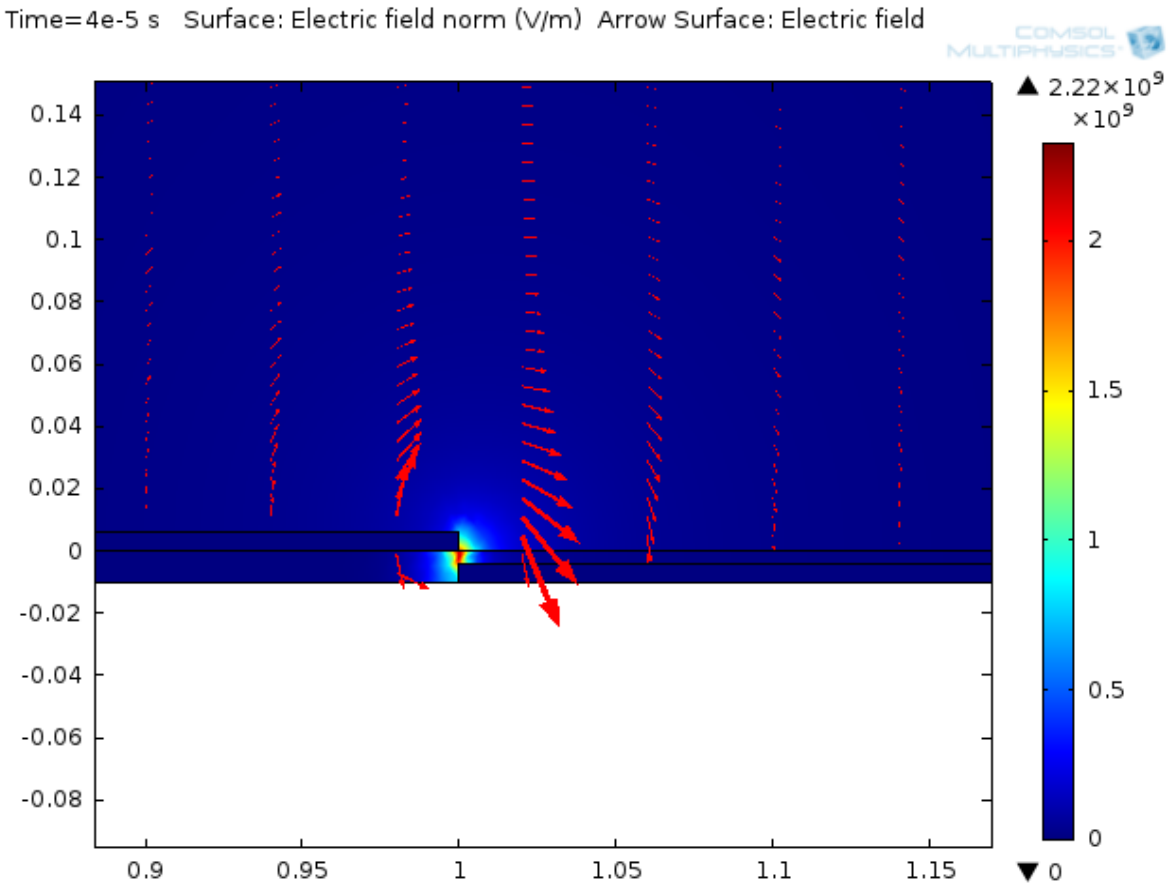
Time=4e-5 s Surface: Electric field norm (V/m) Arrow Surface: Electric field
▲ 2.22×10^9
×10^9
2
1.5
1
0.5
0
▼ 0
0.14
0.12
0.1
0.08
0.06
0.04
0.02
0
-0.02
-0.04
-0.06
-0.08
0.9
0.95
1
1.05
1.1
1.15

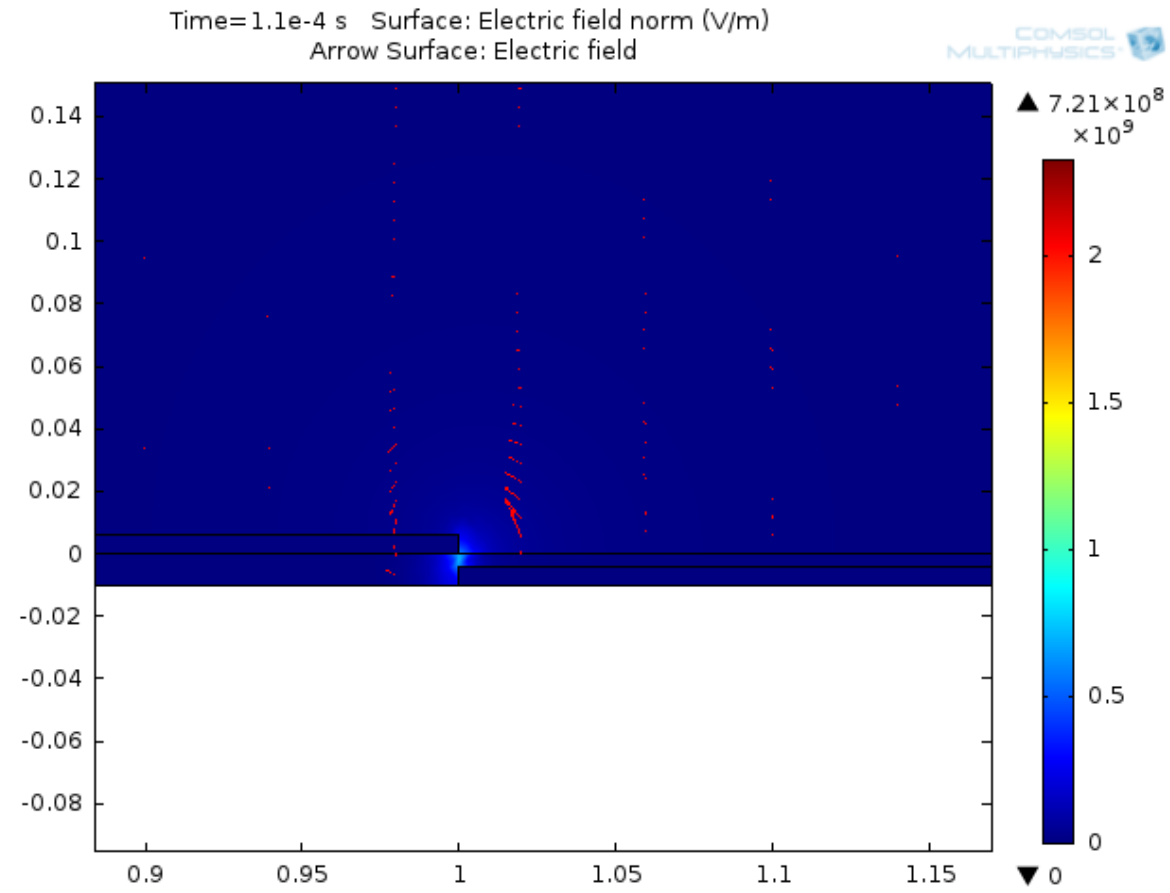
Time=1.1e-4 s Surface: Electric field norm (V/m)
Arrow Surface: Electric field
COMSOL MULTIPHYSICS
▲ 7.21×10^8
×10^9
2
1.5
1
0.5
0
▼ 0
0.14
0.12
0.1
0.08
0.06
0.04
0.02
0
-0.02
-0.04
-0.06
-0.08
0.9
0.95
1
1.05
1.1
1.15

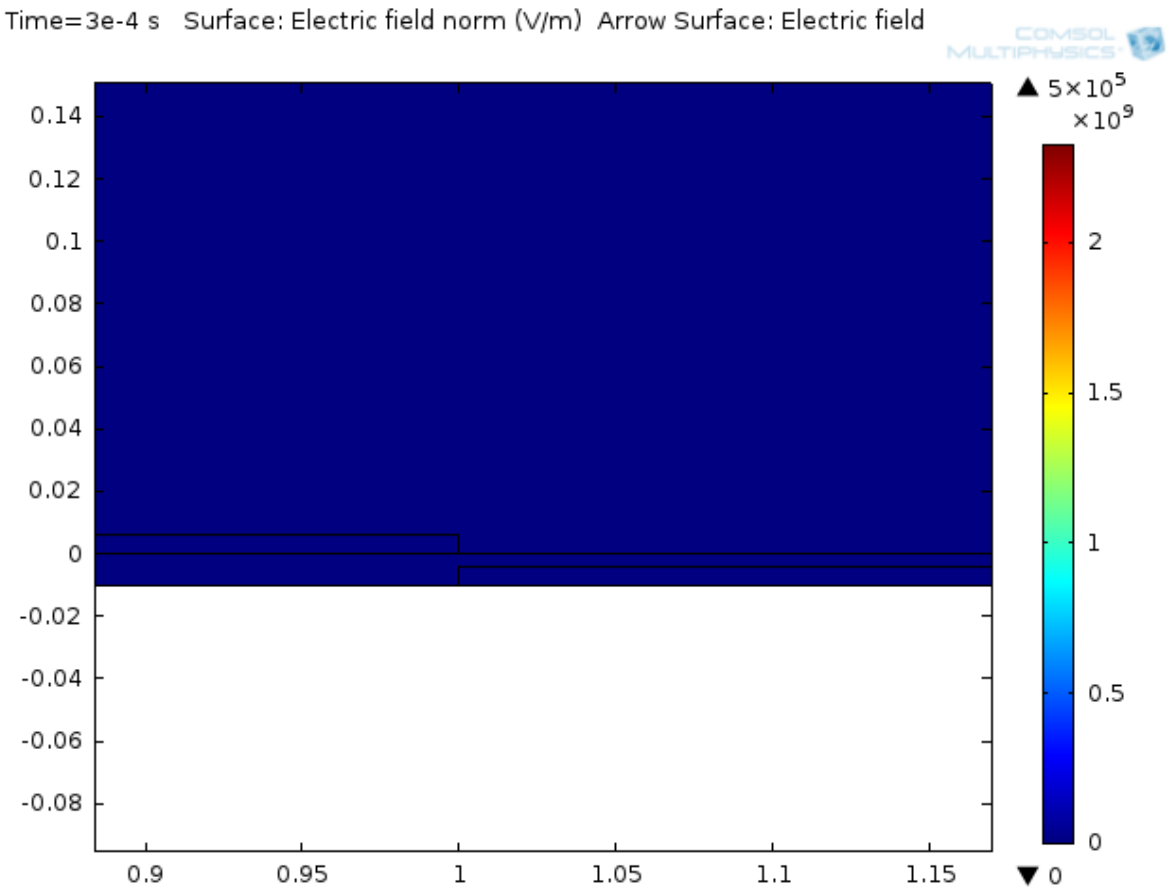
Time=3e-4 s Surface: Electric field norm (V/m) Arrow Surface: Electric field
COMSOL MULTIPHYSICS
▲ 5×10^5
×10^9
2
1.5
1
0.5
0
▼ 0
0.14
0.12
0.1
0.08
0.06
0.04
0.02
0
-0.02
-0.04
-0.06
-0.08
0.9
0.95
1
1.05
1.1
1.15

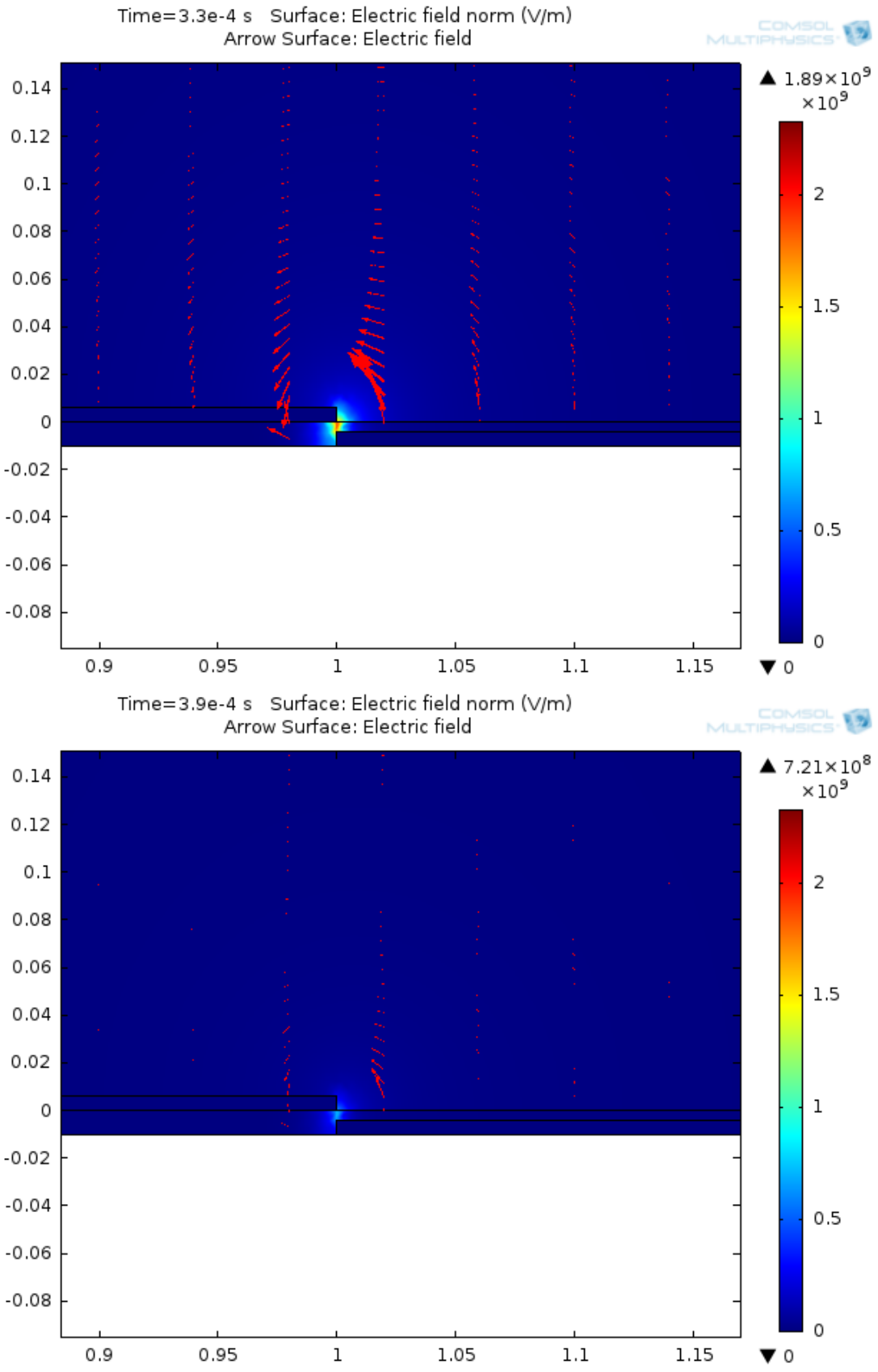

Figure 28 Surface plot and vectors for the electric field with no plasma.

The surface plot and the arrows in Figure 28 represent the Electric field's magnitude and direction. From the results it is evident that the Electric field is the strongest at the edge of the exposed electrode and decreases in the longitudinal and lateral direction. The frequency of the electric field is 10000 Hz and thus the reverse in the electric field direction is replicated by the model as the potential reverses.

This confirms that the boundary conditions for the electrodynamic model 2 are correct. Now, we can proceed to model a Gaussian charge distribution which fluctuates in space and time with the same frequency as that of the applied electric field. This ensures a pseudo-coupling between the charge density and the applied electric field, which is a necessity for an actualistic DBD model.

2. Space and time varying Gaussian charge distribution coupled with the electric field.

Previously in the electrostatic model, we introduced a Gaussian charge distribution in the charge volume adjacent to the exposed electrode. However, it was a static charge distribution which did not fluctuate in time. In real world, the development of charge density in plasma is closely related to the applied electric field. The stronger the electric field magnitude, the higher will be the ionization and quantifiably, the plasma formed will be large. Thus, it can be hypothesized that the charge density fluctuates spatially as well as temporally in response to fluctuations in electric field at that point.

Introducing this coupling between the plasma and the electric field has been a challenge in many numerical and computational studies done so far. For example; Shyy and Jayaraman[19] modelled a static Gaussian charge distribution which is not fluctuating in time. This results in a drawback that the quantified body force is not correctly estimated since in an actualistic plasma actuator computational model; both the charge density and the electric field should vary spatially and temporally; and so does the body force, which is the product of magnitudes of the Electric field and the charge density.

In this study, we model the charge density such that along with being a Gaussian along lateral and longitudinal direction of the plasma actuator, it also fluctuates temporally at the same frequency to that of the applied electric field. We achieve this by adding the temporal component of the applied potential in the charge density boundary condition. This incorporates a pseudo-coupling of the charge density with the applied potential, which shall hopefully provide us with scrupulous body force values.

As stated prior, one of the goals is to get a realistic charge distribution, which fluctuates in space and time, and one that also looks physically realistic.

The results from the simulation are shown in Figure 29. The charge density physically represents a roughly realistic plasma. The density of the plasma is greatest at the exposed electrode edge and decreases in lateral and longitudinal directions. Furthermore as shown in Figure 30, the charge density and the electric potential is plotted at the edge of the exposed electrode. As shown, the charge density fluctuates at the same frequency as that of the applied voltage. This indeed ensures the pseudo-coupling between applied electric field and the charge density.

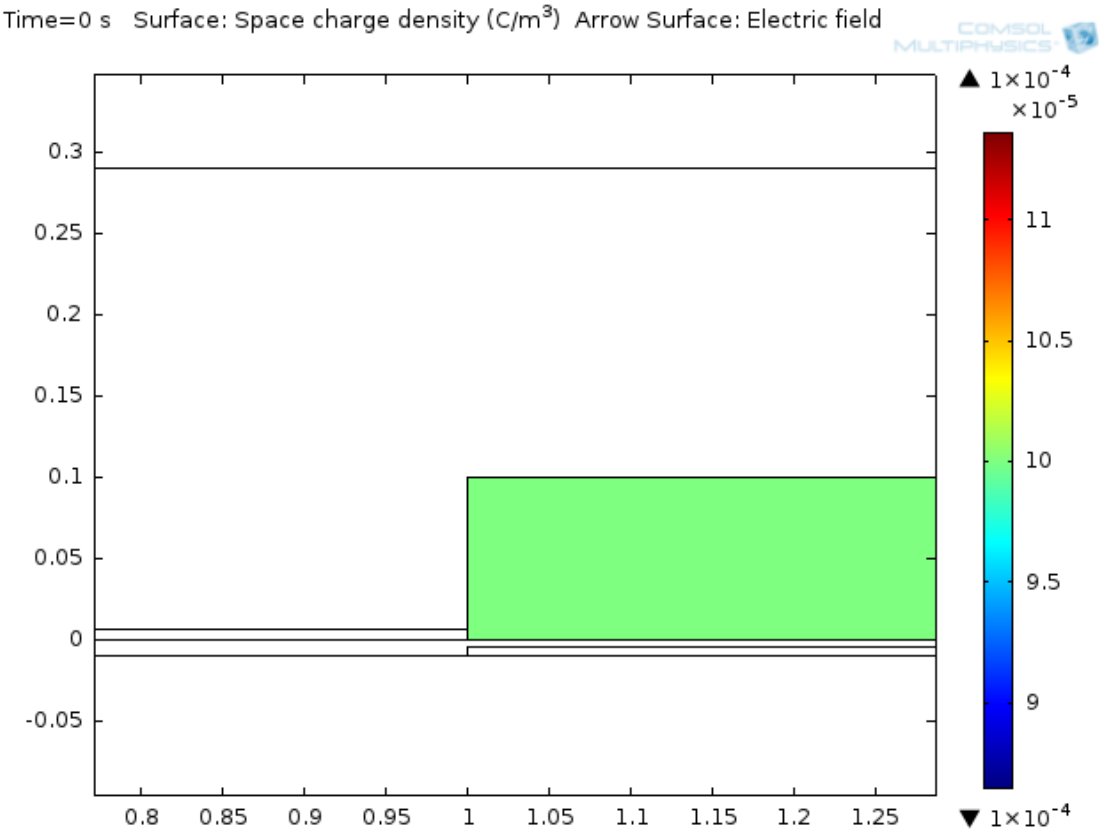
Time=0 s Surface: Space charge density (C/m3) Arrow Surface: Electric field
▲ 1×10-4
×10-5
11
10.5
10
9.5
9
▼ 1×10-4
0.3
0.25
0.2
0.15
0.1
0.05
0
-0.05
0.8
0.85
0.9
0.95
1
1.05
1.1
1.15
1.2
1.25

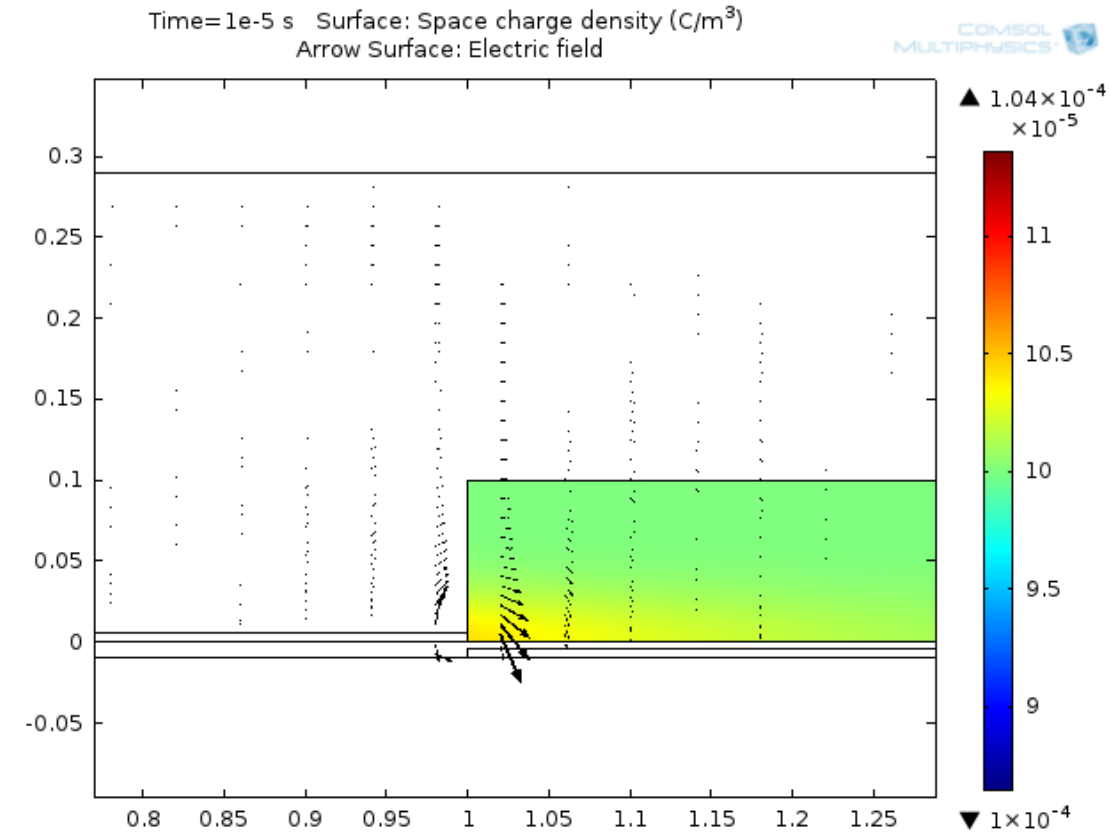
Time=1e-5 s Surface: Space charge density (C/m3)
Arrow Surface: Electric field
▲ 1.04×10-4
×10-5
11
10.5
10
9.5
9
▼ 1×10-4
0.3
0.25
0.2
0.15
0.1
0.05
0
-0.05
0.8
0.85
0.9
0.95
1
1.05
1.1
1.15
1.2
1.25

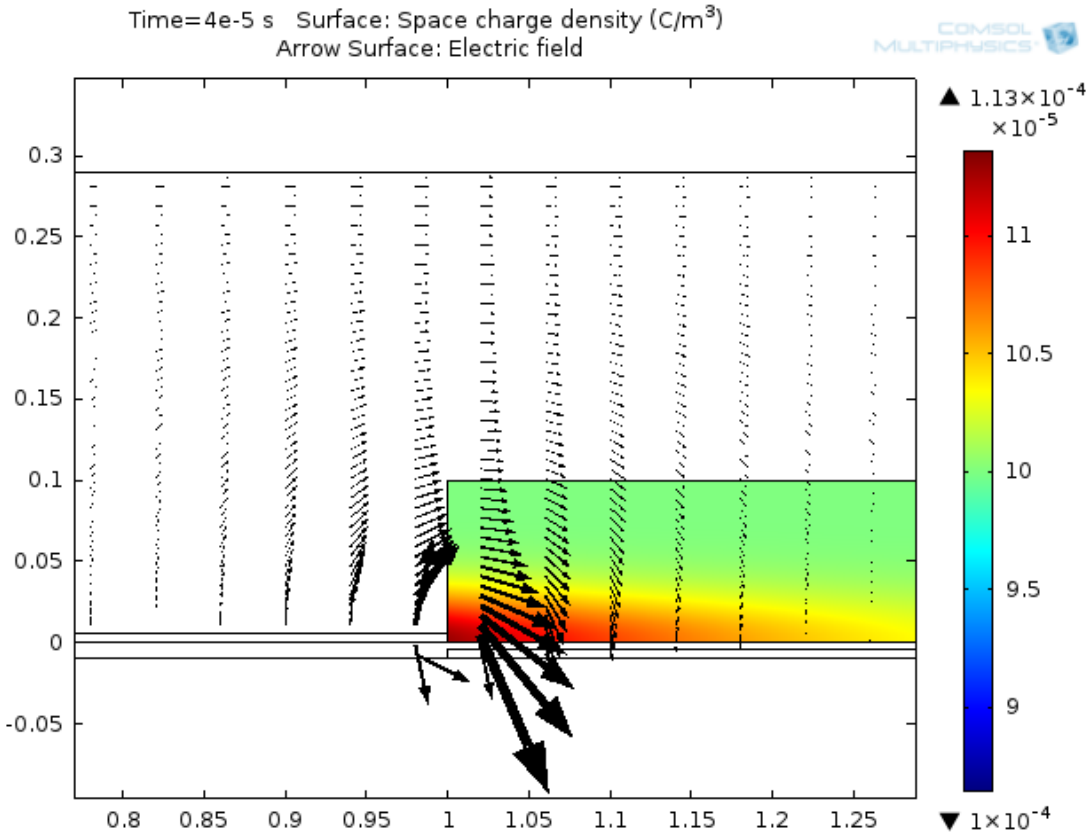
Time=4e-5 s Surface: Space charge density (C/m3)
Arrow Surface: Electric field
▲ 1.13×10-4
×10-5
11
10.5
10
9.5
9
▼ 1×10-4
0.3
0.25
0.2
0.15
0.1
0.05
0
-0.05
0.8
0.85
0.9
0.95
1
1.05
1.1
1.15
1.2
1.25

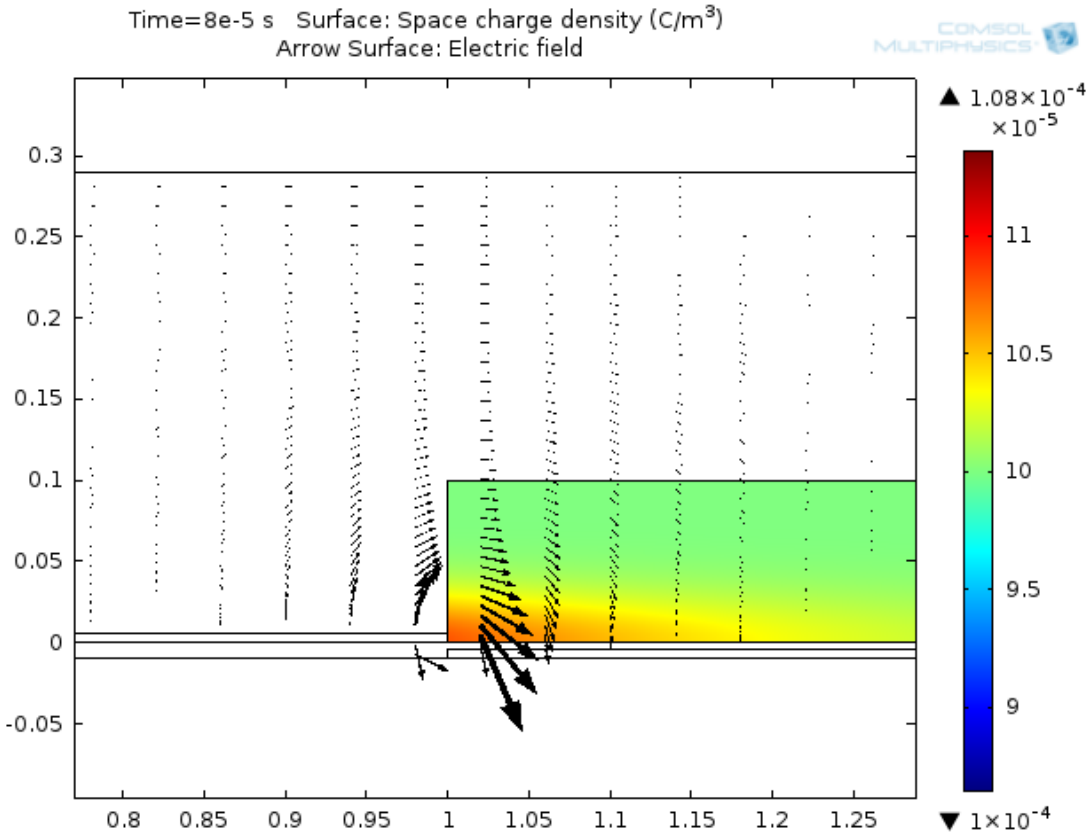
Time=8e-5 s Surface: Space charge density (C/m3)
Arrow Surface: Electric field
▲ 1.08×10-4
×10-5
11
10.5
10
9.5
9
▼ 1×10-4
0.3
0.25
0.2
0.15
0.1
0.05
0
-0.05
0.8
0.85
0.9
0.95
1
1.05
1.1
1.15
1.2
1.25

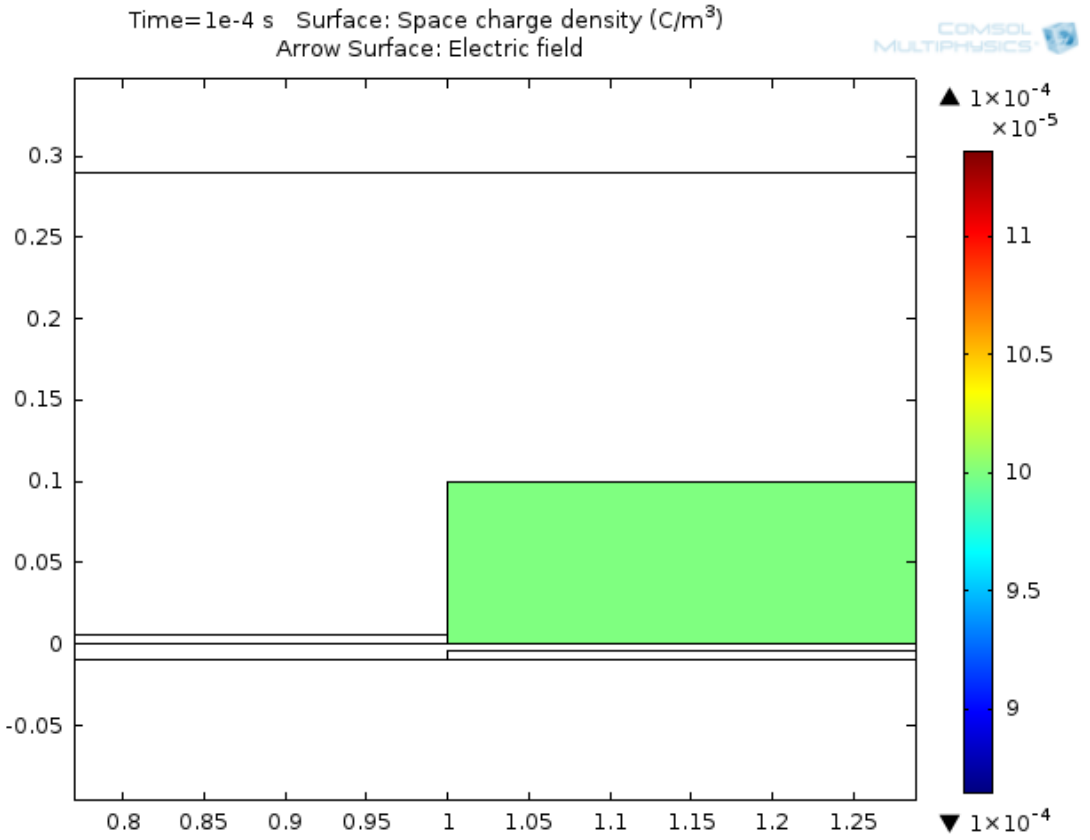
Time=1e-4 s Surface: Space charge density (C/m3)
Arrow Surface: Electric field
▲ 1×10-4
×10-5
11
10.5
10
9.5
9
▼ 1×10-4
0.3
0.25
0.2
0.15
0.1
0.05
0
-0.05
0.8
0.85
0.9
0.95
1
1.05
1.1
1.15
1.2
1.25

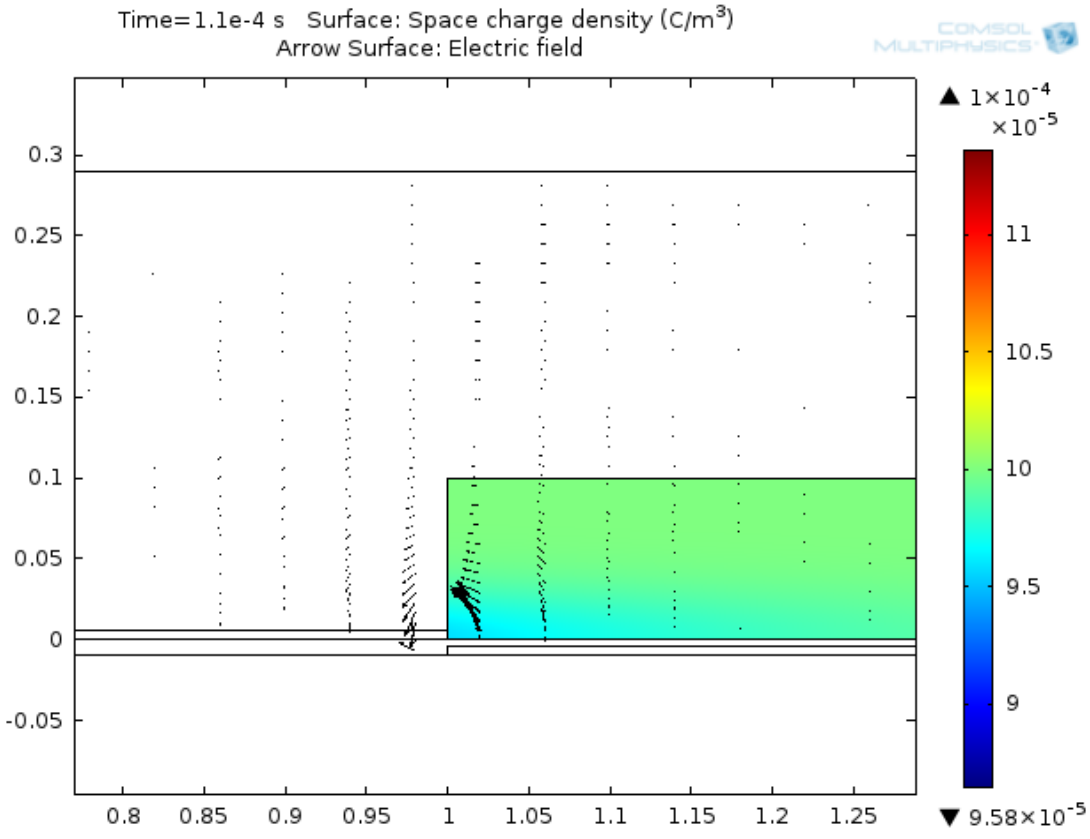
Time=1.1e-4 s Surface: Space charge density (C/m3)
Arrow Surface: Electric field
▲ 1×10-4
×10-5
11
10.5
10
9.5
9
▼ 9.58×10-5
0.3
0.25
0.2
0.15
0.1
0.05
0
-0.05
0.8
0.85
0.9
0.95
1
1.05
1.1
1.15
1.2
1.25

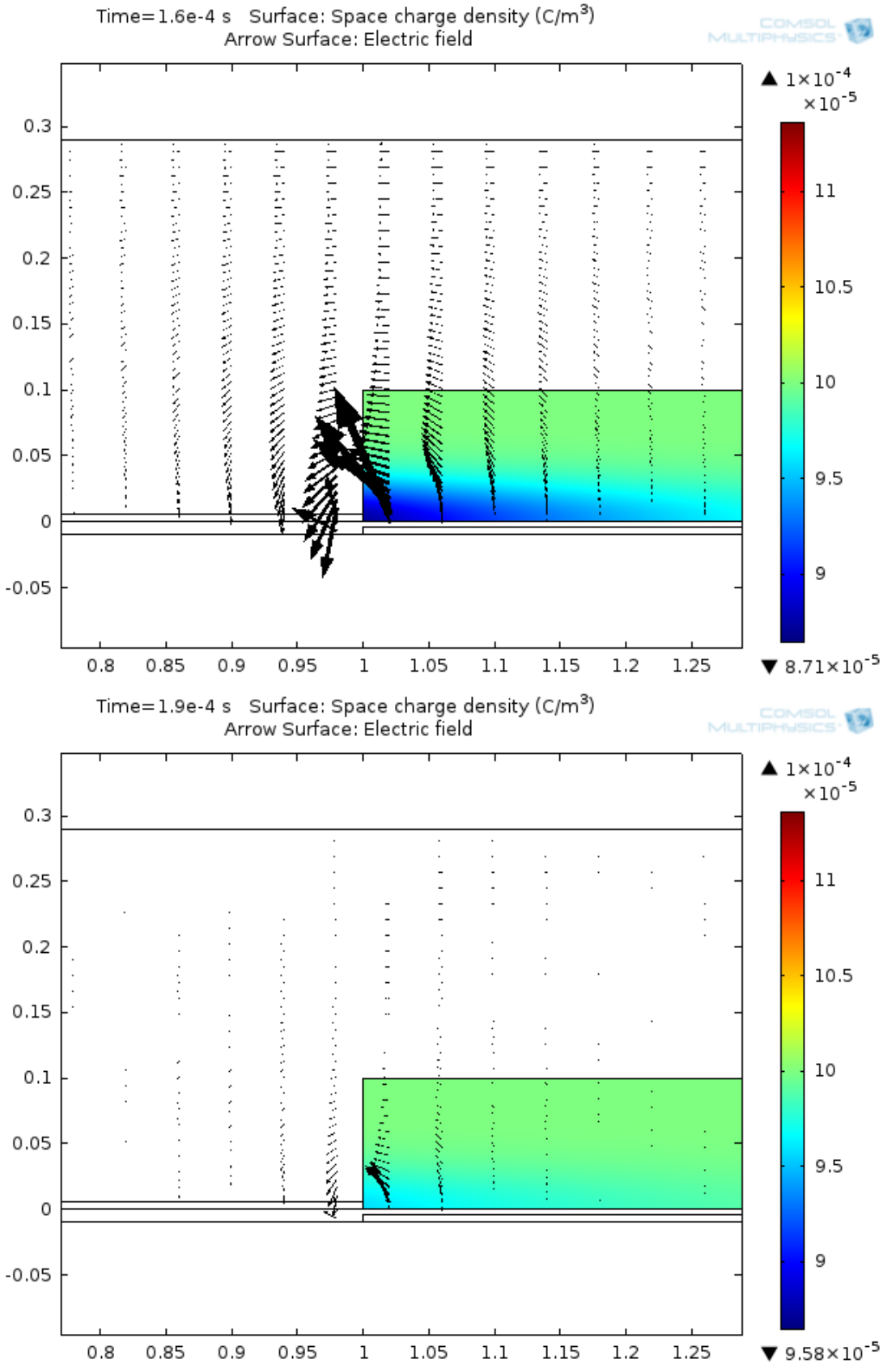

Figure 29 Charge density representing plasma and the electric field lines.

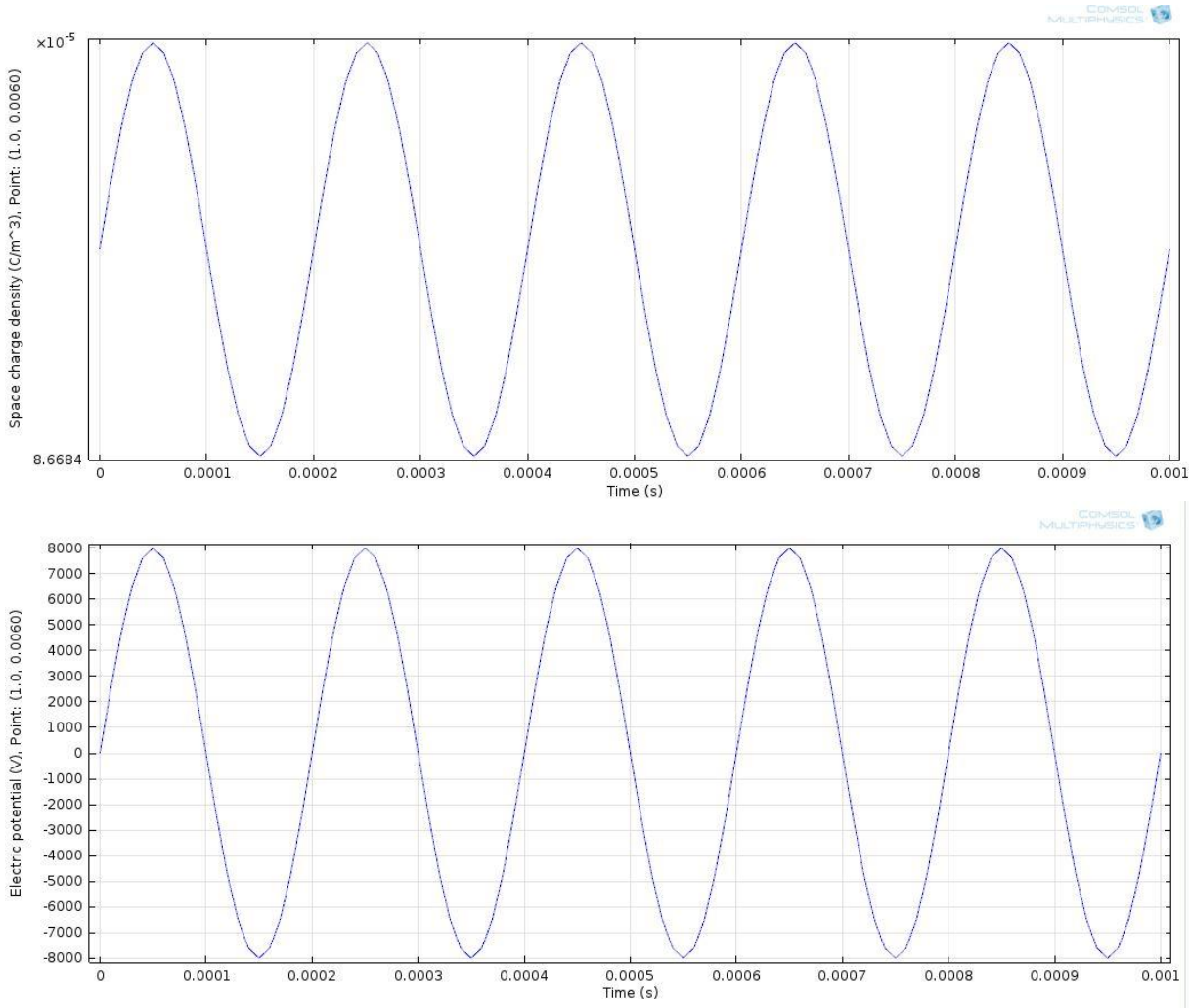

Figure 30 Temporal behavior of Plasma in response to the applied potential.

Next goal is to obtain the magnitude and distribution of spatially and time-varying body force due to the plasma in the volume. This is achieved by integrating the product of the electric field and the charge density in space, in the charge volume. In Figure 31, the resulting body force distribution is shown for one complete cycle. The body force distribution looks realistic and since the phase of charge density and applied potential is same, the body force acts in the same direction i.e; away from the exposed electrode, for both the cycles. But this can easily be altered by adding a phase difference between the charge density and the applied potential.

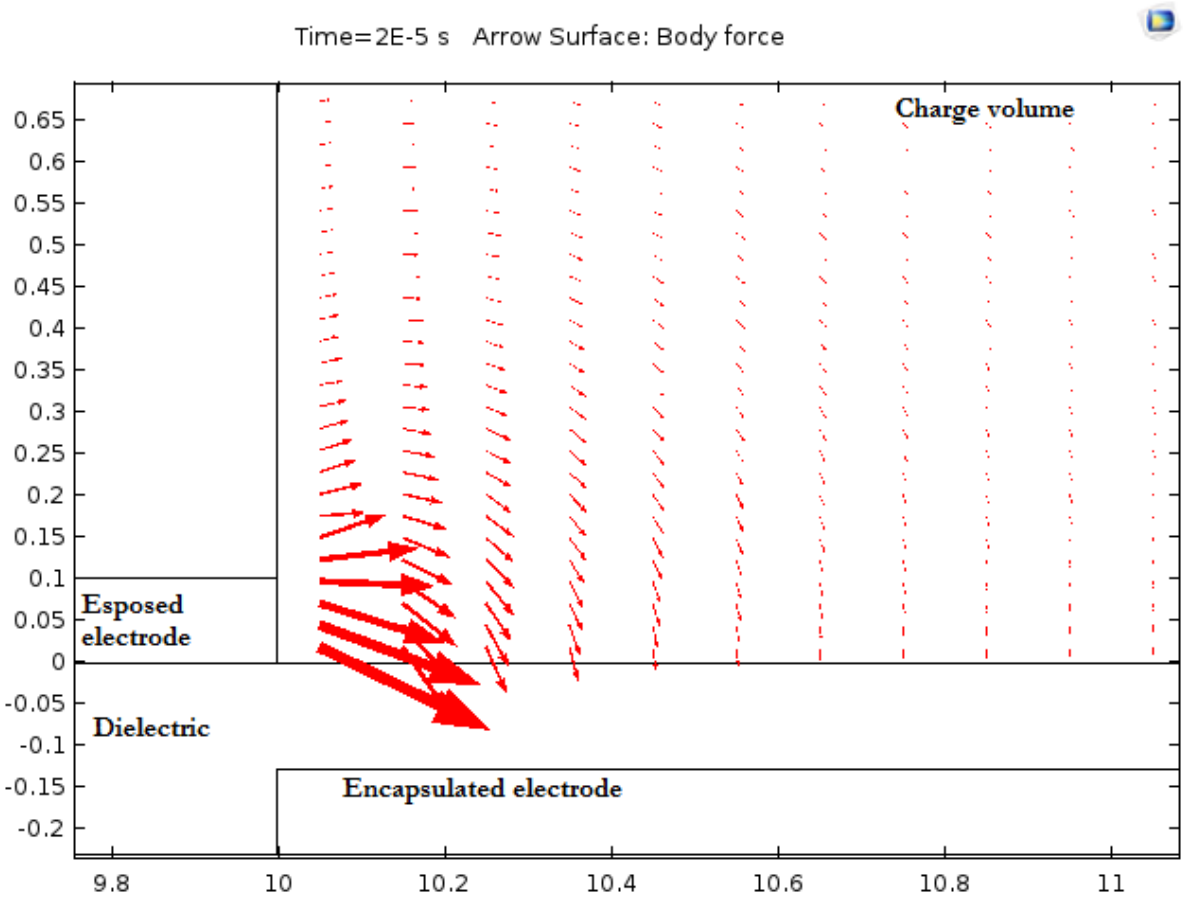
Time=2E-5 s Arrow Surface: Body force
Charge volume
Esposed electrode
Dielectric
Encapsulated electrode
0.65
0.6
0.55
0.5
0.45
0.4
0.35
0.3
0.25
0.2
0.15
0.1
0.05
0
-0.05
-0.1
-0.15
-0.2
9.8
10
10.2
10.4
10.6
10.8
11

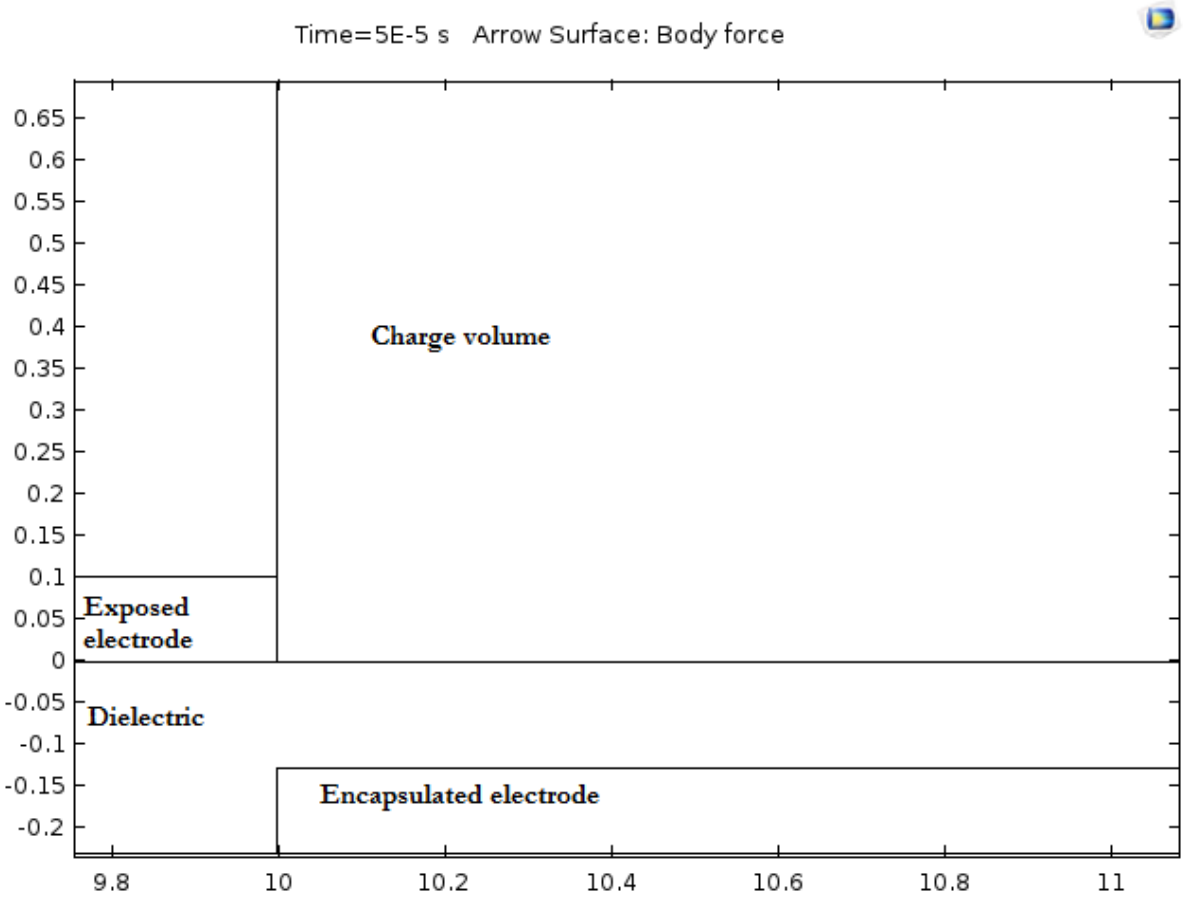
Time=5E-5 s Arrow Surface: Body force
Charge volume
Exposed electrode
Dielectric
Encapsulated electrode
0.65
0.6
0.55
0.5
0.45
0.4
0.35
0.3
0.25
0.2
0.15
0.1
0.05
0
-0.05
-0.1
-0.15
-0.2
9.8
10
10.2
10.4
10.6
10.8
11

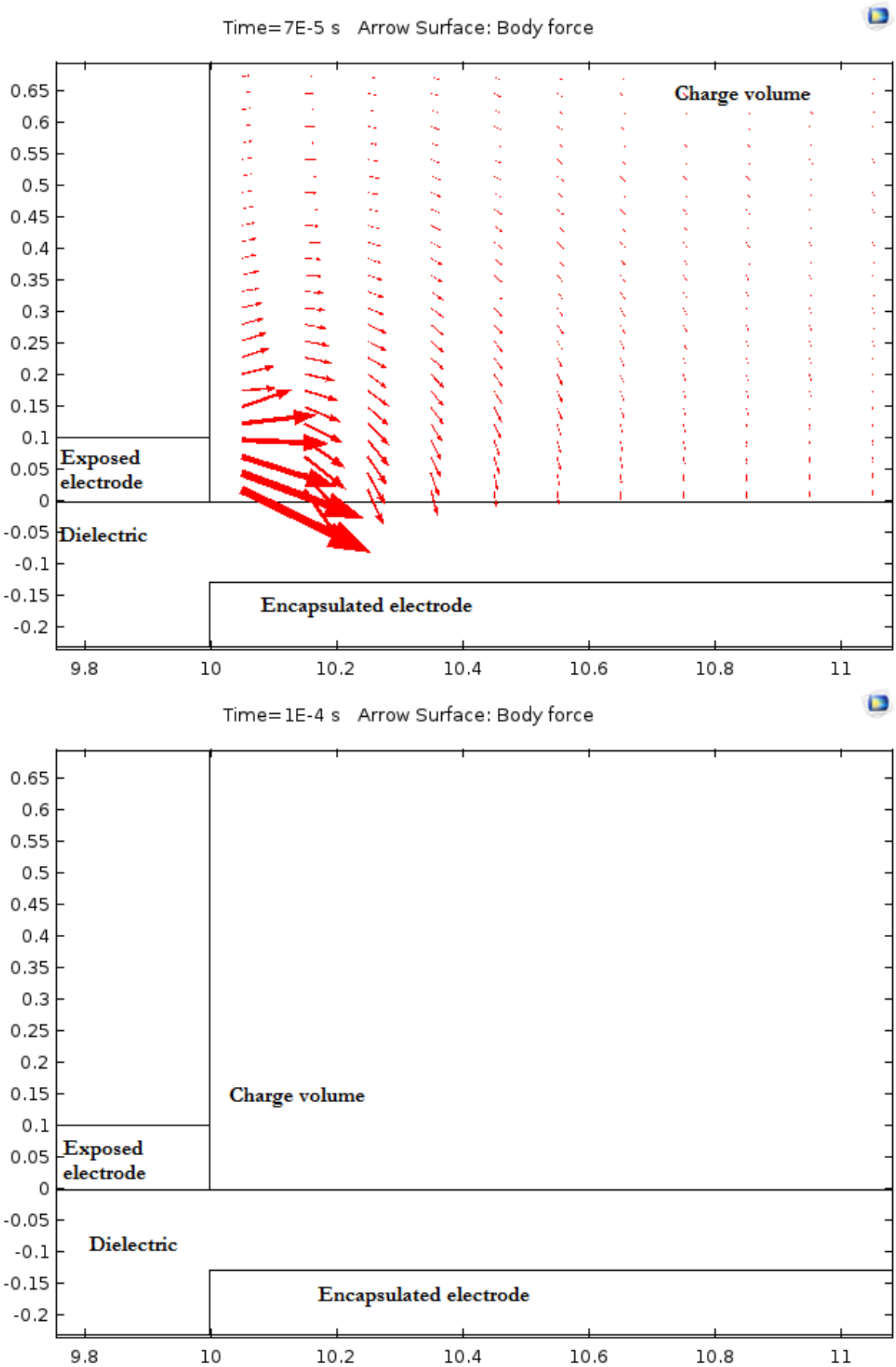

Figure 31 Temporal variation of body force.

For the given conditions, the space integrated and time varying body force magnitude is shown in Figure 31.

Having modelled the body force in the right fashion and imposed the right boundary conditions, we finally proceed to develop a relation which matches the experimental body forces from Kotsonis[10,11] with body force from the computational model. The aim is to develop a relation for the charge density which gives the correct match between the experimental body force (Fe)and computational body force (F_c). In previous cases [Figure 29], the net charge density was a product of Gaussian charge densities along x and y axes multiplied by the temporal component of the applied potential. This relation is not as amenable as one would desire when a change in magnitude of the charge density is wished for to closely match the experimental values. Therefore, we introduce more variables so that we are able to obtain a larger count of charge densities within the desired range. This is desired because we want to obtain a close match between the experimental and computational body forces. Therefore, we introduce two more variables; namely A and B. The new relation for the charge density is shown in Equation 4.1.

Variable A controls the offset of the charge density and variable B controls the amplitude of the charge density. Therefore, we have 3 variables which we can use to control the charge density in order to correctly model the body force, spatially and temporally, and to calibrate our results with the experiments.

These variables are:

1. Phase
2. Variable A
3. Variable B

We shall first calibrate the cases from Kotsonis [Kapton] and Kotsonis [PMMA].

1. A, B values for Fc=Fe for Kotsonis [Kapton].

The formulated spatial and temporally varying charge density equation is given by:

$$B + (A * pw1(x) * pw2(y) * sin(2 * pi * f * t)) \quad 4.1$$

Whereby
$pw1(x)$ is the Gaussian along longitudinal (X) axis, depicted in Figure 32.
$pw2(y)$ is the Gaussian along lateral (Y) axis, depicted in Figure 32.

f is the frequency of the applied potential at the exposed electrode.
t is the time period of the AC waveform of the applied potential at the exposed electrode.

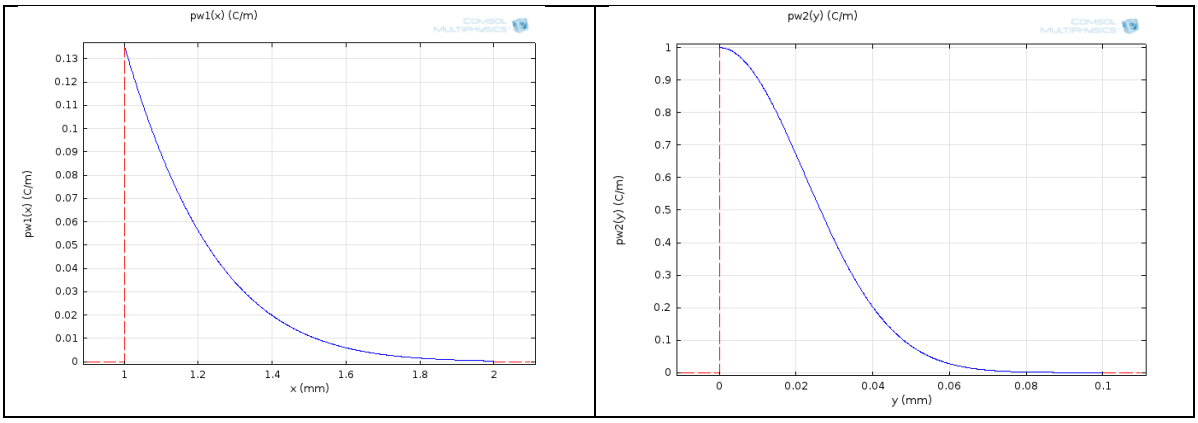

Figure 32 Gaussians introduced in the charge density formulation along longitudinal (x) and lateral (y) directions.

As stated prior, we aim to determine the values of A and B in the charge density equation which give a close match between the experimentally derived space integrated-time averaged body force (F_e) and the same body force from the present computational model (F_c).

In this section, we shall calibrate the body force for each case from Kotsonis's Kapton study[11]. The test cases from Kotsonis's Kapton experiments (PIV measurements) are as given in Table 6. All of these cases are simulated individually and a change in A and B values is made to match F_c with F_e.

Parameter	**Value**
Applied voltage (V)	8-16 KV_{pp} (in steps of 2 KV_{pp})
Frequency (f)	0.5, 1, 1.5, 2, 2.5, 3 kHz.
Lower electrode length	10mm
Upper electrode length	10mm
Dielectric thickness	100 μm

Table 6 Geometrical and electrical parameters from Kotsonis[11].

Figure 33 shows the time averaged body forces per unit length of the actuator from the PIV studies for different voltages and constant frequency of 1 kHz.

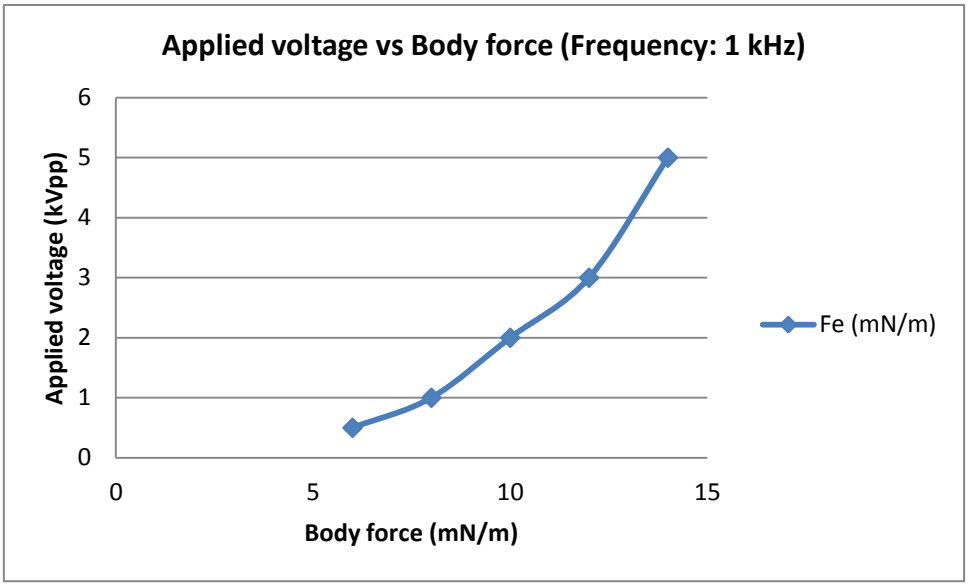

Figure 33 Body force measurements for different applied voltages from PIV studies for electrode length of 10mm and applied frequency of 1 kHz.

The respective A and B values that give the best match between Fe and Fc are shown in Figure 34. Figure 35 shows the match between Fc and Fe for the determined A and B values.

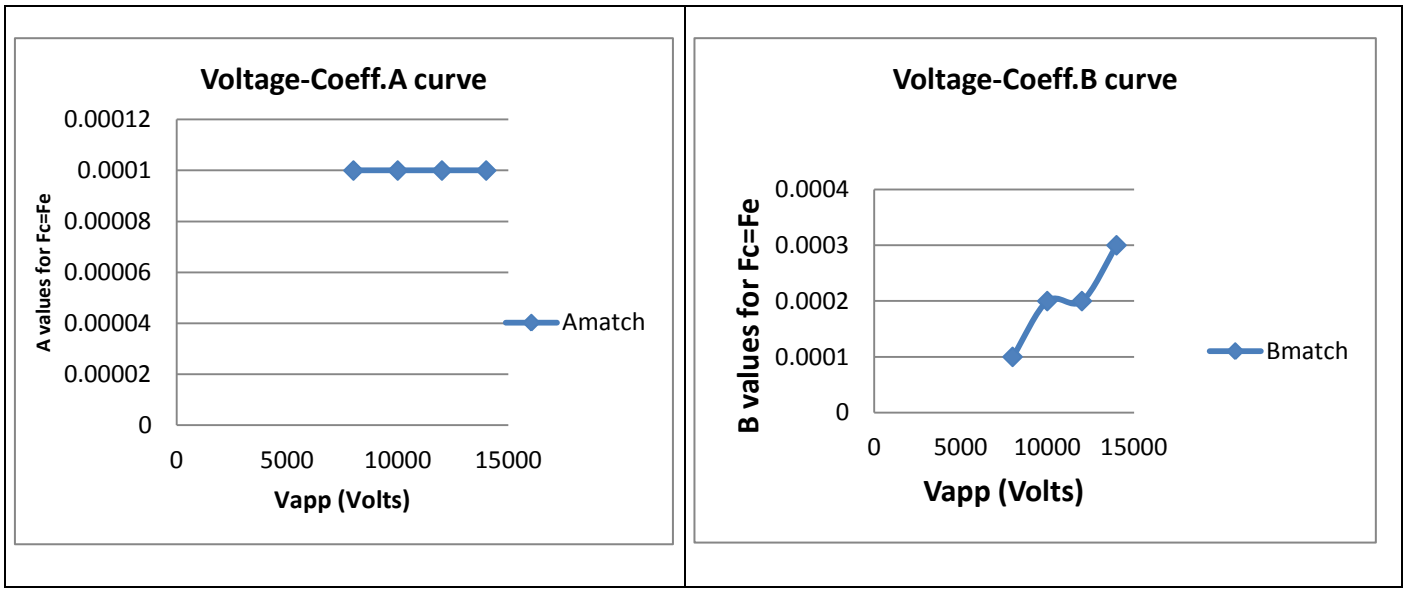

Figure 34 Plot of Applied Voltage vs Variable (A,B) curve for A,B values that give the best match between Fe and Fc.

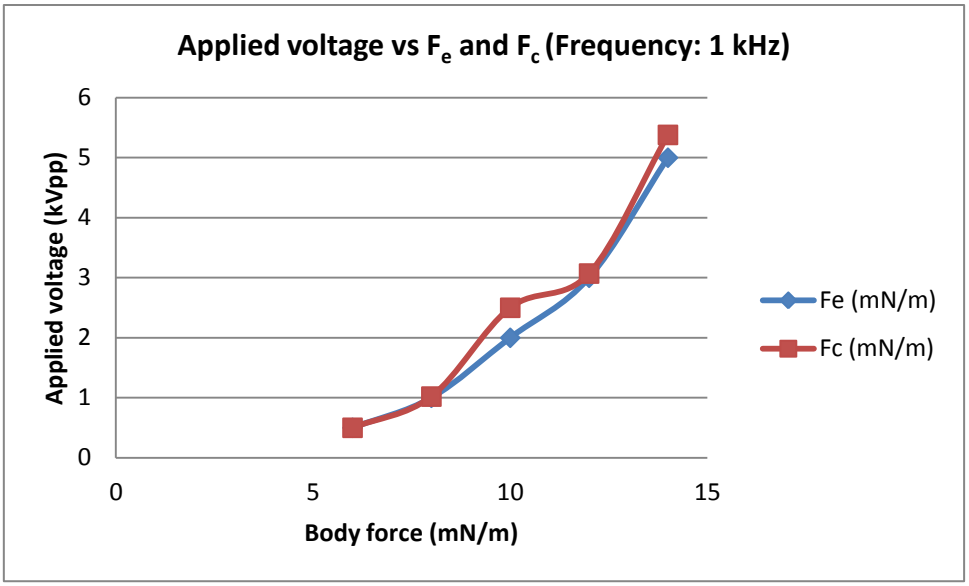

Figure 35 Graph showing the comparison between Fc and Fe for the A and B values.

Thus, once the experimental and computational body forces have been calibrated, the next aim is to duplicate the behaviour of time variable space-integrated body force with the potential behaviour; i.e.; The body force, and thus the charge density due to plasma, in the positive half cycle is less than that in the negative half cycle. The variable that governs the reverse in magnitude of the charge density is the phase. For a zero phase, the behaviour of the body force with the applied potential is shown in Figure 36 [Right].

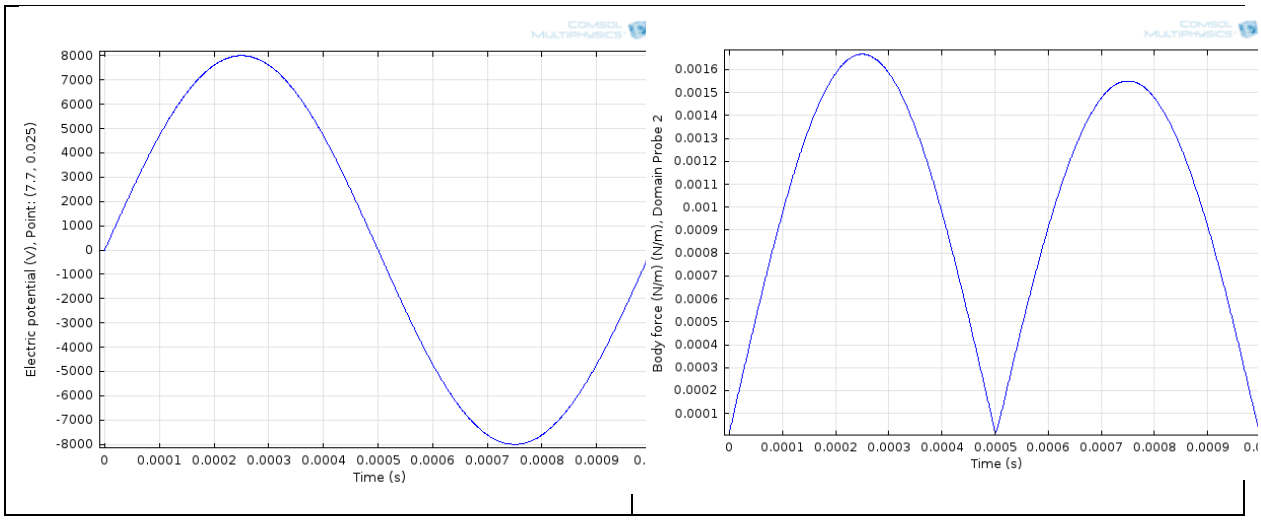

Figure 36 [Left] Electric potential at the exposed electrode [Right] Space integrated body force.

Thus, the correct behaviour is not replicated for a zero phase since it depicts a large body force for the positive going half cycle compared to the negative half cycle. However, this behaviour can be easily altered by simply adding a phase difference of 180 degrees between the applied potential and the charge density.

2. A, B values for Fc=Fe for Kotsonis [PMMA].

In this section, we shall calibrate the body force for each case from Kotsonis's PMMA (Plexiglass) study [10]. The test cases from Kotsonis's PMMA experiments (PIV measurements) are as given in Table 7. All of these cases are simulated individually and a change in A and B values is made to match F_c with F_e, for the frequency of 2 kHz

Parameter	Value
Applied voltage (V)	20-40 KV_{pp} (in steps of 5 KV_{pp})
Frequency (f)	2 kHz.
Lower electrode length	10mm
Upper electrode length	10mm
Dielectric thickness	100 μm

Table 7 Electrical and Geometrical parameters from Kotsonis's PMMA study[10].

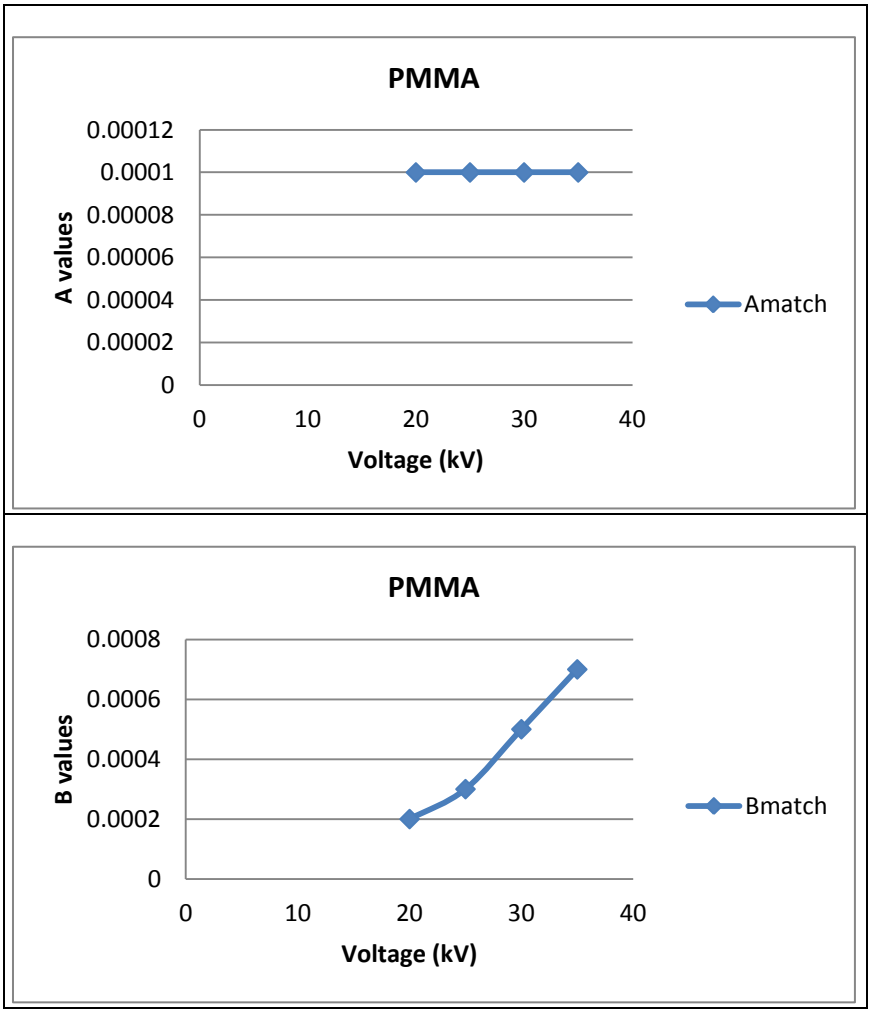

Figure 37 Sensitivity of variables A and B to the applied voltage.

It is evident from Figure 37 that variable A has a very low sensitivity while variable B has considerably high sensitivity to the change in applied voltage.

Figure 38 shows the match between Fc and Fe for the determined A and B values shown in Figure 37, that give a best match between the computational and experimental values.

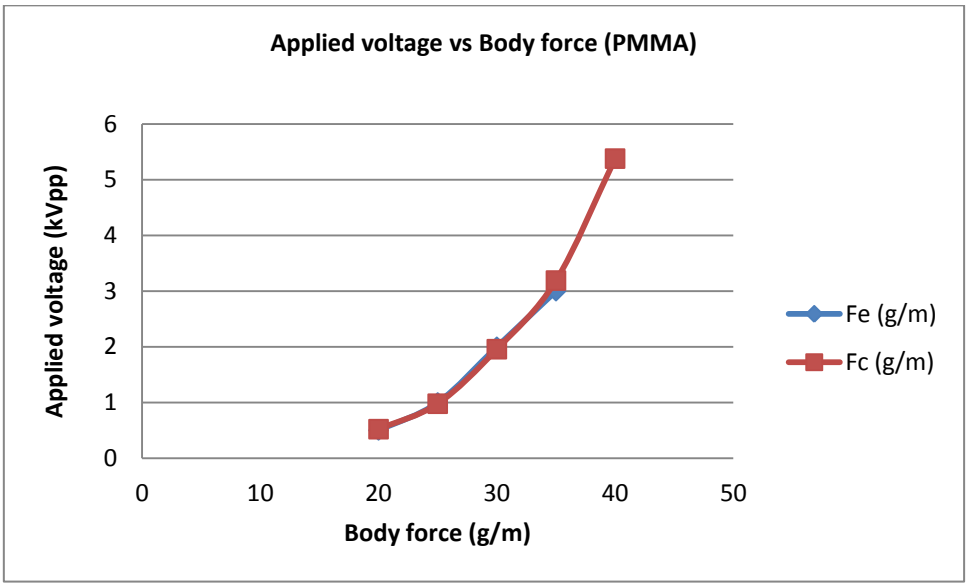

Figure 38 Calibrated experimental and computational body force for the A and B values that give the best fit.

The body forces calibrate quite well for all 5 cases for the given relation with fitting A and B values.

4.4 2-D Electrodynamic-Fluid model

The magnitude of the body force at a point depends solely on the charge density due to plasma and the Electric field, at that point. This body force acts on the ambient fluid and adds momentum to it, preventing flow separation. Thus, when developing a computational model for the plasma actuator, it is desired to see the effect of the body force on the ambient fluid; in other words, see the resulting velocity and pressure distributions. And this is the next objective of this thesis.

Having successfully developed an Electro-dynamic model for the AC-DBD and having calibrated the results with experiments, we proceed to couple the Electro-dynamic model with a fluid model. This CFD study is aimed to get the pressure and velocity distributions that result due to the momentum exchange between the plasma and the ambient fluid. This necessitates the body force to be coupled with the ambient fluid flow in an equation that governs the motion of a fluid, taking into account the finite viscosity of the fluid. This equation is the Navier-Stokes equation, discussed in Chapter 3.

The body force resulting from the Electrodynamic model at each nodal point in the mesh is plugged in the Navier-Stokes equation as a source term and then they are solved for. The solution gives us the velocity and pressure distributions.

However, our CFD study takes a long time to converge (typically 3 weeks using a Xeon E7 Processor), for the dimensions that we have been working with so far, therefore we had to scale down the model considerably. Also since, we have to perform a check on the boundary conditions for the coupled model; it is not feasible to carry on with the previous dimensions of the model.

4.4.1 Computational model and Setup.

In order to reduce the computation time the original model used for the Electrostatic model has been scaled down to $1/10^{th}$ of its original size and is used as the computational geometry for this model. The scaled down model is shown in Figure 39.

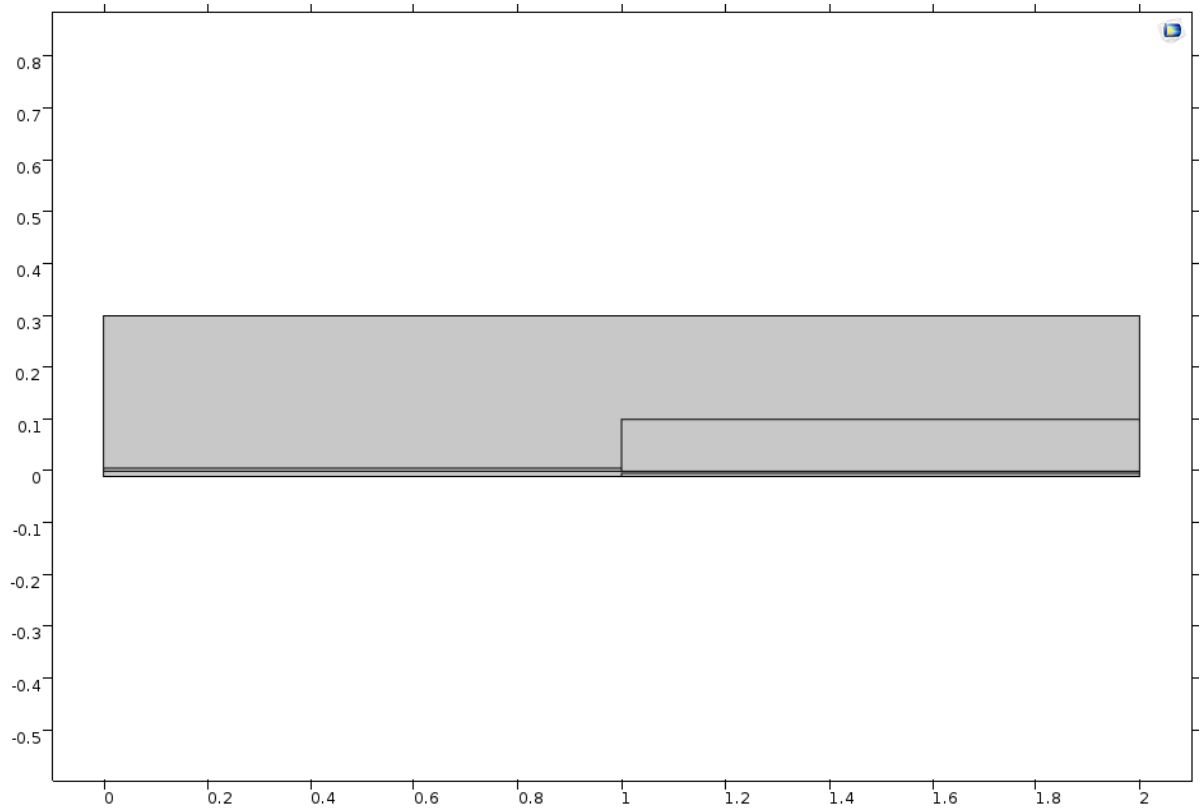

Figure 39 Computational model and set-up for the Electrodynamic-Fluid model.

Boundary conditions

The Navier-Stokes equation is solved for the fluid-domain and the coupled Poisson equation is solved for all the domains.

Discretization.

Meshing is one of the challenges of this study. The right mesh distribution is not only critical to achieving convergence but also crucial for getting the accurate values and resolving relevant

details. Too fine a mesh results in long solver run and too coarse a mesh can result in inaccurate values or lead to solver not converging. Fluid dynamics simulations require quite high quality meshes in both, element shape and smoothness of sizes changes. Thus, the goal is to find a mesh distribution that converges and resolves relevant details sufficiently while also keeping the computational costs in check.

Close up of the mesh distribution is shown in Figure 40. The mesh distribution is not uniform. A much finer custom mesh is used in the Plasma volume and surrounding edges, respectively, in order to obtain accurate body force values while a pre-defined custom fine mesh for CFD simulations is used for the rest of the fluid domain. Total number of mesh elements amount to 1282594.

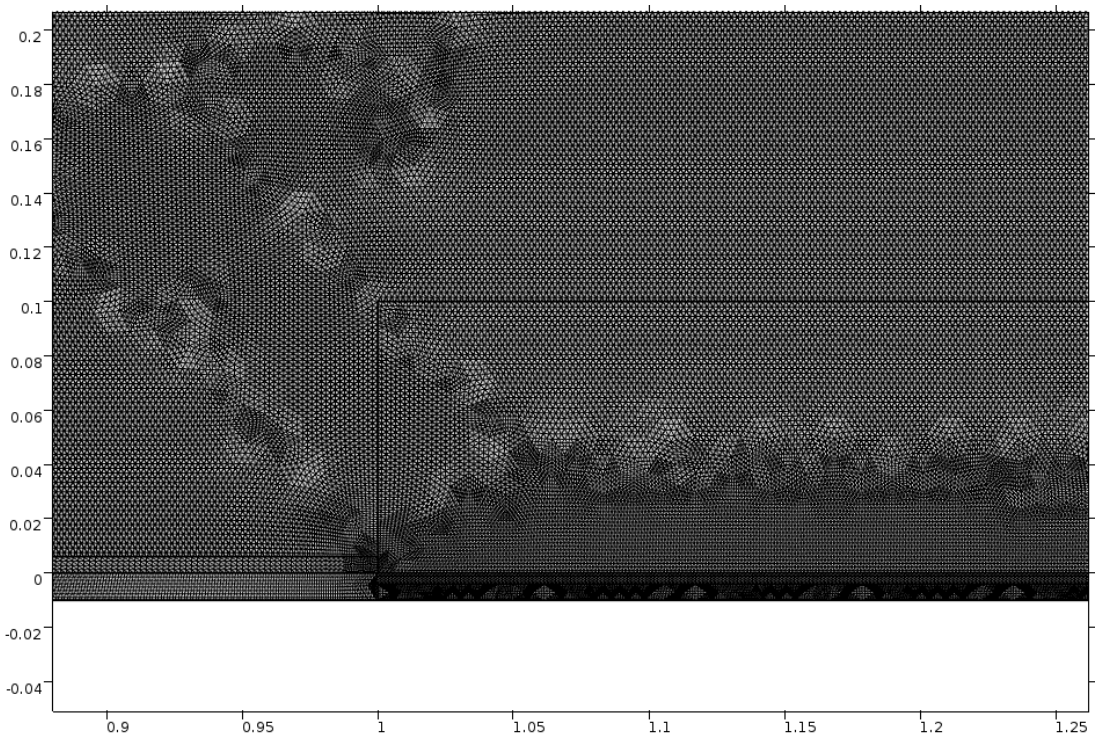

Figure 40 Meshed computational domain for the Electrodynamic-Fluid model.

Initialization

The time range for the simulation starts at 0 seconds and converges at the final time step of 10^{-2} seconds in steps of 10^{-5} seconds. The simulation is first run without charge density to check the boundary conditions for the fluid flow. In the second simulation the spatial and time varying charge density is introduced, in the volume adjacent to the exposed electrode and the velocity and pressure distribution is obtained. A realistic distribution of the body force was already obtained in the Electrodynamic model 2, and in this model we are interested in the increase in velocity on the ambient flow due to the action of the body force.

4.4.2 Results and discussion

- **No charge density.**

Initially we simulate without any charge density in the Plasma volume in order to check if we have correctly implemented the boundary conditions for the CFD model. The operating conditions for Electrodynamics are shown in Table 8 while the operating conditions for CFD simulation are shown in Table 9. The computation time is 2 hours and 4 minutes with the available computing power.

Temperature	293.15 K
Pressure	1 atm
V_0 (Voltage at the exposed electrode)	8000*sin(2*pi*5000[1/s]*t)
V (Voltage at the encapsulated electrode)	0
ρ_v (Charge density)	0.0001+(0.0001*pw1(x)*pw2(y))*sin(2*pi*5000[1/s]*t)

Table 8 Operating conditions for Electrodynamics.

Temperature	293.15 K
Pressure	1 atm
ρ(Density of the fluid)	1.223 kg/m^3
μ (Dynamic viscosity of the fluid)	171.291 Pa.s

Table 9 Operating conditions for CFD.

The velocity distribution at the concluding time step 10^{-2} seconds for this study is shown in Figure 41. The model converges well and the velocity distribution looks realistic. There is a velocity deficit as the flow gets closer to the wall, due to the finite viscosity of the fluid and this confirms that the No-Slip condition has been properly implemented.

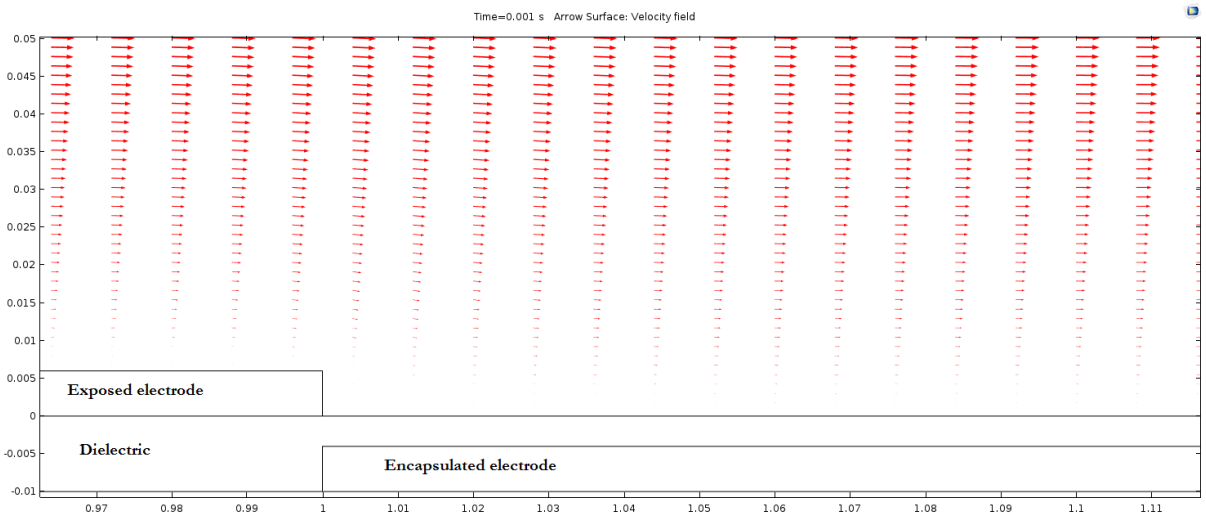

Figure 41 Velocity field without charge density at the concluding time step of 10^{-2} seconds.

Figure 42 shows the contours for Potential and Electric field vectors. The plots are similar to the ones we obtained in the Electrodynamic model. This confirms the implementation of correct boundary conditions and the coupling of the Electrodynamic model with the Navier-Stokes equation.

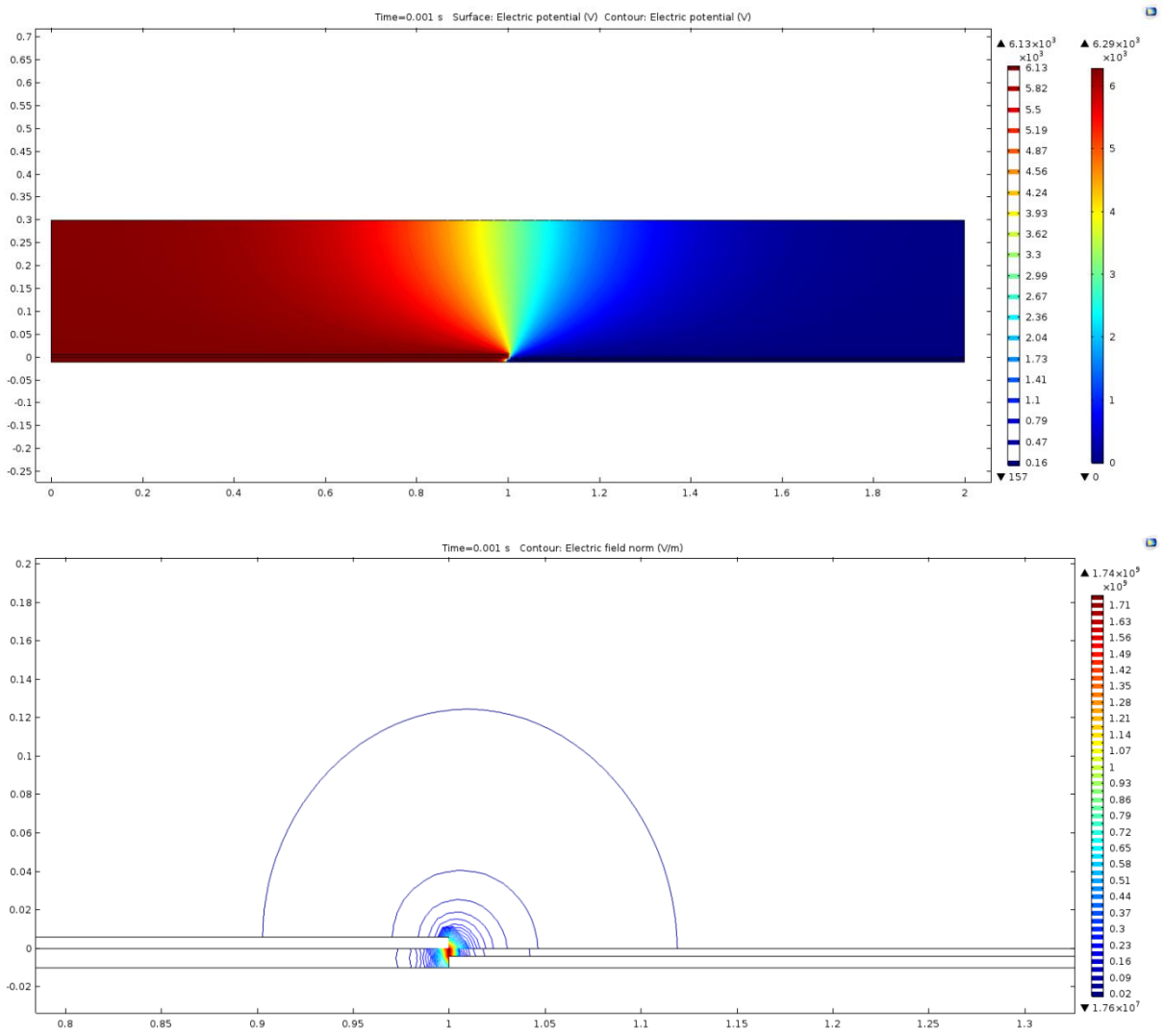

Figure 42 Potential and Electric field at concluding time step of 10^2 second of the Electrodynamic-Fluid model. The results corroborate with the results of Electrostatic model [Figure 18, 19] confirming the correct implementation of boundary conditions and the coupling of NS-equations with Poisson equation.

- **With charge density.**

Next, we introduce the equation for the half Gaussian charge density along X and Y axes, that we had formulated earlier in the Electrodynamic model. We aim to confirm some phenomenon's suggestive from literature with this model, which are as follows;

- The Push-Pull behaviour of the body force.

- The increase in velocity magnitude, which should be largest at the exposed electrode edge for all time steps.
- The spatial and temporal variation of the velocity field.

In the subsequent sections, we shall discuss the results apropos to each of the abovementioned objectives.

- **The Push-Pull behaviour of the body force.**

  In the scientific community, the proponents of the Push model are alike to the proponents of the Pull behaviour of the body force. For the presently developed model, we can model both; the push behaviour of the body force and the pull behaviour, for a range of A, B values. However, important is to note that this is a very rough modelling, but considering that the charge density of the plasma is always positive, our model will always replicate the Push model (opposite in both cycles) for a positive charge density. This is because the product of charge density and the Electric field reverses for the negative going cycle since the Electric field vector reverses direction for the negative going cycle, thus resulting in the reversal of the total body force. The reversal of body force is evident from Figure 43.

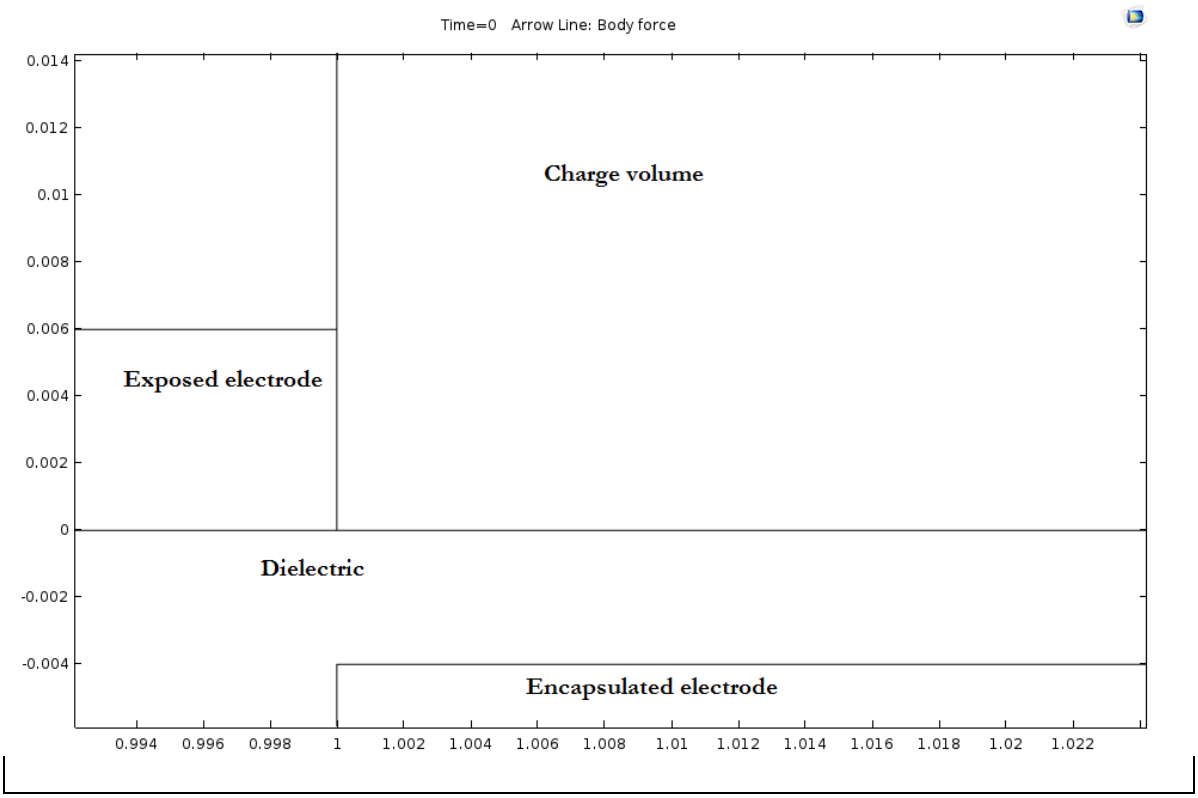

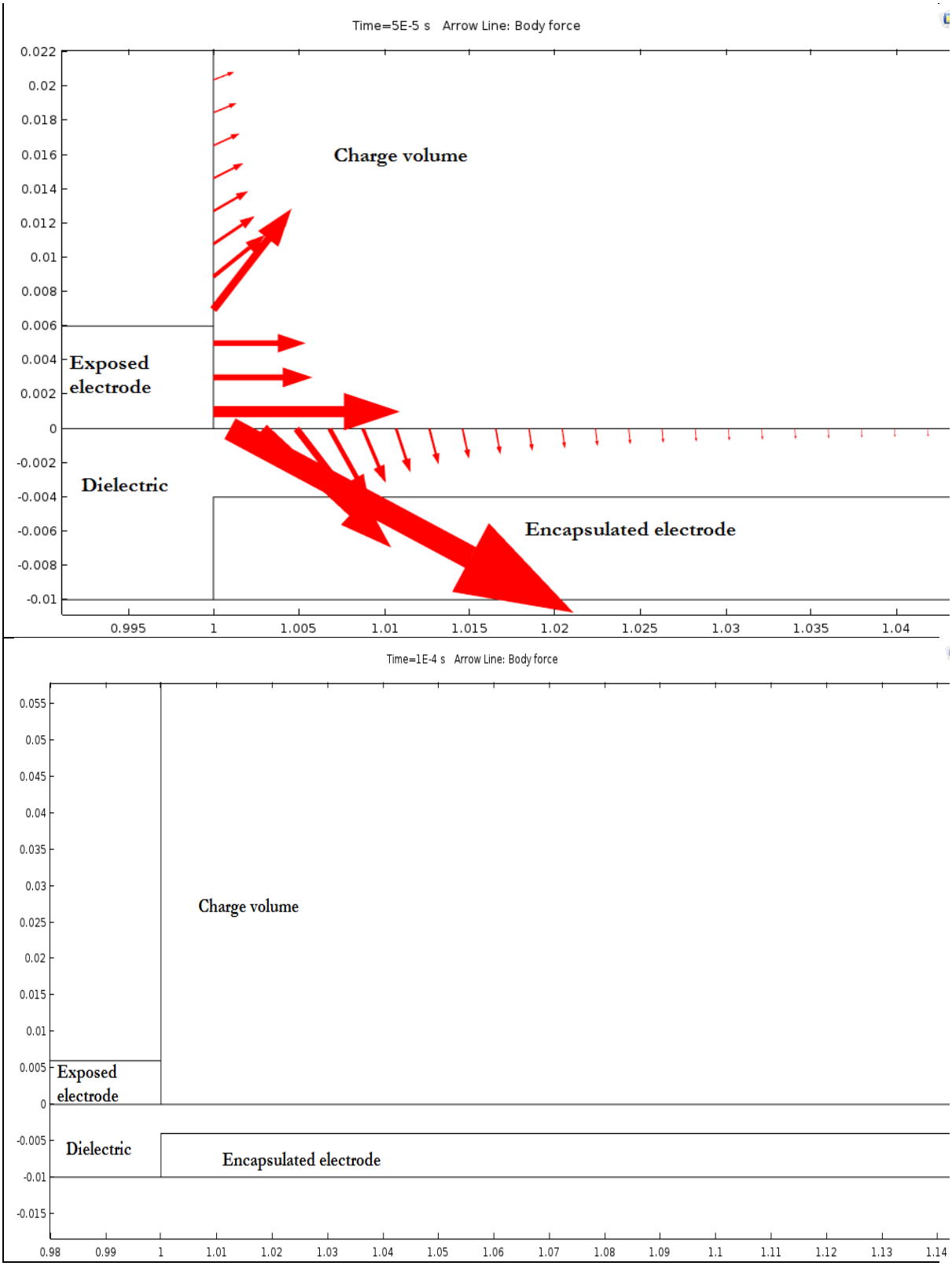
Time=5E-5 s Arrow Line: Body force
Charge volume
Exposed electrode
Dielectric
Encapsulated electrode
Time=1E-4 s Arrow Line: Body force
Charge volume
Exposed electrode
Dielectric
Encapsulated electrode

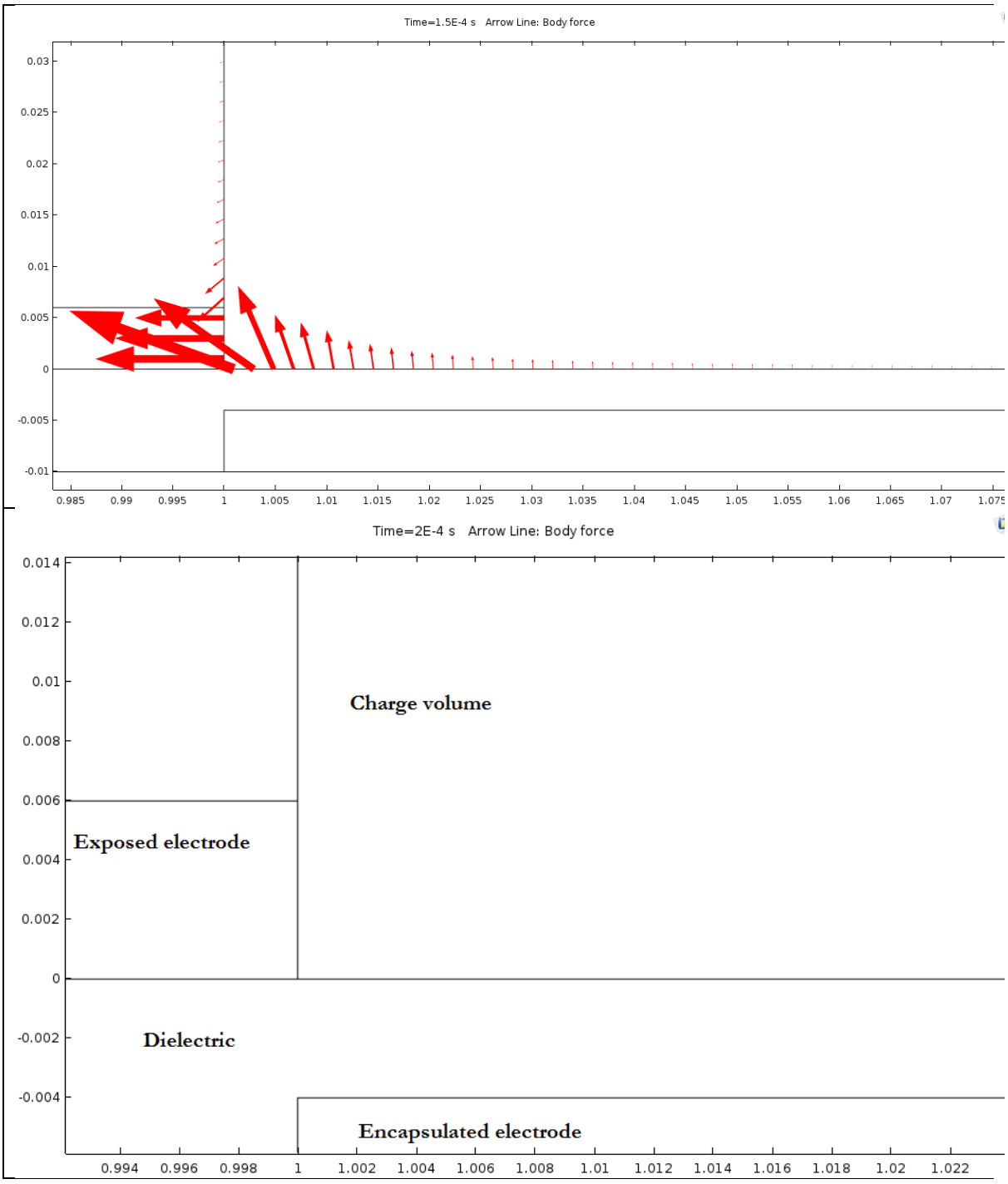

Figure 43 Spatially and temporally varying body force distribution and for one complete cycle from t=0 seconds to t=2e-4 seconds with frequency of 5000 Hz.

- **Increase in the magnitude of velocity.**

  The body force adds momentum the ambient fluid. Thus, compared to the No-Plasma case, we expect to have an increase in the magnitude of velocity near the charge density region. Figure 45 shows the plot for the velocity vector field for quiescent conditions.

  Thus, the Electrodynamic-Fluid model is able to establish the behaviour established from the experiments.

  Furthermore, from the literature, for the quiescent conditions, it is observed that a wall-jet issues near the exposed electrode and spreads along the dielectric surface, as shown in Figure 44, from Kotsonis[11]. This wall-jet ultimately reaches a steady state and further voltage cycles don't affect its magnitude. Thus, in our model, we expect the spatial and temporally varying velocity to reach a steady state in order to resemble this behaviour.

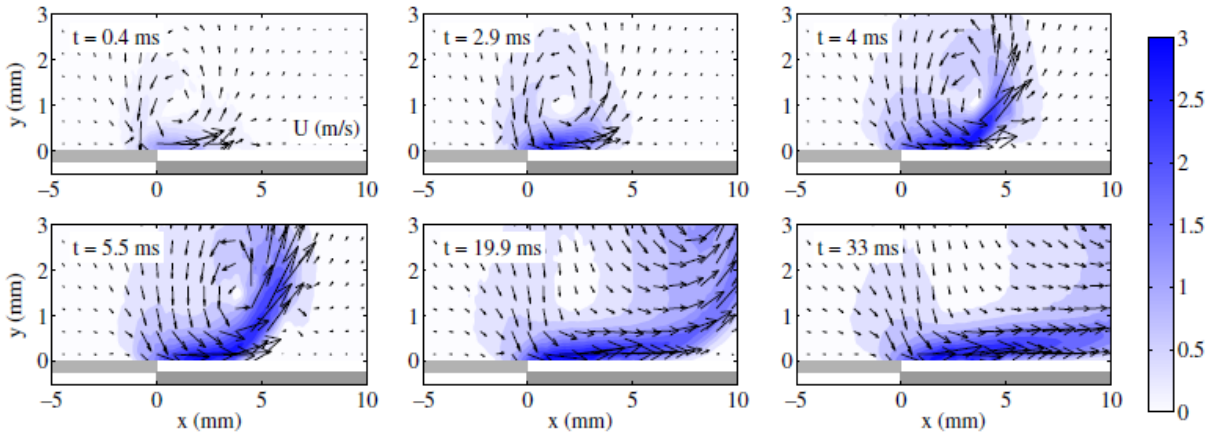

Figure 44 Velocity ditribution and issuing of wall jet under quiescent condition, evident from Kotsonis[11]

The velocity distribution from Figure 45 build up in a similar manner which is evident from the literature. However, it doesnt reach steady state because it is not simulated for a farther final time. Thus, it can be hypothesized that if we run the simulation for longer time, then it will reach a steady state.

- **The spatial and temporal variation of the velocity field.**

  For the quiescent conditions, the velocity of the ambient fluid is zero m/s. However, as the plasma forms, it exchanges momentum with the ambient fluid, or in other words, the body force acts on the ambient fluid, transferring a finite velocity to it. Since the body force varies spatially and temporally, we expect the velocity of the ambient fluid also to vary spatially and temporally, in sync with the body force. This is quite well suggested by our model. The plots at various time steps in Figure 45 show the variation in velocity field of the ambient flow. Clearly, the velocity magnitude will be highest where the body force and hence the product of charge density and electric field is maximum. Thus, the max-min points for the body force have also been plotted in Figure 45 which confirms that the body force is maximum near the edge of the exposed electrode. Thus, the result is in coherence with the literature.

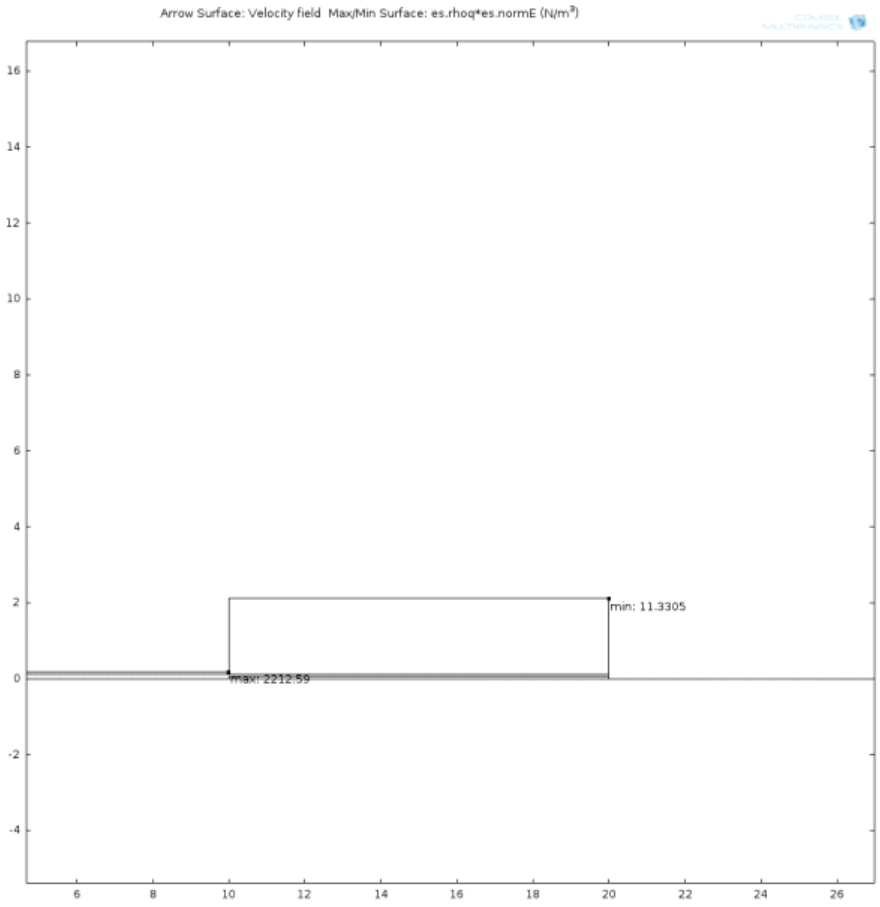
Arrow Surface: Velocity field Max/Min Surface: es.rhoq*es.normE (N/m³)
16
14
12
10
8
6
4
2
0
-2
-4
6
8
10
12
14
16
18
20
22
24
26
min: 11.3305
max: 2212.59

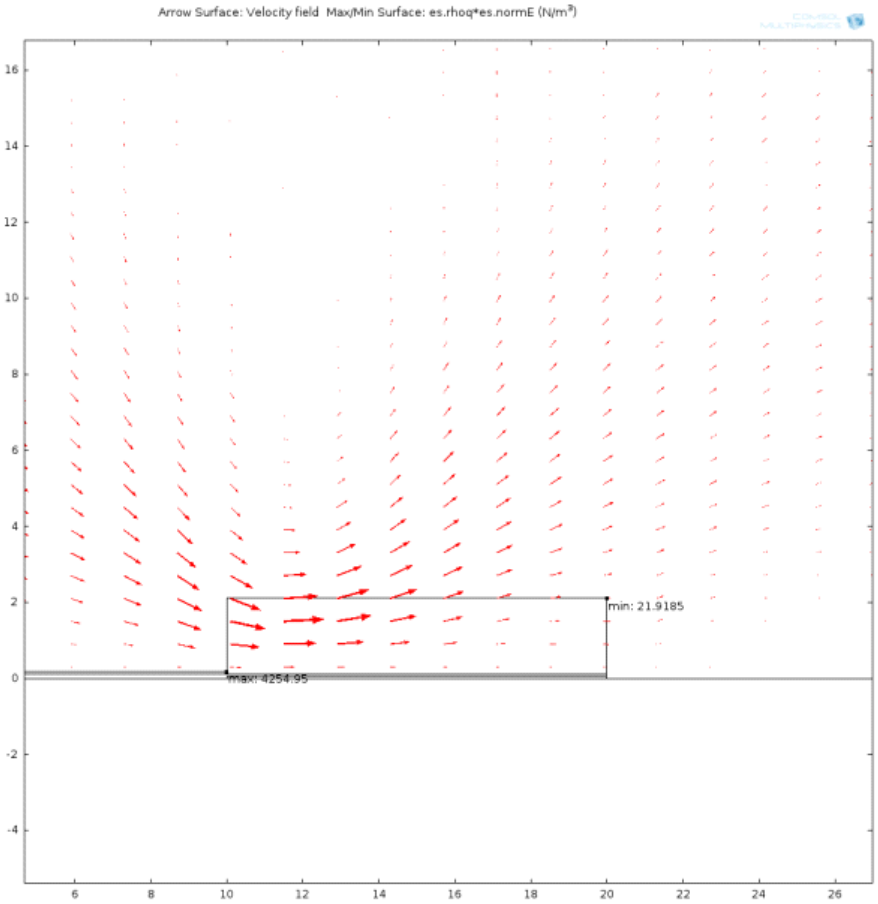
Arrow Surface: Velocity field Max/Min Surface: es.rhoq*es.normE (N/m³)
min: 21.9185
max: 4254.95

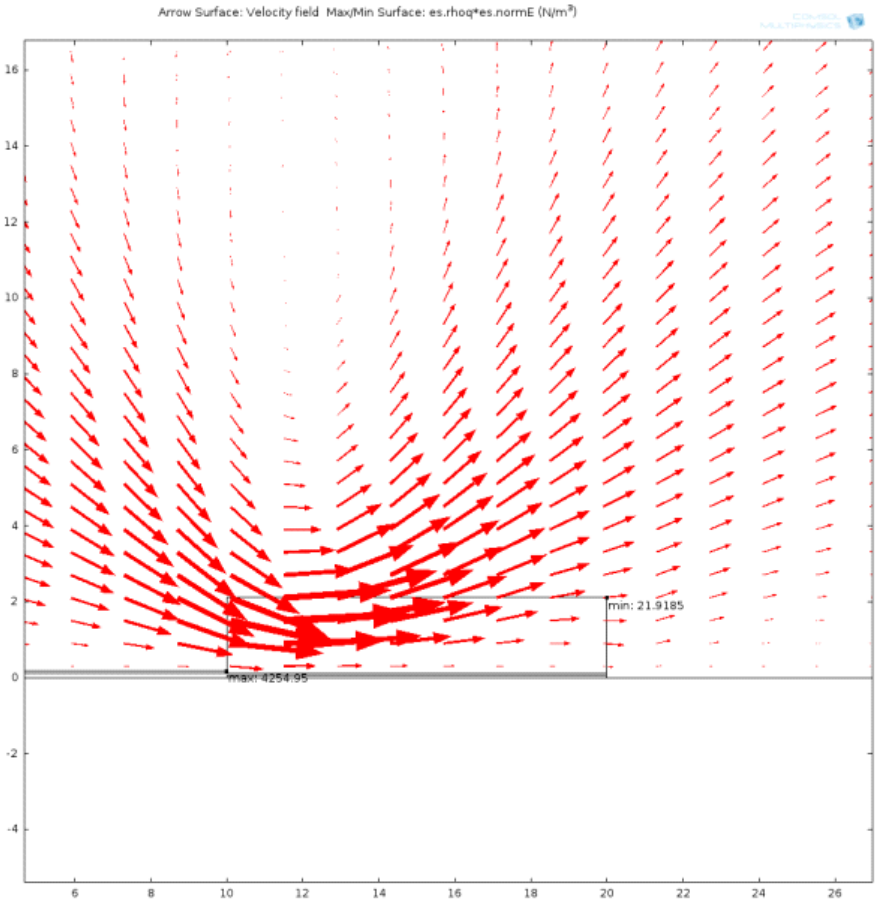
Arrow Surface: Velocity field Max/Min Surface: es.rhoq*es.normE (N/m³)
min: 21.9185
max: 4254.95

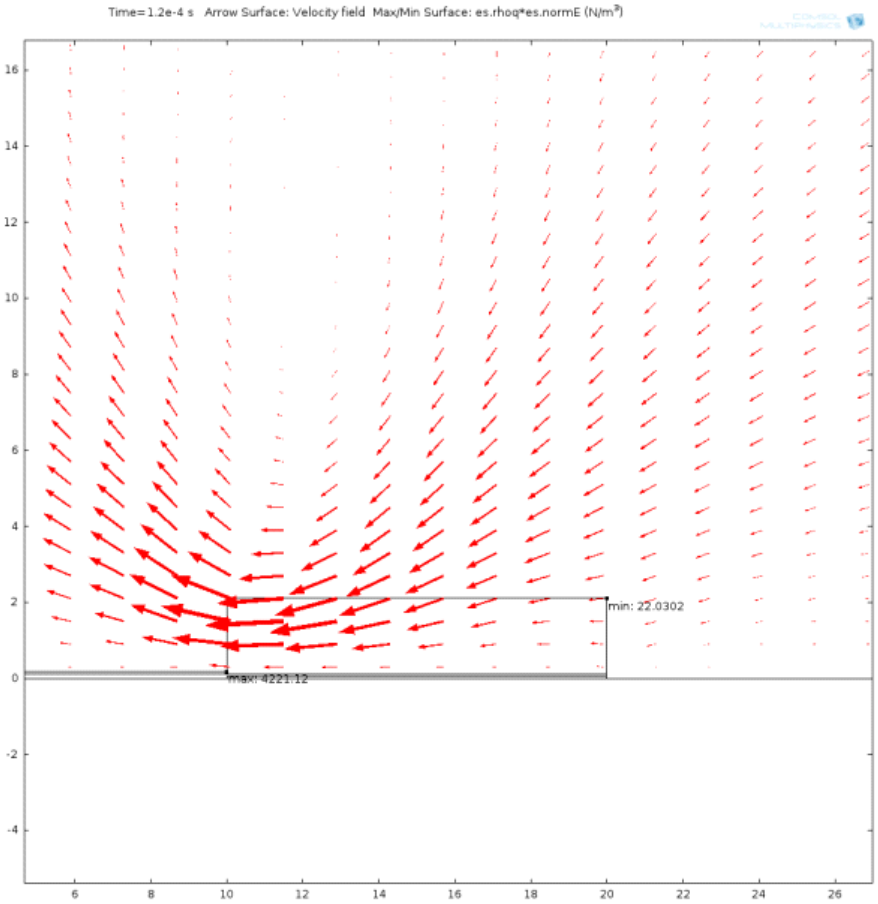
Time=1.2e-4 s Arrow Surface: Velocity field Max/Min Surface: es.rhoq*es.normE (N/m³)
min: 22.0302
max: 4221.12

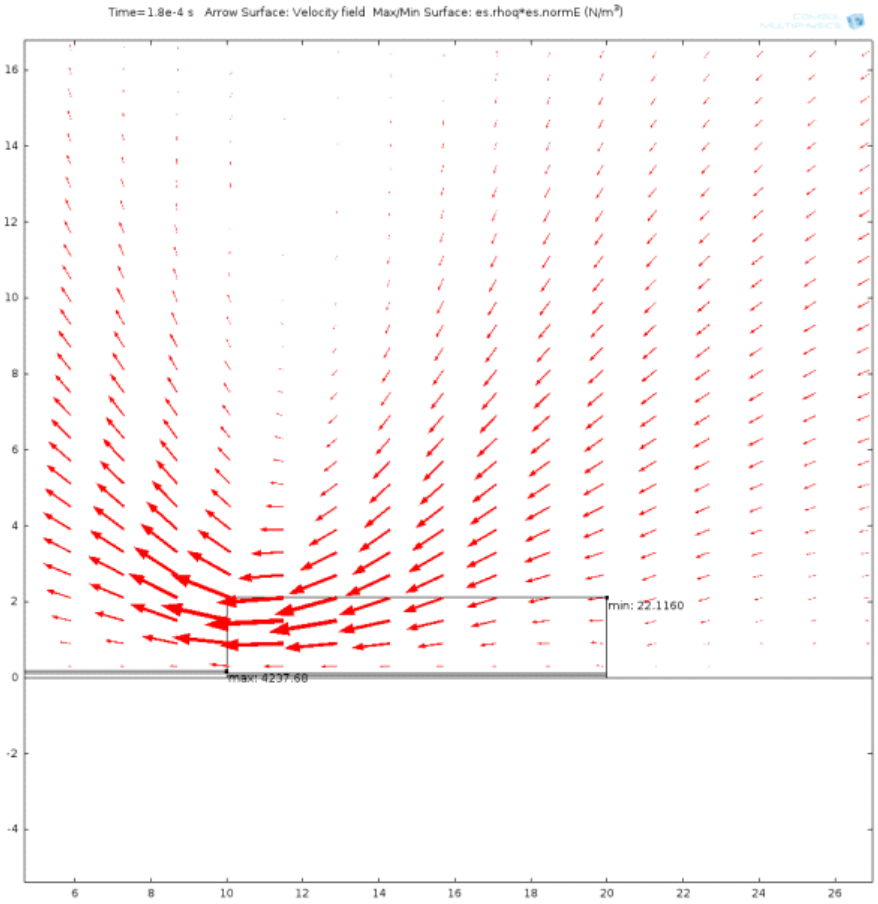
Time=1.8e-4 s Arrow Surface: Velocity field Max/Min Surface: es.rhoq*es.normE (N/m³)
min: 22.1160
max: 4237.68

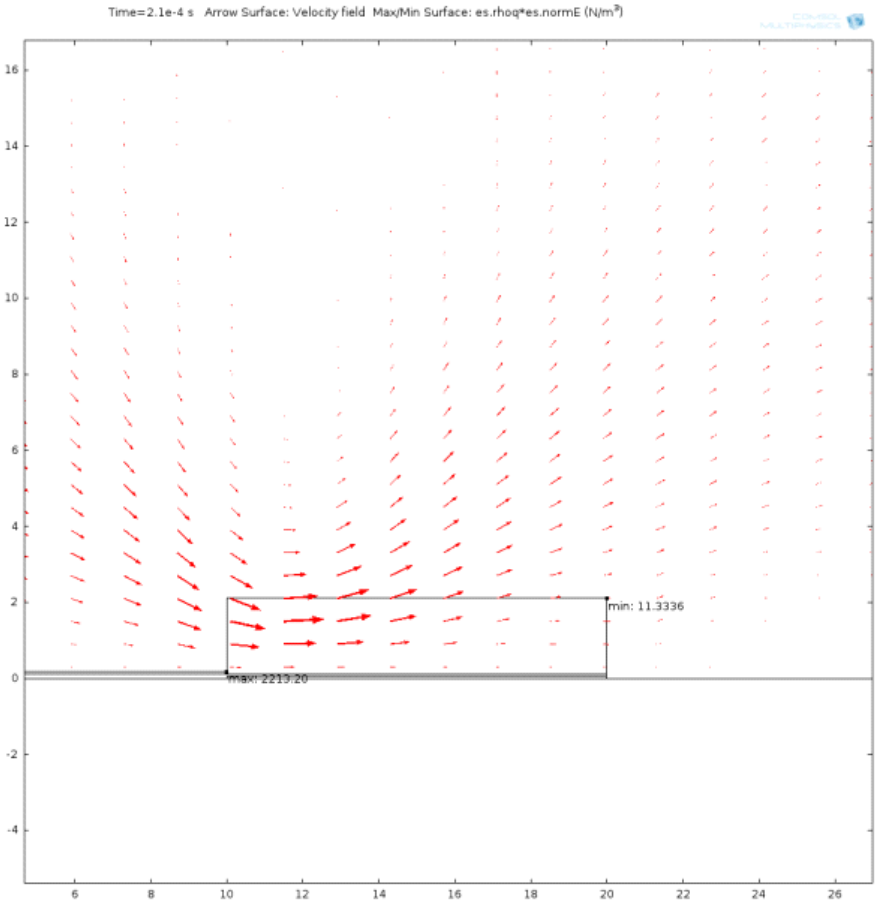
Time=2.1e-4 s Arrow Surface: Velocity field Max/Min Surface: es.rhoq*es.normE (N/m³)
min: 11.3336
max: 2213.20

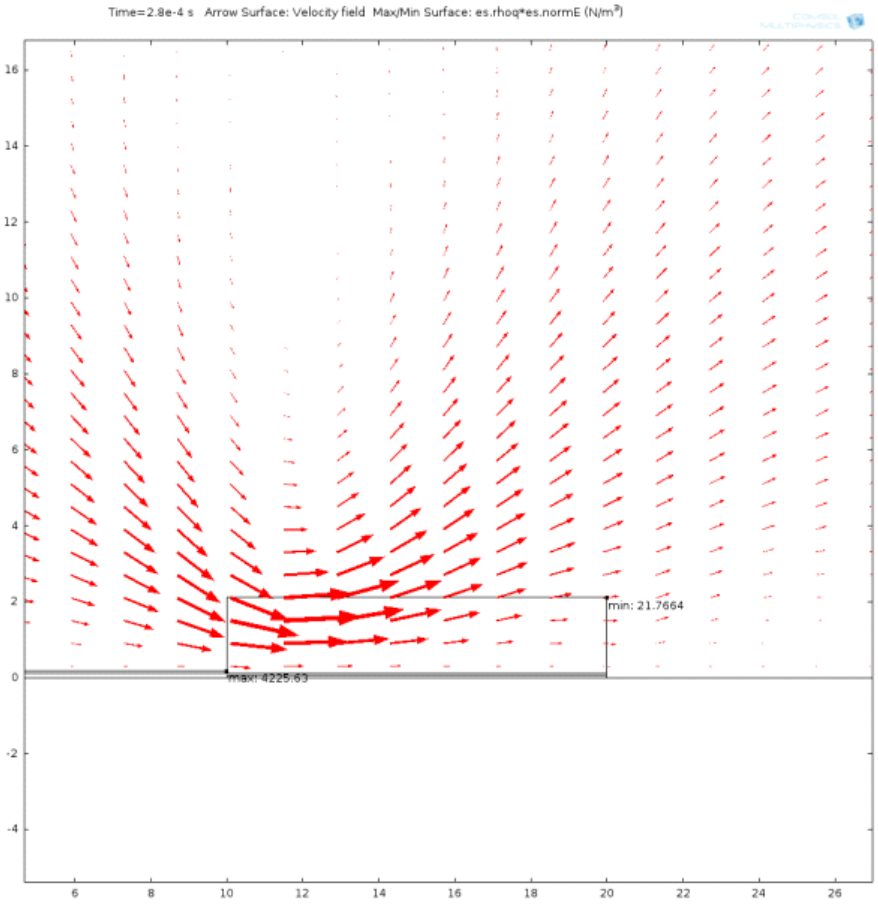
Time=2.8e-4 s Arrow Surface: Velocity field Max/Min Surface: es.rhoq*es.normE (N/m³)
min: 21.7664
max: 4225.63

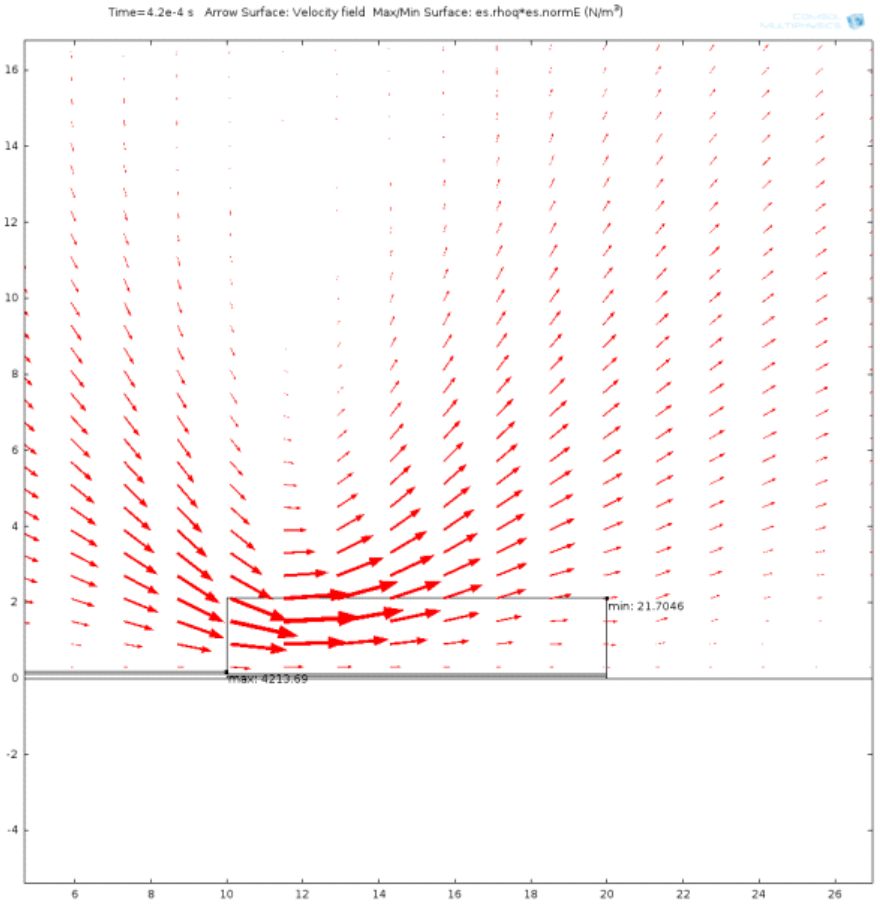
Time=4.2e-4 s Arrow Surface: Velocity field Max/Min Surface: es.rhoq*es.normE (N/m³)
min: 21.7046
max: 4213.69

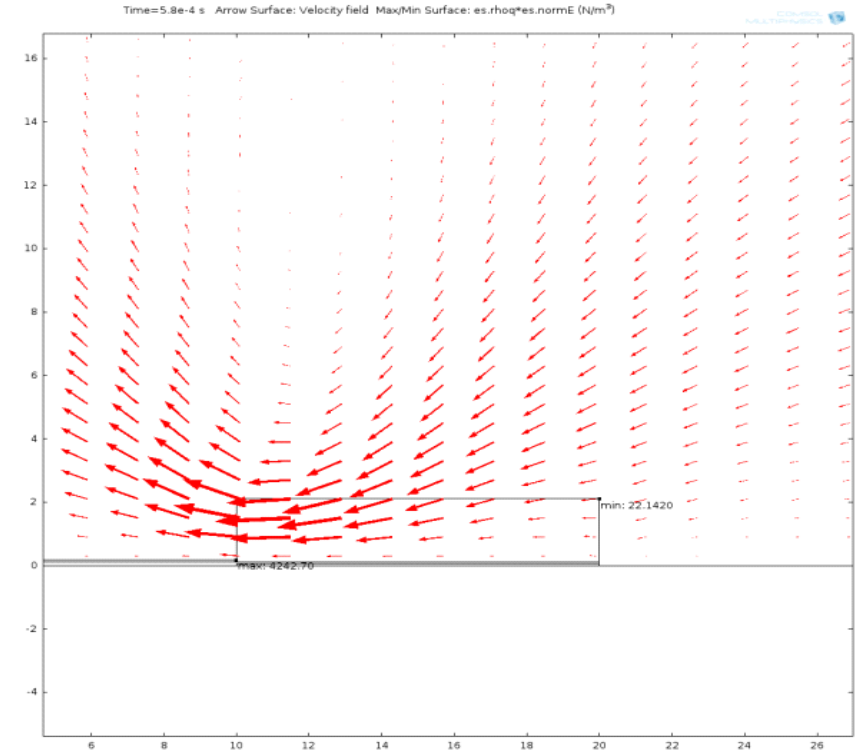
Time=5.8e-4 s Arrow Surface: Velocity field Max/Min Surface: es.rhoq*es.normE (N/m³)
min: 22.1420
max: 4242.70

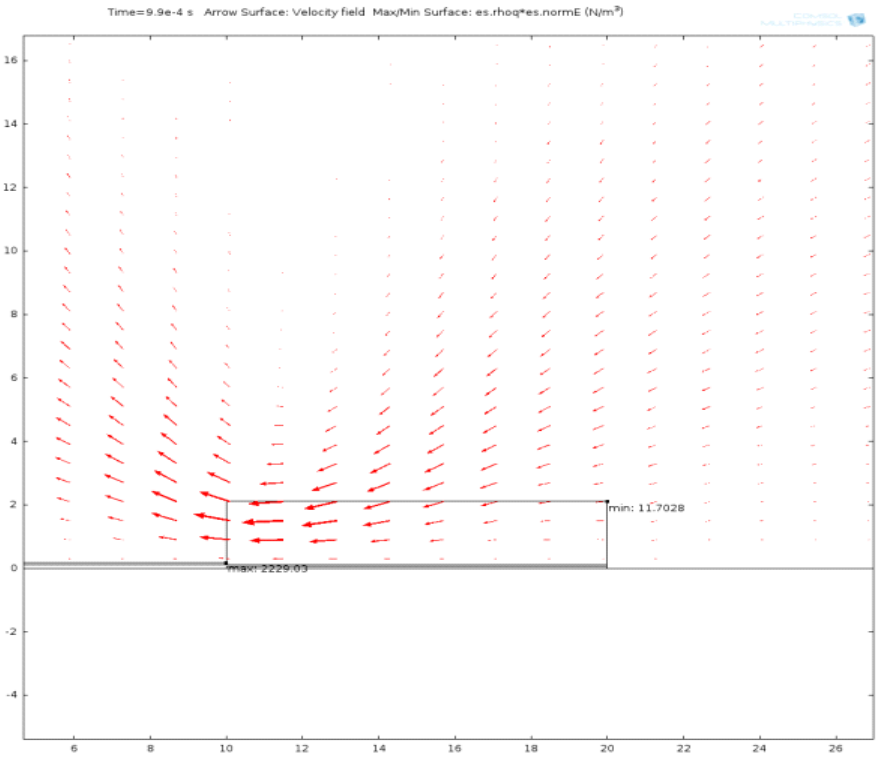

Figure 45 Velocity vectors for a series of time steps for the Electrodynamic-Fluid model.

Chapter 5

Conclusions & recommendation

This chapter presents the conclusions and recommendations of this thesis respectively.

Conclusions

1. Results from the Electrostatic model corroborate well with the computational studies done in the past. The Potential and the Electric field distribution bolster the fact that the Poisson equation has been correctly implemented and solved for, for the Electrostatic and later for the simplified Electrodynamic model. Thus, the Electrostatic model has been developed successfully.

2. In order to develop a 2D self-consistent Plasma Actuator model, involving positive species, it is not recommended to continue with COMSOL 4.2a[27]. However, this might not be the case for the newer COMSOL versions (5.0, 5.1).

3. A rudimentary model for a Plasma Actuator can be developed in COMSOL. So far, it is the best software which can be used to fundamentally model a Plasma Actuator in the simplest and least time consuming manner.

4. The Electrodynamic-Fluid model replicates the initial behaviour of the velocity field. Since, the model is computationally extensive, it wasn't allowed to converge to a steady state. However, since the initial behaviour corroborates well with the literature, it can be hypothesized the model shall converge to a steady state condition.

5. 1-D DBD Models have already been developed. However, these models are valid for very simple plasma chemistry, involving only a few reactions. To model close to experimental scenario, the model should incorporate hundreds to thousands of reactions. Higher the number of reactions involved, longer will be the time taken by the solver to converge.

6. Computationally modelling a DBD which specially solves for all the associated process, is very computationally intensive. For the present study, a 4 core(s), 3.40 GHz Intel Xeon Processor with 8 Gigabytes of RAM was used. The Xeon Processor has a proven reliability in handling large computations and therefore the only limitation is the RAM of the system.

7. For future Plasma Actuator modelling studies which involve a "ground-up" development of the Plasma Actuator model, starting from modelling the Plasma, the associated chemistry etc, coupling with a CFD study, it is strongly recommended to have a student from Plasma Physics or Electromagnetics background.

References

1. Gad-el-Hak, M., *Flow control.* Applied mechanics reviews, 1989. **42**(10): p. 261-293.
2. Post, M.L. and T.C. Corke, *Separation control on high angle of attack airfoil using plasma actuators.* AIAA journal, 2004. **42**(11): p. 2177-2184.
3. Matlis, E. and T. Corke. *Boundary Layer Instability on a Sharp Cone at Mach 3.5*. in *APS Division of Fluid Dynamics Meeting Abstracts*. 1998.
4. Corke, T.C., et al., *Application of weakly-ionized plasmas as wing flow-control devices.* AIAA paper, 2002. **350**: p. 2002.
5. Ramakumar, K. and J.D. Jacob. *Low Pressure Turbine Blade Separation Control Using Plasma Actuators*. in *Proceedings of the 45th AIAA Aerospace Sciences Meeting and Exhibit, Reno, NV, Jan*. 2007.
6. Van Ness, D., T.C. Corke, and S.C. Morris, *Turbine tip clearance flow control using plasma actuators.* AIAA Paper, 2006. **21**: p. 2006.
7. Thomas, F.O., A. Kozlov, and T.C. Corke, *Plasma actuators for bluff body flow control.* AIAA paper, 2006. **2845**: p. 2006.
8. Choi, K.-S., T. Jukes, and R. Whalley, *Turbulent boundary-layer control with plasma actuators.* Philosophical Transactions of the Royal Society of London A: Mathematical, Physical and Engineering Sciences, 2011. **369**(1940): p. 1443-1458.
9. Visbal, M.R. and D.V. Gaitonde, *Control of vortical flows using simulated plasma actuators.* AIAA paper, 2006. **505**: p. 2006.
10. Kotsonis, M. and S. Ghaemi, *Performance improvement of plasma actuators using asymmetric high voltage waveforms.* Journal of Physics D: Applied Physics, 2012. **45**(4): p. 045204.
11. Kotsonis, M., et al., *Experimental study on the body force field of dielectric barrier discharge actuators*. 2010: American Institute of Aeronautics and Astronautics (AIAA).
12. Corke, T.C., C.L. Enloe, and S.P. Wilkinson, *Dielectric barrier discharge plasma actuators for flow control*.* Annual Review of Fluid Mechanics, 2010. **42**: p. 505-529.
13. Enloe, C., et al., *Mechanisms and responses of a single dielectric barrier plasma actuator: plasma morphology.* AIAA journal, 2004. **42**(3): p. 589-594.
14. Orlov, D.M., *Modelling and simulation of single dielectric barrier discharge plasma actuators*. 2006.
15. Thomas, F.O., et al., *Optimization of dielectric barrier discharge plasma actuators for active aerodynamic flow control.* AIAA journal, 2009. **47**(9): p. 2169-2178.
16. Enloe, C.L., et al., *Mechanisms and responses of a dielectric barrier plasma actuator: geometric effects.* AIAA journal, 2004. **42**(3): p. 595-604.
17. Likhanskii, A.V., et al., *Modeling of dielectric barrier discharge plasma actuator in air.* Journal of Applied Physics, 2008. **103**(5): p. 053305.
18. Hoskinson, A.R., N. Hershkowitz, and D.E. Ashpis, *Force measurements of single and double barrier DBD plasma actuators in quiescent air.* Journal of Physics D: Applied Physics, 2008. **41**(24): p. 245209.
19. Jayaraman, B. and W. Shyy, *Modeling of dielectric barrier discharge-induced fluid dynamics and heat transfer.* Progress in Aerospace Sciences, 2008. **44**(3): p. 139-191.
20. Suzen, Y. and P. Huang, *Simulations of flow separation control using plasma actuators.* AIAA paper, 2006. **877**: p. 2006.
21. Orlov, D.M., T.C. Corke, and M. Patel, *Electric circuit model for aerodynamic plasma actuator.* AIAA paper, 2006. **1206**: p. 2006.

22. Kotsonis, M., et al., *Measurement of the body force field of plasma actuators.* Journal of Physics D: Applied Physics, 2011. **44**(4): p. 045204.
23. Abe, T., et al., *Experimental study for momentum transfer in a dielectric barrier discharge plasma actuator.* AIAA journal, 2008. **46**(9): p. 2248-2256.
24. Gregory, J.W., et al., *Force production mechanisms of a dielectric-barrier discharge plasma actuator.* AIAA paper, 2007. **185**: p. 2007.
25. Forte, M., et al., *Optimization of a dielectric barrier discharge actuator by stationary and non-stationary measurements of the induced flow velocity: application to airflow control.* Experiments in Fluids, 2007. **43**(6): p. 917-928.
26. Orlov, D.M. and T.C. Corke, *Numerical simulation of aerodynamic plasma actuator effects.* AIAA paper, 2005. **1083**: p. 2005.
27. Mamunuru, M., et al., *Plasma actuator simulation: Force contours and dielectric charging characteristics.* AIAA Paper, 2010(1221): p. 1-9.
28. A. Bouchmal, *Modeling of Dielectric-Barrier Discharge Actuator* (Master of Science thesis), Delft University of Technology, 2011.
29. http://www.comsol.nl/blogs/solutions-linear-systems -equations-direct-iterative-solvers
30. COMSOL Plasma Module User Guide.